2007

THE USE OF SELECTIVE ANNEALING FOR SUPERPLASTIC FORMING OF MG AZ31 ALLOY

Michael Christopher Cusick
University of Kentucky, mccusi2@uky.edu

ABSTRACT OF THESIS

THE USE OF SELECTIVE
ANNEALING FOR SUPERPLASTIC
FORMING OF MG AZ31 ALLOY

A recent study on the Post-Formed properties of Superplastically Formed Magnesium AZ31B has shown that the heating time prior to testing has a major effect on the Post Forming properties of the superplastically material. To this point, there has been very little examination into the effect of pre-heating or annealing on superplastic forming (SPF) properties. In this work, the effects of annealing prior to the SPF of Mg AZ31 alloy were examined. Both high temperature SPF tensile and bulge specimens were formed after annealing. Multiple annealing temperatures were examined to produce specimens with grain sizes ranging from 8 μm to 15 μm for comparison with traditional SPF results. The results show that the effect of annealing can be suitable for the improvement of thinning and possibly the forming time of superplastically formed Magnesium alloys through the control of the microstructure.

KEY WORDS: Superplastic Forming, Magnesium Alloy, Manufacturing, Annealing, Microstructure gradient.

Michael Christopher Cusick

November 26th 2007

THE USE OF SELECTIVE ANNEALING FOR SUPERPLASTIC FORMING OF MG AZ31 ALLOY

By

Michael Christopher Cusick

Dr. Marwan Khraisheh
Director of Thesis

Dr. Scott Stephens
Director of Graduate Studies

November 26th 2007

RULES FOR THE USE OF THESES

Unpublished theses submitted for the Master's degree and deposited in the University of Kentucky Library are as a rule open for inspection, but are to be used only with due regard to the rights of the authors. Bibliographical references may be noted, but quotations or summaries of parts may be published only with the permission of the author, and with the usual scholarly acknowledgments.

Extensive copying or publication of the thesis in whole or in part also requires the consent of the Dean of the Graduate School of the University of Kentucky.

A library that borrows this thesis by its patrons is expected to secure the signature of each user.

Date	Name

THESIS

Michael Christopher Cusick

The Graduate School

University of Kentucky

2007

THE USE OF SELECTIVE ANNEALING FOR SUPERPLASTIC FORMING OF Mg AZ31 ALLOY

THESIS

A thesis submitted in partial fulfillment of
the requirements for the degree of Master of Science in the
College of Engineering
at the University of Kentucky

By

Michael Christopher Cusick

Lexington, Kentucky

Director: Dr. M.K. Khraisheh, ME Director of Undergraduate Studies

Lexington, Kentucky

2007

Acknowledgements

The following thesis, while an individual work, benefited from the insights and direction of several people. First, my Thesis Chair, Dr. Marwan Khraisheh, exemplifies the high quality scholarship to which I aspire. In addition, Dr. Fadi Abu-Farha and Dr. John Balk as well as technicians Serge Tovar and Sabine Leroux provided timely and instructive comments and evaluation at every stage of the thesis process, allowing me to complete this project on schedule. Next, I wish to thank the complete Thesis Committee: Dr. Keith Rouch, Dr. Marwan Khriasheh, and Dr. Ibrahim Jawahir. Each individual provided insights that guided and challenged my thinking, substantially improving the finished product.

In addition to the technical and instrumental assistance above, I received equally important assistance from family and friends. Finally, mother and father, Kim and Howard Cusick, instilled in me, from an early age, the desire and skills to obtain the Master's degree.

Table of Contents

List of Figures

List of Tables

List of Files

Electronic Thesis & Dissertation

CHAPTER 1 INTRODUCTION

Problem Definition

As the lightest structural alloy on earth, the desire to use Magnesium alloy continues to increase day by day. The purpose for many magnesium applications is weight savings, particularly in the automotive industry. Magnesium alloys are becoming more common in application, specifically parts manufactured by casting. But for Magnesium to experience the success that the Aluminum industry has experienced, several obstacles must be navigated about. One such obstacle is the cost of the alloys with respect to Aluminum alloys. A second obstacle is the supply of Magnesium. Though the use of magnesium alloys in manufacturing has been continuously increasing for the last decade or so, the large scale availability of magnesium is still questionable. The final obstacle, which is the most influential, is room temperature formability of Magnesium. Magnesium alloys are characterized with poor formability at room temperature. This poor characteristic has been preventing Magnesium alloys from being applied in applications which include sheet metal forming, pressing, and die forging. Such applications account for a large percent of the parts produced in the transportation industry for which it has been strongly desired to incorporate Magnesium alloys for major weight savings and thus obtain substantial energy savings.

Superplastic forming (SPF) is a process in which sheet metal parts are produced at elevated temperatures (greater than 0.5 T_m) using an inert pressurizing gas to force the sheet into the shape of a die. Large ductility generally greater than 200% and a fine equiaxed microstructure, usually less than 15 μm are typically required of the material for application with SPF. Several Magnesium alloys show good SPF characteristics which

have led to the study of their deformation properties and constitutive modeling. The results of the models are used to generate forming pressure – time profiles, finished part properties such as thickness, and process optimization. But even with all the work that has been completed to date, the forming characteristics and results are not good enough for the application of Magnesium alloys thus far. The forming times are still too slow to be applied in the automotive industry, the primary applicant for Magnesium alloys for weight savings to combat the rising energy cost of fossil fuels as well as global warming do to the high amount of green house gases produced during combustion.

Brief Review

Development of new processing technology for microstructure control is a continuous cycle. Equal Channel Angular Extrusion (ECAE) is a bulk extrusion process which has been studied extensively over the last decade. ECAE has been shown to produce refined equiaxed microstructure with a grain size of the micron and sub micron scale. As for selective (non-bulk) microstructure control, Friction Stir Processing (FSP) has been a growing process in both research and industry. FSP produces a refined equiaxed microstructure though severe plastic deformation within a material without melting. FSP generally reduces the grain size, though in the correct circumstances, it may promote grain growth, but only in material with submicron or near submicron grain size prior to processing. Another state of the art grain size controlling process is ion bombardment, which has been used in crystalline materials. Finally, selective heating has been used to selectively anneal a metal which generates selective grain growth.

The development of constitutive models for the modeling and prediction of formed parts in SPF has been quite significant over the last decade. The initial models

proposed for Lead-Tin alloys have been adjusted and modified for the use with the SPF modeling of titanium alloys, aluminum alloys, stainless steels, and magnesium alloys. The models have been used to predict final sheet properties from thickness profiles and grain size distributions in research to the optimization of forming for industrial processes. These constitutive models have had a major effect on the direction of research in the SPF, especially for the use of magnesium sheet metal in the automotive industry. In the automotive industry, weight savings is crucial to reach the 100km/liter of fuel efficiency mark. This has lead the automotive industry to search for possible forming processes that can permit the use of magnesium alloys in sheet metal form since it is the lightest structural alloy available. SPF is the plausible forming process for magnesium alloys. Though, the forming process is still weak with respect to the forming time constraints required by the automotive industry. Therefore, modeling has become crucial in aiding the prediction of the forming results.

Motivation

With modeling, the control of the strain rate in the material is used to determine the forming pressure profiles. Grain size in SPF has a major effect on the strain rate sensitivity and optimum forming strain rate. FSP has been mixed with SPF to show this effect. Finite Element (FE) simulations have also been used to show that microstructure in bulk form as well as gradients can significantly affect the forming parameters. Experimentally, the results have been shown in both a Zn-Al alloy and Ti-6Al-4V to have a positive effect. This leaves magnesium and the automotive industry in need of exploration with microstructure gradients for the aid in process improvements if application of magnesium alloys in sheet form are to be realized.

Objectives

This work is to show that there is positive benefit when the bulk microstructure is modified locally prior to forming in SPF. Works with other alloys have shown that there is a significant benefit in the decrease of thinning when the microstructure has been modified locally. It is clear though that microstructure has a major effect on the strain rate properties in SPF forming processes and therefore it is possible that the forming time may be positively affected with locally modified microstructure, which is to be investigated as well.

The first task will be the determination of a static grain growth curve over the range of annealing temperatures. This curve will then be used to determine experimental procedures for the remaining two tasks. The second task in this work is to locally modify the microstructure in several sheet samples and to SPF bulge form them for preliminary experimental evidence in the affects to thinning and forming properties. The third and final task will be the preliminary determination of annealing effects to the strain rate sensitivity and stress strain curves for Mg AZ31 alloy. The grain size will be the primary constraint for these tasks. Thus, it is to be determined if the annealing temperature or time (note: the same grain size in a specimen can be achieved for different annealing temperatures and times) changes the forming properties when the specimen grain size is the same. These results can then be used to determine the relevancy of further pursuit into locally modified microstructure.

Methodology

To complete task one, annealing at 4 selected temperatures will be preformed over a time range of 24 hours to permit the fit of the single phase static grain growth

curve. The samples will then be examined optically to acquire the grain size at each selected point of the experiment. Once the results have been tabulated, the static grain growth parameters will be fit and used to select temperature and annealing time profiles for tasks two and three.

Task two is to be completed by first evaluating and selecting an appropriate means for locally heating sheet specimens. Once the means for selectively heating the specimens has been determined, specimens will be generated for testing and examination. The specimens generated will be duplicated to allow for microstructure examination and validation. The remaining specimens will be SPF bulge formed and then compared to non modified bulge samples to reveal the experimental out comes. This will permit the determination of the validity of the constitutive model used for AZ31. The results will also be used to determine the necessity of continuation of task three.

The third task will be the property examination of annealed AZ31 tensile specimens. Two annealing temperatures will be used for the experiment. For each annealing temperature, two annealing times will be used. The microstructure will be verified by optical examination. The specimens will then be used for SPF tensile testing at 400 C. Both stress strain curves for 3 strain rates will be evaluated for each time-temperature category of specimens as well as 2 strain rate jump tests. These results will then be compared to the as received material properties to determine if long term annealing has a major effect of the SPF properties and thus will require an in depth examination to permit proper modeling of Mg AZ31 alloy bulge samples that have locally modified microstructure.

CHAPTER 2 Background

Magnesium alloys are the lightest structural alloys known to man. With a density of 1.74 g/cc, Magnesium is about ¾ the density of steel, ⅔ the density of Aluminum and ⅜ the density of Titanium, making Magnesium one of the most desirable alloys in manufacturing for weight savings. Magnesium alloys are of hexagonal close-packed (HCP) crystalline arrangement with respect to the alloys atomic arrangement. Similarly, Titanium has a HCP atomic crystalline arrangement where as Aluminum consists of a face centered cubic (FCC) atomic crystalline arrangement and steel consists of a body centered cubic (BCC) atomic crystalline arrangement. The atomic crystalline arrangement is very important for ones understanding of metals ductility. At room temperature, a metal plastically deforms through the movements of dislocations and vacancies along slip planes. Slip planes are the planes that consist of the largest atomic density in the crystalline unit cells. HCP metals have up to 5 slip planes where as BCC metals have 48 slip planes and FCC metals have about 12 slip planes. Due to the lack of slip planes, it is easy to understand the low room temperature ductility for light weight Magnesium and Titanium alloys (1).

Along with the low ductility of Magnesium alloys at room temperature, Magnesium is one of the more expensive alloys to produce. Magnesium is found in the natural form of Magnesium Oxide (MgO_2) in the earth's oceans. Magnesium Oxide is one of the salts which explains why it is the 2nd most abundant source for any metal on earth behind Titanium Oxide (TiO_2) which is found in the earth's crust and thus is more abundant. The process of Mg extraction from the oxide form is known as electrolysis,

which is the use of large electric charges to break the oxide bounds. This process has been used largely for Aluminum extraction since the turn of 20th century. Initially, with the understanding that Titanium alloys are the strongest of the metals, one might wonder why there is a need for Magnesium alloys, since Titanium is found in a similar oxide form, is more abundant, and its strength is capable of offsetting the density gap with Magnesium alloys. But though the above statements are true, there is a hidden expense for the formation of Titanium alloys due to the high reactivity of the Titanium element (Ti) with nearly any element in the periodic table requiring highly expensive manufacturing and processing techniques leading to a cost of almost twice that of Magnesium alloys. But it should also be mentioned that Magnesium alloys are still well more expensive than Aluminum alloys due to its low reactivity compared to Aluminum, lack of industrial demand and thus lack of production worldwide as well as a slightly larger energy intensive extraction process.

The over haul of Magnesium alloy production currently trying to be implemented shows that the manufacturing use of Magnesium is still desired and on the rise even though its current production expense is well above Aluminum alloys, Magnesium's most prominent competitor. With this, promise of implementing Magnesium alloy use for weight savings in order to aid in consumable energy reduction has been growing in such industries as the automotive industry, which has been and is currently even more pressured to conform to current and potential future pollution reduction laws. Currently, approximately 36% of the 360,000 tons of Magnesium alloys annually produced are used in the automotive industry with the automotive industry comprising of the primary Magnesium alloy industrial application (2,3). Outside of the automotive, Magnesium

alloys have found use in the Aerospace industry, both military and commercial for weight savings purposes, as well as the Nuclear power, metals, and Audio and Electronics industries (4). Magnesium is though making a run at industrial applications currently due to the realized manufacturing property benefits.

When compared to the Aluminum alloys, steels and plastics that Magnesium alloys are looking to replace, different Magnesium alloys exhibit high quality advantages. Beginning with the primary advantages currently being combined for application today, Magnesium alloys have a lower latent of heat than all cast and molded competitors. This leads to shorter casting realized up to 50% currently which combines to reduce production costs up to 50% as well due to a possible 25% increase of manufacturing efficiency (5). Other Magnesium alloy casting properties include surface quality characteristics that provide the ability to cast parts with thicknesses as thin as 1.0 – 2.0 mm versus 2.5 – 3.5 mm for Aluminum alloys. This can be combined with the ability for Magnesium alloy casts to be designed with draft angles of 1 to 2 degrees which is nearly ½ that of Aluminum alloys (5). The surface characteristics also allow tolerances of up to twice that of Aluminum casted alloys or ± 0.001 mm which is significant when machining is required after casting. Magnesium Alloys have low strength characteristics compared to Aluminum alloys and steels which lead most people perceive as a major weakness but the lower strength provides the manufacturing industry with the added benefit in terms of power reduction by nearly 50% due to the lower horsepower and larger material removal rates used in post casting machining operations (5). All of these characteristics promote the reduction of material waste leading to more production cost savings and thus increasing the desire to use Magnesium alloys in the automotive

industry. With these benefits, Magnesium cast parts now account for 30% of Magnesium industry use today, up from 15% prior to the mid 1990's when nearly 55% of Magnesium used in industry was in the form of alloying agents for Aluminum alloys (6). Figure 1 and Figure 2 show several examples of the current magnesium parts manufactured in the automotive industry.

Though Magnesium has had success in the automotive industry for die-cast parts, there is still a large desire to develop techniques of forming that will allow the sheet metal and extrusion applications of Magnesium alloys. There are several primary benefits of these desired applications including weight reduction as mentioned above for both aerospace as well as automotive to reduce fuel demands and green house gas emissions. Damping and thermal characteristics of Magnesium alloys versus Aluminum alloys are desired for stability and thermal controls necessary for such applications as satellites robots and other future structures in space (7,8). All of the possible ideas currently researched for Magnesium may lead to a major increase in required production. Researchers from both private R&D and Academia have expressed believe that a more unified effort can lead Magnesium into the 21st century as a primary alloy source for the future if collective efforts can pull together and create a research infrastructure where material property ↔ process technology ↔ construction methods are realized with a hand in hand vision (7,9).

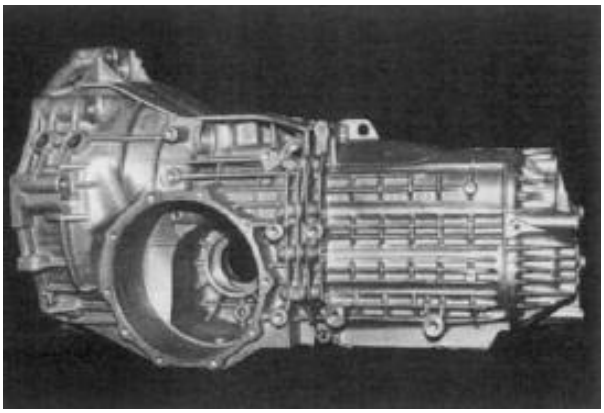

Figure 1 Magnesium gear box housing (10)

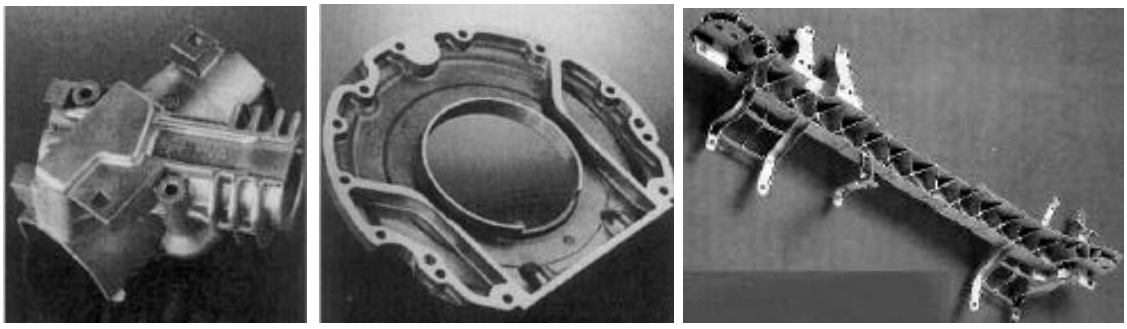

Figure 2 (a) Steering column lock housing (b) sealing flange (c) Steering column (2,11)

Magnesium alloy application is primarily accomplished by die-casting as previously mentioned, but researchers continue to search for more processing techniques. Currently, SPF is the primary forming technique for sheet metal in R&D facilities. Room temperature formability has led to many studies for the optimized forming temperature of magnesium extrusions and sheet metal. Lack of initial success has led to the investigation of combined processing and forming techniques such as combining Friction Stir Processing (FSP) prior to both room temperature or elevated temperature formability testing (12-15) or deep drawing at elevated temperatures in hopes of utilizing the elevated temperature properties for processing time reductions more favorable to industry (16). Research in the area of equal channel angle pressing (ECAP) has also provided promise for material preprocessing for the generation of processed wrought alloys with

microstructure properties slightly more desirable for room temperature forming though largely more desirable for the elevated forming processes including SPF (17). But even with the combination of technologies, the formability is still limited and SPF by itself remains the most probable forming technique. With this, microstructure and modeling efforts have led the way to today's knowledge of Magnesium alloy SPF formability.

SPF is a forming process that utilizes select materials elevated temperature properties permitting large plastic elongation by means of blow molding. A material capable of large plastic elongation is classified as a Superplastic material. Superplasticity is the ability of a material to undergo plastic strains generally greater than 200% fairly uniformly prior to failing. Figure 3 provides a visual reference of superplasticity from a tensile test of the Eutectic alloy mixture of Lead (Pb) and Tin (Sn) tested at 125 ˚C. The result was an elongation of nearly 4850% percent, though it should be noted that the only use of the Pb-Sn alloy is for the research of understanding and modeling of superplastic materials.

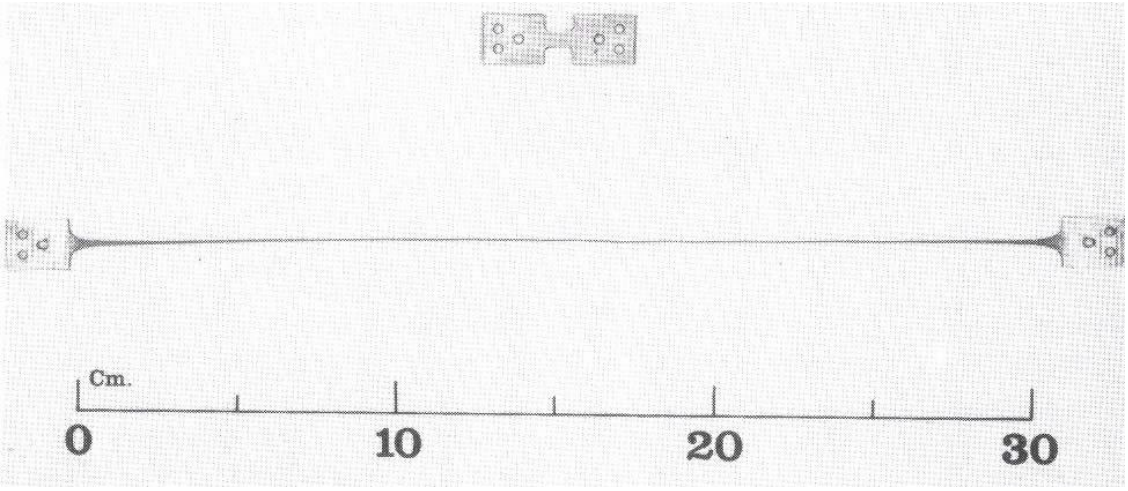

Figure 3 Superplasticity in a Pb-Sn alloy pulled in tension to 4850% elongation at 140˚C (18)

Instinctively, the superplastic materials that have been discovered or generated encompass nearly the entire realm of alloys. Though of surprise is the selectivity for such alloys, especially those of the Aluminum base. Aluminum alloys with superplastic behavior have been limited to those of the Supral 5000 series and Neopral which have been used primarily for art and decoration applications until recently and AA7475, Supral 100, 150, and 250 for the use in structural application (19). Figure 4 illustrates a few of the decoration applications. As for the structural aluminum applications, Figure 5 illustrates the use of Aluminum for the body panels of the Aston Martin Vanquish (a) and a Morgan Aero 8 (b). Aluminum AA5083 sheets have also been recently implemented into the aerospace industry as presented in Figure 6 (20).

Figure 4 Superplastic forming used for art and architectural applications (21)

Figure 5 Superplastic forming used for automotive applications (a) Aston Martin Vanquish (b) Morgan Aero 8 (1)

(a) Air intake Lip Skin

(b)Wing Tip **(c) Leading Edge of an Engine Mount**

Figure 6 Superplastic forming used for airplane applications (a) Eclipse 500 Jet (b) Boeing 777 (c) Boeing 737 (21)

Titanium alloys Ti-6Al-4V and Ti 6Al-2Sn-4Zn-2Mo have been used quite successfully in the Aerospace industry but only when hot rolled into sheet metal with the $\alpha + \beta$ phase present (22). SPF Titanium is also a major reason for the success of metal in replacing wood for the golf club industry (23). The use of SPF Titanium alloys has increased readily in the last few years for the aerospace industry due to the ability to join the parts together without fasteners with a technique call Diffusion Bonding (DB) (24,25). The SPF success in the aerospace industry is permitting the commercial airlines to operate with lower fuel consumption costs due to the decrease in mass with the decrease in parts and rivets during the manufacturing of the airplanes. There have also been results of superplasticity for many Iron based alloys including sink tops for aerospace as well as cookware involving duplex stainless steels (23). SPF has also began to enter the medical field, specifically the dental area though work in non-dental prostheses has been studied by a fellow University of Kentucky masters student Daniel Thomas. The primary researcher of the dental prostheses is a Dr. Richard Curtis who is also working with Daniel Thomas. As for the current results of Dr. Curtis, dental implants as seen in Figure 7 have shown success and continue to be researched (2,27-29). Finally, SPF applications for Magnesium alloys are still in the research and development stage for the many desirable applications.

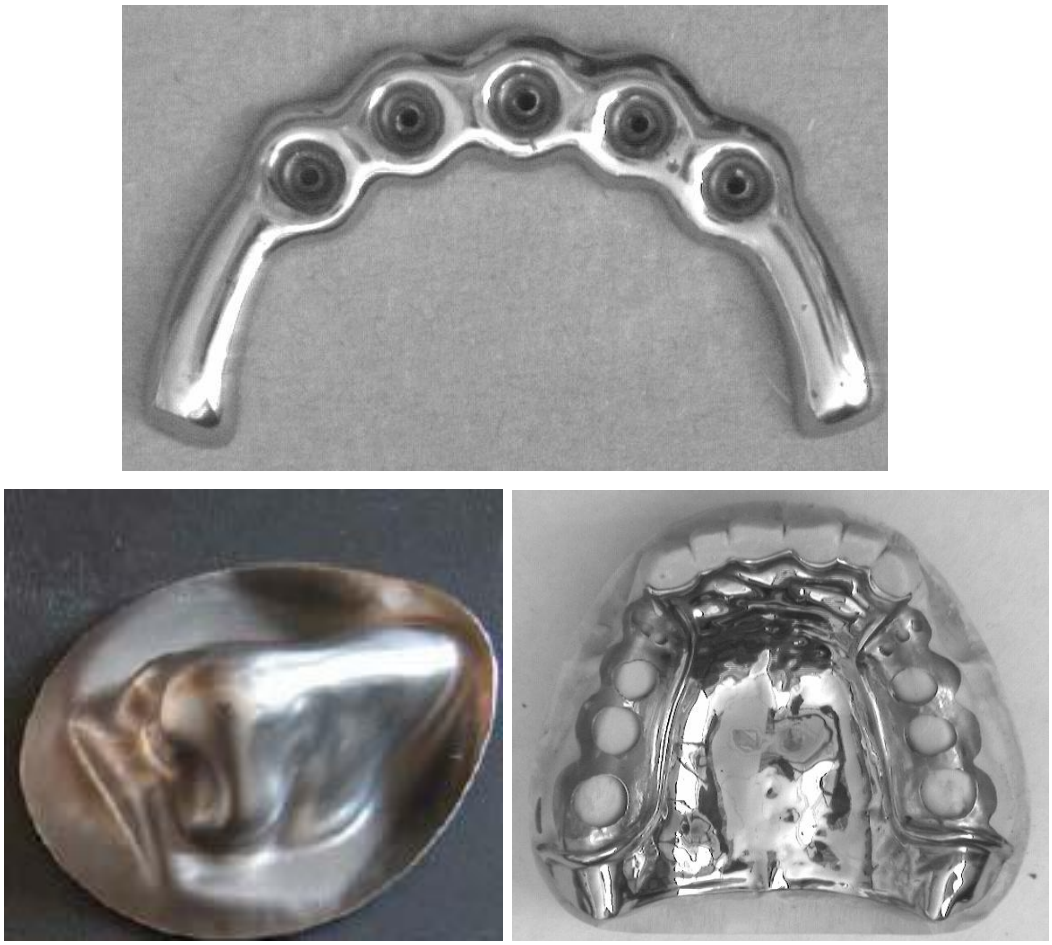

Figure 7 Superplastic forming used for medical applications (3)

Superplastic Forming

As the name suggests, superplastic forming is an extreme plastic deformation process. Figure 8 provides a visual of the SPF process. The process begins with the preheating of the sheet metal to be formed. Once the material has reached the desired forming temperature, an inert gas is used to pressurize the forming chamber to stretch the material into the die below the material. With the extreme stretching, the material thins severely and takes the shape of the die. The rate of deformation process is controlled with the pressure of the forming gas where the maximum strain rate of the material is used to adjust the forming pressure to prevent failure or extreme thinning.

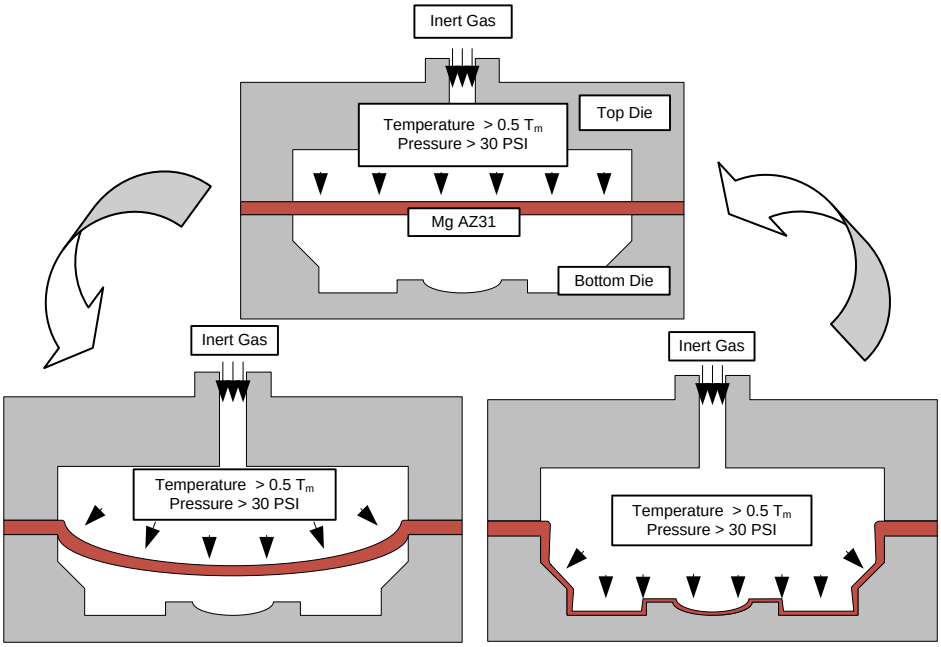

Figure 8 Schematic of the Superplastic forming process

Superplastic forming has traditionally been characterized by four properties of either the preformed sheet or the forming results of the material. The properties are as follows (4):

- Greater than 200 % elongation prior to failure in tensile stretching
- Equiaxed and stable microstructure of a grain size less than approximately 15 μm
- Forming strain rates typically between $1x10s^{-1}$ and $1x10^{-5}$ s^{-1}
- Forming temperature greater than ½ melting temperature

Superplasticity

Superplasticity has been a known phenomenon for nearly a century, though it is unclear who actually discovered the material property. Arguments over the initial observation include those for USSR and UK but without proof are believed to be sometime in the 1920's. Pearson's discovery in 1934 that he generated a tensile

elongation of 1950% without failure using a Bismuth (Bi) – Tin (Sn) eutectic alloy was the first well known report of extreme plastic deformation. Though there are the supposed properties listed above for material requirements to permit superplasticity, literature publications do provide plenty of reports currently that superplasticity has been achieved with grain sizes well above 100 μm (5-7) and signs of strain rates above the traditional values in the range up to $2x10^{0}$ s^{-1} for Magnesium alloys with grain sizes in the realm of 500 nm (8).

Superplasticity is a deformation process that is rooted in the rate-dependant material deformation model. The general model for such material deformation is presented in equation 3.1. In a rate-dependent material model, the stress, σ, is proportional to the strain rate, $\dot{\varepsilon}$, in the form of a power law where the exponent is the rate sensitivity coefficient, *m*. *K* is the proportionality constant.

$$\sigma = K\dot{\varepsilon}^{m} \qquad (3.1)$$

For superplastic materials, the strain rate sensitivity coefficient typically falls between 0.3 and 0.7. Values greater the 0.5 are preferred because the ductility of materials formed in this region are typically capable to be used in industrial environments. Equation 3.1 is presented graphically in Figure 9. Figure 9 is known as the superplastic sigmodial stress/strain rate curve which is a characteristic graphical portrayal of superplastic materials dependence of stress and strain rate sensitivity coefficient.

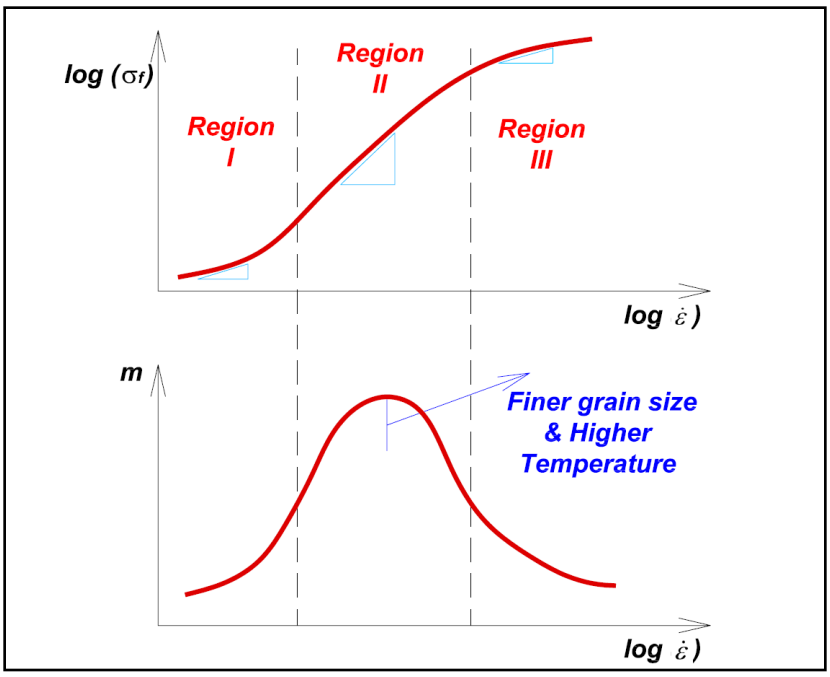

Figure 9 Typical sigmodial shaped logarithmic stress-strain rate curve for superplastic materials (9)

In Figure 9, the strain rate axis is theoretically broken up into 3 regions (10,11). Region I is a non superplastic region where the deformation mechanism is generally considered to be threshold limited due to the extremely low strain rates. Region II is considered to be the superplastic region of a material. The deformation mechanism for region II is accepted to be a combination of grain boundary sliding and dislocation glide climb. Finally, a transition to non superplasticity takes place as the deformation mechanism of power law creep over takes grain boundary sliding in region III at the elevated strain rates (12).

As expressed by the figure, the region II can be shifted to the right by decreasing the grain size and/or increasing the temperature which is highly favorable due to the decrease in optimum cycle time from the increase in the optimum forming strain rate. But of course, region II can also be shifted to the left which is unfavorable by the same parameters. The sigmodial curves in Figure 9 are the primary projection of experimental

results from SPF testing. They appear in literature for current and future industrial materials such as Titanium alloys (12-16), Aluminum alloys (17,18) and Magnesium Alloys (19-22). Friction stir processing resulted in the decrease of grain size for the both Aluminum publications showing the slight shift right and up for the sigmodial curve. All for Magnesium alloy references provided the sigmodial curve to express the primary region of superplasticity of the alloys tested as received from material suppliers. Constitutive model comparisons and tested microstructural alterations have also been published by many researchers as the realm of modeling and optimization in superplasticity continue to move towards industrial application (13,16,18,23-27). Superplastic materials encounter many processing, experimental and computational steps before application. Figure 10 represents the traditional material flow path for today's current SPF applications in of dental and aerospace (3,28-30). SPF materials are produced in wrought form at the mills prior to commercial processing to produce the sheets necessary before suppliers may purchase them. In the past, Titanium alloys were specifically processed additionally to produce the fine grain microstructure desired by the aerospace industry, but due to the consolidation of the Titanium processing plants in industry, this additional process no longer occurs. Thus, the fine grain microstructure used in SPF research and industry is that resulting from sheet rolling. This has been acceptable for many years now. After a material was observed to exhibit superplastic behavior, mechanical testing is employed to verify initial observations and provide the extent to which a material is ductile. With this information known, future work with the material can be decided upon by the possible new observations one might find when testing the material or if the material may be useful for application, research towards

material deformation models and SPF process optimization is carried out to further information knowledge base. Finally, the SPF material is applied with the continuation of

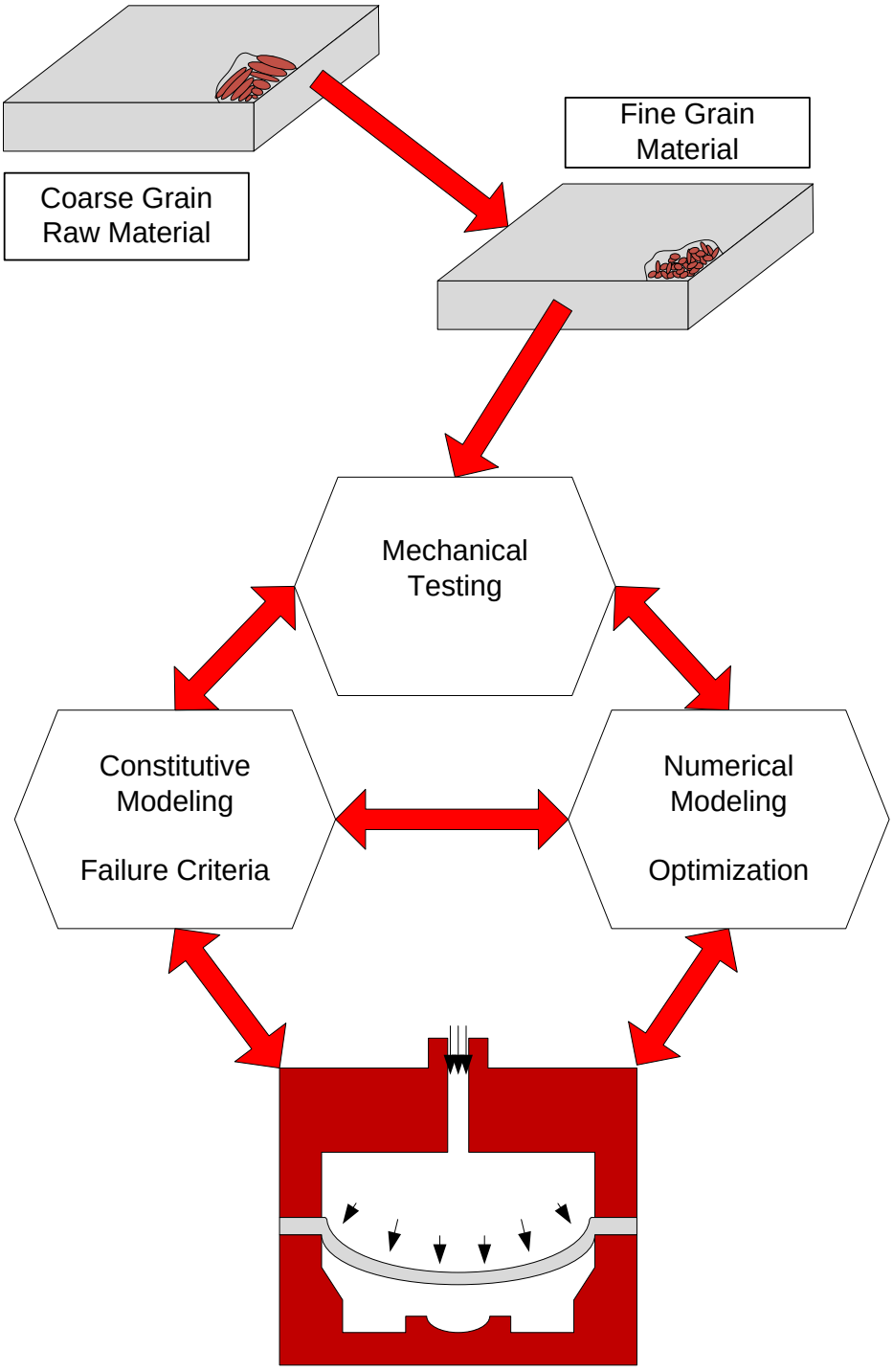

Figure 10 Material flow diagram for Superplastic forming

to application with continued research and modeling to move the material and SPF process in a more economical and sustainable direction.

SPF Research: Contributions and Objectives

SPF has many advantages that continue to drive research in order to provide the means of high production rate application, such as:

- Complex shape formability is a single sheet forming step. This permits many simple parts formed separately and assemble to be combined into a single step.
- Many very difficult to form materials exhibit Superplastic properties which permits the possible industrial application. For Example, wrought Magnesium alloys are formable by SPF where as there less than 8% room temperature ductility has prevented there use in many applications to date.
- Greater design flexibility due to the large ductility of SPF materials.
- Ability to extensively reduce energy consumption by automobiles which is the source of the majority of the United States green house gas emissions.

Of course, there are also disadvantages to SPF currently which is the reason future SPF research is vital to the hopes of high production rate applications, such as:

- Strain rates below $1x10^{-3}$ s^{-1} are rather unlikely to permit high production rate industrial application.
- Predictive capabilities to allow applications in such circumstances without trial and error tooling setup. This is extremely important to prevent extensive material waste in both tooling material and product material.

SPF constitutive modeling has been the primary tool for determining where the technique stands for industrial applications whether used or not. There are two bases for the

constitutive models used today (31). Either the models are based in Continuum Mechanics or Atomistic mechanics. In the area of continuum mechanics models, researchers either base their modeling efforts on the description of the macroscopic mechanical responses of the material (32-34) or the activation energy of material flow determined with the measured macroscopic forces (35). There have been a few efforts put forth to create analytical models for pressure curve equations (36), initial sheet thickness and sheet thickness after forming (37-38). Though the analytical solutions are accurate, there use is very limited due to the restriction that the formed shape must be a hemispherical dome. But the pressure profile is useful for initial SPF parts to validate constitutive models. The Atomistic mechanics models were the focus of many SPF researchers who studied the deformation mechanics microstructurally. Models based on Grain Boundary Sliding or Dislocation Glide Climb have been developed and occasionally applied in the application of Ti-6Al-4V for the initial SPF application to aerospace (11,39-41). The most popular constitutive models currently in development and in use today have taken the properties of viscoplastic material deformation and added atomistic properties of deformation to create microstructural viscoplastic constitutive models (29,42-46). The constitutive models have become the most common in SPF modeling efforts of late, especially in the area of dental application (28,29) and Magnesium alloys (42,43). Due to the success of the recent constitutive models, research for SPF application in the automotive industry is slowly shifting the new work towards that of increasing the cycle times and decreasing the thinning during SPF. With this, work towards models with reduced microstructure components to permit faster R&D testing of new materials has come about (34). New hybrid forming techniques are being developed

such as deep drawing with SPF (47) and reverse bulging and moveable male die forming (48). With these hybrid techniques, researchers are hoping to determine a highly applicable means to implementing SPF in high production rate processes. On the other hand, other researchers as mentioned previously have been focusing efforts in obtaining and proving that material with microstructure in the sub-micron scale are capable of permitting forming strain rates in the order of industrial application rates around $1x10^{0}$ s^{-1} (8,49).

Though the research in SPF has shown much progress in the moving the process to industry, there are still many areas that need to be improved in. The Simulation models for today's materials from Titanium alloys to Magnesium alloys are clearly applicable as test after test is performed using both FE and Numerical software but the cost of material and post material forming properties are hindering the transition of SPF to a main stream process. Industrial researchers have expressed that the ability for SPF to fully integrate into the industrial realm lies primarily now in manufacturing cost and supply (50,51). The primary concern for the application of Magnesium alloys in cars today is the low rate of production. Currently, the world's rate of Magnesium alloy production is approximately 360,000 tons/year. That is with an average use of Magnesium alloys of 2 kg/vehicle. If the projected 100 kg/vehicle of Magnesium alloy use is reached in the future, an increase of annual production of 5,000,000 tons will need to be realized (52). This alone will be a major problem especially since the cost will need to be maintained or even reduced to compete with aluminum alloy use. The metals processing technology used for generating such alloys desired for industrial application is still that of the 1950's and 60's. With this, the cost of desired alloys is still uncompetitive resulting in the resistance of transition,

especially in the automotive industry. As for the post formed properties of SPF formed parts, initial research is just beginning to surface (53). The post forming properties are necessary for designers to create product designs that are safe and marketable. To accomplish such tasks, collaboration between industry and academia will be crucial if SPF is to be successful.

Many automotive researchers have published articles to provide a basis on where the current research efforts on SPF are at and the direction of future work (51,54-58). The work is driven by their needs to meet the Kyoto treaty and US fuel economy regulations which states that the world automotive industry must provide vehicles with fuel economy at least as good as 3 Liters/100 km (80 mpg). Currently, the use averages are 27.5 mpg (8.7 Liters/100 km) for cars and 20.5 mpg (9.8 Liters/100 km) for trucks (58). To do this, automotive manufacturer Ford is focusing on the application of more Aluminum and high strength low alloy (HSLA) steels formed by means of SPF (51). Other automotive researchers including Volkswagen, GM, and Toyota are looking to apply Magnesium alloys (54,55,58- 62) to lighten vehicles. Energy conservation is being approached in many ways with respect to vehicles. One long term direction is the goal to create a useable fuel source in Hydrogen since the theoretical by product is environmentally friendly water. Shorter versions of alternative fuel sources include electric-gas hybrids currently in production for small economy cars and diesel and ethanol generated from corn providing combustible fuels with less green house gas emissions. Though, currently in use, neither of the short term alternatives are beneficial enough to provide much relief in terms of the pollution control currently.

The automotive researchers mentioned above have all been providing studies and results of what is now felt to be the most promising solution to pollution reduction all based in the reduction of vehicle mass. Figure 11 describes the breakdown of the current energy consumption percentages for the entire life cycle of a vehicle from manufacture to recycling. The largest energy consumption section is the actual fuel burned during the time the vehicle is driven, which is of no surprise with the distances Americans travel every year by vehicle. Thus, the driving fuel consumption category was broken down further to permit researchers to understand what manufacturing changes will be most beneficial. With this breakdown, the fuel savings due to mass reduction while driving can be graphically estimated (61), which is presented in Figure 12.

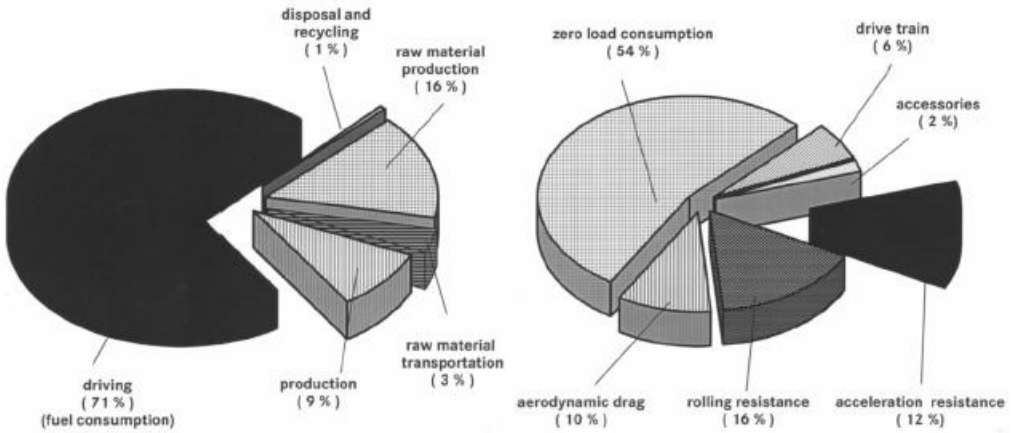

Figure 11 (a) Energy consumption during full life cycle (b) Impact of vehicle weight on total fuel (62)

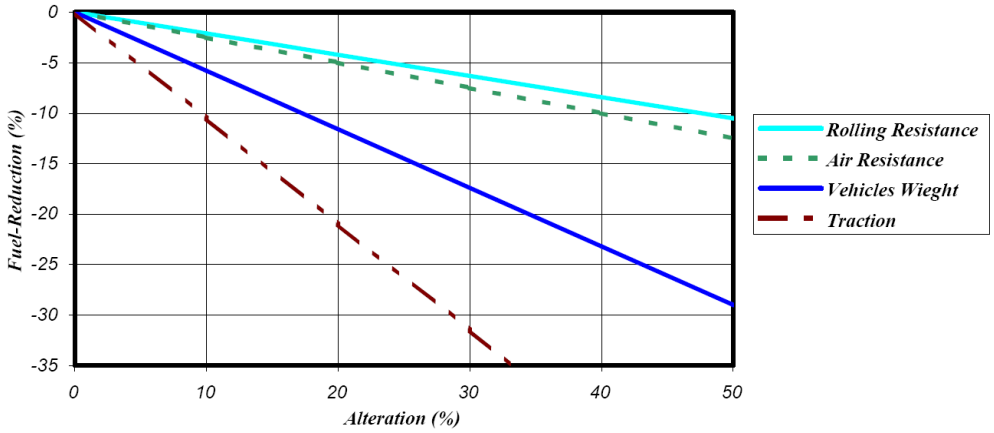

Figure 12 Means for reducing fuel consumption (61)

Figure 12 shows that a reduction of mass of 20 % is necessary to generate a decrease of almost 10% in fuel consumed by a vehicle. To actually generate such weight reductions, the material used for nearly the entire vehicle will need to be that of a small density. Fiber composites and Magnesium alloys would be capable of producing such reductions. It has been shown that an all-aluminum car would provide a weight reduction of 30 to 50% while further reductions would require Magnesium and plastic composites (62).

To accomplish the feat of fuel consumption reduction, magnesium use has been on the increase and material producers and manufacturers have been planning for and working towards the increase of Magnesium alloy use in industry. Dead Sea Magnesium and the Magnesium Research Institute are both examples of such efforts. Specifically between Volkswagen and Israeli (63).The primary Magnesium alloys manufactured are for die cast use. Such alloys are Mg AZ91, Mg AM 20, Mg AM 30, Mg AM 30, Mg AM 60, and Mg AE42 (64). The name signifies the primary alloying elements and the numbers stands for the nearest whole percent of the alloying agent. For example, AZ stands for Aluminum and Zinc, and AM stands for Aluminum and Manganese. For sheet metals currently being research, typical alloys are Mg AZ31, Mg AZ91, and Mg ZK60,

where ZK stands for Zinc and Potassium (22). The US government published an initial report in the early 1980's for the department of the Interior (22). The purpose was to determine how applicable magnesium alloys in wrought form would be for future industrial use. After this initial report, very little research was performed for wrought metal processing. Research was common for magnesium casting alloys due to their extensive use by Volkswagen just after World War II in the Beetle and then again with the establishment of the join Magnesium alloys research and production entities in Israeli (63).

With the results pointing to Mg AZ31 as the most formable Magnesium alloy (22), it was chosen by many researchers for formability and application research when Magnesium SPF research picked at the turn of the 21st century. Initial investigations of Mg AZ31 superplasticity began with the determination of the most effect way of material processing techniques. Extrusion properties of alloys from cast, rolled and extruded billets were re-extruded to evaluate recyclability and grain refinement properties in order to generate better superplastic characteristics (19,64,65).

After the work on material processing research, material properties began to be examined, usually in cohorts with the microstructure present prior to forming. Coarse-Grained Mg AZ31 sheet metal has been tested in uniaxial loading to examine the effects of grain size (5). It was concluded that the microstructure was rather irrelevant but it is important to know that the grain size of the SPF tests were between 130 μm and 320 μm. This size of microstructure was considered to be superplastic based on the results but grain sizes on the order of 10μm are generally necessary for superplasticity.

Wrought Magnesium formability was again the basis of several researchers who were trying to show that Mg AZ31 is formable whether at warm forming temperatures or SPF temperatures by applying deep drawing at elevated temperatures (47), rectangular pan shaped bulge formed samples (66), and boss forming which is similar to reverse extrusion for electrical applications (67). Until recently, very little formability results and SPF material properties had been examined. One of the first published works on SPF properties for uniaxial testing was for temperatures of 200 –500˚C but with constant cross head speeds (68). Though the work was the first, no description of gripping techniques were discussed or presented leaving the results to be considered as an intro to property testing. This is due to the slipping that is present with traditional gripping techniques, which was examined several years later (20). Desire to present constitutive material models for the Magnesium materials lead to an increase in material and deformation property analysis including the texture and cavitation development as well as the microstructural evolution, both static (during the preheat) and dynamic (during forming) (69-72). The uniaxial properties of Mg AZ31 between room temperature and 250 ˚C have been examined but primarily for the analysis of texture evolution (73). This did however provide a microstructural basis for the determination of grain boundary sliding as the deformation mechanism, though the formability of the material was absent. The formability of Mg AZ31 in the temperature range of 300 – 400 ˚C has been examined but at constant cross head velocity leaving the results segregated from the form desired results form for modeling and industrial analysis (72). Until the works performed by Dr. Abu-Farha and Dr. Khraisheh (9,20,21,43,53), there was no significant material property database for the SPF of Mg AZ31 in uniaxial deformation and for the modeling that

included the evolution of the microstructure and cavitation. With the material properties determined and microstructure evolution equations, a viscoplastic with microstructural evolution included material model was developed and validated (9,44). The simplified model generated is presented as equation 3.3.

$$\dot{\bar{\varepsilon}} = \frac{k}{d^p}\left[\frac{\bar{\sigma}}{(1-f_a)}\right]^{\frac{1}{m}} \qquad (3.3)$$

Where $\dot{\bar{\epsilon}}$ is the effective strain rate, $\bar{\sigma}$ is the effective stress, m is the strain rate sensitivity, d is the grain size k is a material parameter, p is the grain growth exponent and f_a is the fraction area of voids. This model was input to the FE Abaqus and used for modeling of pressure profiles in order to optimize the SPF of Mg AZ31 as well as determining the thinning distribution. One important modeling effort proceeded to evaluate the effect of grain size distribution differences in a SPF sheet prior to forming (74). A modeling with different grain sizes and the material flow stress properties associated with the different grain sizes was carried out and provided clear thickness distribution effects due to the starting grain sizes. The grain sizes were generated by friction Stir Processing work elsewhere (75) with their respecting uniaxial properties. Though the results were positive, they were only modeling predictions, no experimental evidence was provided. Several other researchers have also studied the effect of grain size on the superplastic formability of SPF materials. The effect of a microstructure gradient on a Zn 22% Al alloy in bulge forming has been experimentally examined but with nominal success (76). Selectively heat treated Ti-6Al-4V tensile and bulge form specimens with a step shaped die were attempted as well (77). Though the results did show physically a deformation localized in the tensile neck area selectively heated, the heat treatments were too rapid to permit selective grain growth thus resulting in unsatisfactory results. Clear evidence of grain size

influences in uniaxial SPF of an Yttria-stablilized tetragonal Zicronia polycrystal has been provided (78). The microstructure tested was between 0.3 μm and 1.8 μm and showed a tremendous variation in flow stress, ultimate stress and ductility for the Zicronium crystal.

Work on the dependence of the random microstructural gradients generated from material rolling processes used to produce sheet materials has also produced interesting modeling results (79,80). The results did show significant modeled ductility and stress effects but the only way to control such distributions is with Friction Stir Processing do to the non–ideal deformation that occurs during the rolling process. But Friction Stir Processing has been proved to be capable of generating controlled microstructure sizes by adjusting the rotational speeds (75,81- 83). The only other work with thickness distribution control consists of either modeling of microstructure size differences without experimental validation (84,85) of initial thickness profiling by machining a blank to a specific thickness profile before forming (86). This leads to the basis of the work that follows.

Thickness control is crucial for SPF due to the large amounts of deformation that the sheets are subject to. Currently, the solution is to start with a thicker sheet than desired so that the final thickness in the most stretched area of the sheet is of the desired thickness. As discussed above, there has been work published for methods of thickness control. One of the most successful published works to date involved the idea of machining a thickness profile but produces undesired material waste and would require large milling machines that are not of economical means in industry (86). Friction Stir Processing would be another possibility but much research needs to be performed yet in

developing models for resulting grain sizes with respect to processing parameters so that FE analysis can produce necessary processing paths for the materials used. This will also require work to acquire material properties for each resulting microstructure at different processing parameters. With this information, it might be possible to apply Friction Stir Processing to sheets prior to SPF one day, but again, Friction Stir Processing equipment of the necessary scale would be expensive and difficult to prove economically favorable. Finally, Selective heating is a possible route to the desired microstructure for SPF sheets and may possibly be much more economically favorable if proper research is performed to demonstrate the applicability of UV light, plasma, induction heating, and even laser equipment available and much more portable and adjustable than milling machines or Friction Stir Processing machines.

To accomplish such a task, a logical order of research is necessary and is laid out in the following chapters of work in this report.

CHAPTER 3 AZ31 Mg ALLOY STATIC GRAIN GROWTH

Overview

Static grain growth is the third stage of annealing. Annealing is the heating of a material for an extended period of time typically to relieve internal stress or to homogenize the materials microstructure. The three stages of annealing a metal are recovery, recrystallization and static grain growth. Before a material will experience static grain growth recovery and recrystallization must occur. Recover is when energy applied to the material is used for initial defect and stress releasing. If the energy input is large enough, clusters of material defects such as dislocations and grain boundaries permit the nucleation of new grains to minimize the energy state of a material (87). Once recrystallization is complete, the energy consumed by the metal will be transferred to static grain growth which is the growth of the grain size by the movement of the grain boundaries away from the center of the grains. During the static grain growth period, smaller grains will be consumed by the larger grains and after a long enough period, grain size distributions that may be present after mechanical deformation such as rolling and extrusion will dissipate to a more uniform microstructure.

"Physical Metallurgy Principles" 3rd Edition (87) provides a section of the theoretical basis for describing static grain growth. The first explanations were based on 2-D soap bubble analysis and how the bubbles grow eventually into a single bubble. It was proposed that the change in the size of the soap bubbles was proportional to the curvature of the soap bubbles. And the curvature of the soap bubbles of course are inversely proportional to the diameter, thus the theoretical ideal growth rate of the

diameter of the grain size was concluded to be that of equation 4.2 which was derived from equation 4.1.

$$\frac{dD}{dt} = \frac{k}{D} \tag{4.1}$$

$$D^2 - D_o{}^2 = kt \tag{4.2}$$

Where K is the grain growth constant D is the grain size diameter. Though equations 4.1 and 4.2 were based in the theory of radius growth with respect to the energy required to increase the boundary size, experimental evidence, including what will be shown below, does not fit to such a simple mathematical description. The most commonly used model currently is that of equation 4.3.

$$D = kt^n \tag{4.3}$$

Where n is the grain growth constant and k is accepted as the typical activation energy constant. But a very important property of equation 4.3 is that n is always a radium function of temperature and the activation energy is never determined to be a single value on a repeated basis. Table 1 provides a collection of n and K values experimentally determined for several material values from literature and this work that will be present to be fully described below.

The purpose of this static grain growth work is based on the desired outcome of this work. As discussed earlier, the thinning that SPF materials encounter after forming are large due to the extensive plastic deformation that a material under goes when forming. This work is on the use of controlled grain growth to reduce thinning of Mg AZ31B H24 during forming and possibly determining if increased forming rates might be possible.

Table 1 Static grain growth exponent and constant for several materials

Material	Temperature (K)	n	K ($\mu m^n sec^{-1}$)
Zn-22%Al (88)	495	4.8	$3.4x10^{-5}$
	472	4.7	$1.0x10^{-5}$
	523	4.9	$1.1x10^{-4}$
Ti-6Al-4V (88)	1200	4.8	$1.0x10^{-3}$
	1223	3.2	$2.4x10^{-1}$
Fe-25.7Cr-6.6Ni (88)	1273	4.5	$4.4x10^{-1}$
Sn-Bi (88)	293	2.0	$8.6x10^{-5}$
Mg AZ31B H24	498	1.6	$4.0x10^{-1}$
	573	1.2	$5.4x10^{-1}$
	648	1.1	$6.5x10^{-1}$
	723	0.5	$1.3x10^{0}$

Due to the dependence of SPF on a materials microstructure, grain size has been shown to alter a materials flow stress and ultimate stress as mentioned above. Attempts to use this property have also been discussed above, but as mentioned, little significant success has occurred to date for the Zn 22% Al and Ti-6Al-4V alloys tested. In this work, the alloy chosen has been a Magnesium alloy due to its importance to the automotive industry. Titanium alloys are primarily used for aerospace applications which are low production, large margin products so this type of work is not over whelmingly important. Also, static grain growth in Titanium alloys is bit more difficult due to the multiple phases that exist. But since Magnesium is the hopeful structural alloy that will permit the automotive industry to reduce the mass of vehicles in order to reduce green house gas emission, the amount of material that would be used if ever economical will be very important and thus simply increasing the thickness of the sheets to be formed will not be the most desirable choice. Thus, with Mg AZ31B H24 being a single phase and low

melting alloy, controlled static grain growth should be more realizable and applicable. Table 2 provides the composition of Mg AZ31B H24.

Table 2 Element breakdown for Mg AZ31B

Element	Mg	Al	Zn	Mn	Si	Fe	Cu	Ni
Percentage (%)	95.27	3.29	0.991	0.412	0.028	0.0041	0.004	0.0007

Experimental Procedure

The ASM Handbook volume 2 (89) presents the recrystallization temperature of Mg AZ31B H24 alloy as 300˚C. So, for the static grain growth experimental work, four temperatures were chosen between 225˚C and 450˚C. The annealing times for the material varied from 15 minutes to 24 hours to provide contour plot for later use in selective heating and SPF research. Table 3 is the experimental matrix used for this part of the research. In Table 3, "+" are the annealed samples that were used to generate the annealing curves while "-" stand for the annealed samples that were not used due to the lack of available accurate equipment (15 min 225˚C), mounting or etching problems (15 min 375˚C, 30 min 300˚C, 90 min 375˚C and 450˚C, etc.), and optical analysis or time requirements (150, 165, 210, 300 min etc.).

The Magnesium AZ31B H24 samples annealed were cut to a size of approximately 10mm x 20mm. Specimens annealed at 225˚C and 300˚C were heated in a furnace while the 375˚C and 450˚C specimens were heated in an electrical resistance heating (*environmental*) chamber that provides a maximum temperature of 610 *ºC*, maintaining a temperature variation of ±1 ºC. After annealing, 3 specimens of sheet thickness 1.07 mm and 2 of sheet thickness 3.22 mm were mounted for polishing in EPOAR resin and EPOES epoxy from Struers which was a cold mounting set up.

Table 3 Annealing Experimental Matrix

		Temperatures (˚C)			
		225	300	375	450
Time (min)	15	-	+	-	+
	30	+	-	+	+
	45	+	+	+	+
	60	+	+	+	-
	75	+	+	+	+
	90	+	+	-	-
	105	-	+	-	-
	120	-	-	+	+
	135	-	+	-	-
	150	-	-	-	-
	165	-	-	-	-
	180	+	-	+	+
	210	-	-	-	-
	240	+	+	-	+
	270	-	+	-	-
	300	-	-	-	-
	330	-	-	-	-
	360	+	+	+	+
	390	-	-	-	-
	420	-	-	+	-
	450	-	-	-	-
	480	+	+	+	+
	540	-	-	-	-
	600	-	-	+	+
	660	-	-	-	-
	720	+	+	-	+
	1440	+	+	+	+

Sample preparation for microstructural examination was carried out according to the ASM standard procedures, ASM Handbook 1999 (89). After several grinding thence polishing steps, Acetic Picral was used to etch the samples, in order to reveal its microstructure. The microstructure was analyzed by optical microscopy. The grain size for the as received and selective heating experiment specimens were determined using the mean

linear intercept method. A magnification of 1000x was used for as received specimens, 500x was used for all selective heating specimens and 625x was the magnification used to generate the static grain growth curves presented below.

Results

Figure 13 through Figure 17 are pictures of the microstructure of Mg AZ31B-H24 received from Thyssen Krupp Cooper Division Copper and Brass. Figure 13 is an image of the as received Mg AZ31B alloy at 500x magnification. With this image, it is clear that the microstructure is still stressed with twinning and abnormal shaped. The same microstructure is shown in Figure 14 at 1000x revealing the microstructure more clearly and the large variation of grain size within the sheet. The variation of grain sizes is one of the most important properties of sheet metal when attempting to understand static grain growth and selective heating for such work. When fitting the grain growth data, the large grain size variations lead to fit curves with poor R^2 fit results. This also makes it difficult to provide confident selective static grain growth results because you must rely on the accuracy of a single specimen for optical measurements when determining grain size gradients later in chapter 5.

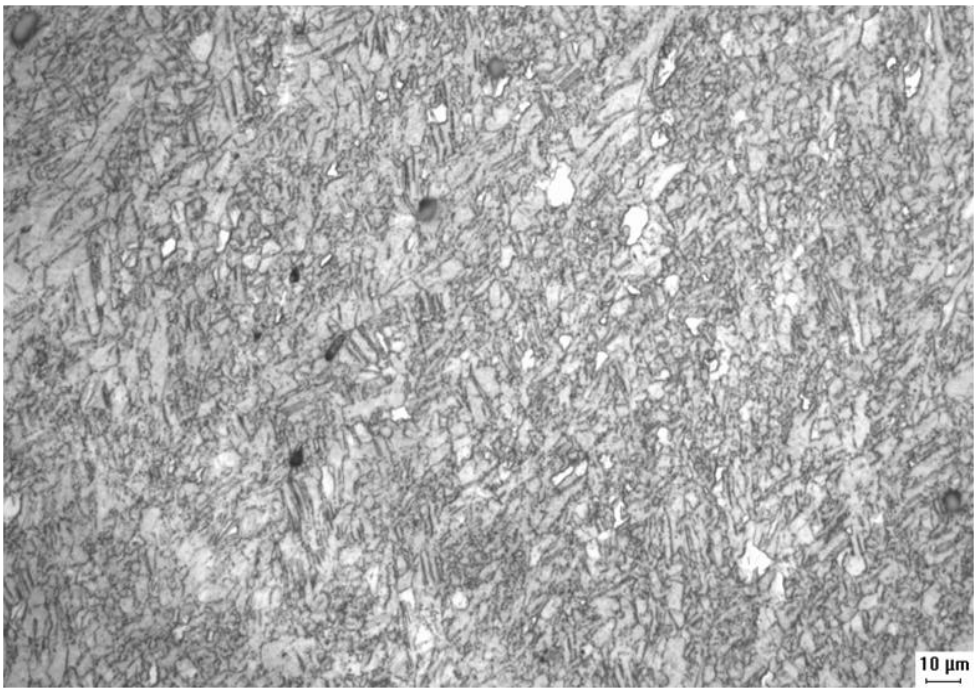

Figure 13 Optical image of AZ31B Mg Alloy As received from commercial supplier at 500 times magnification

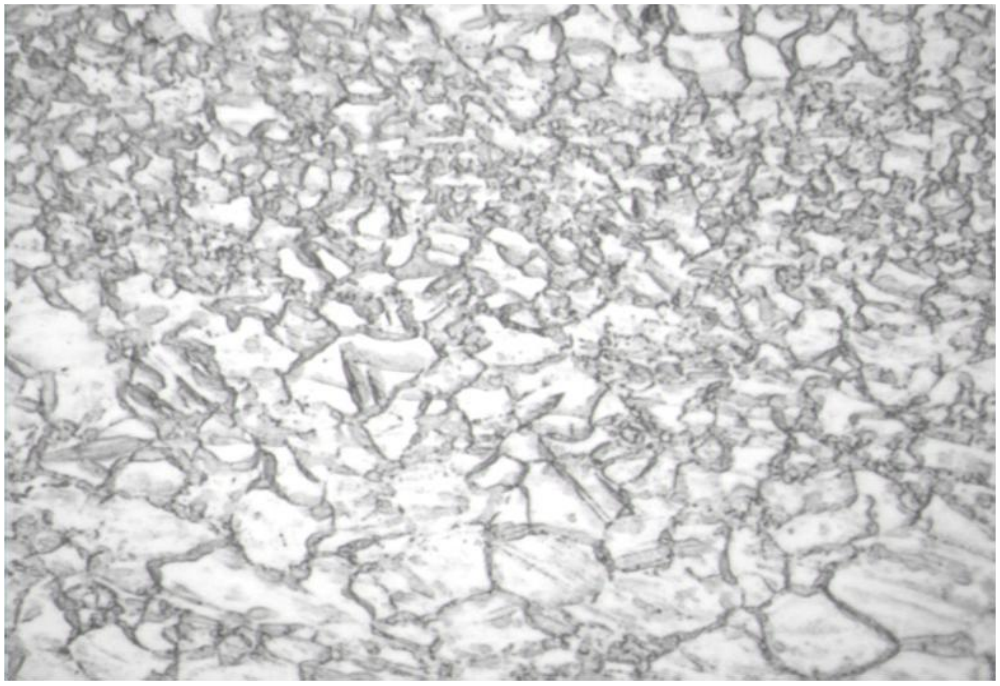

Figure 14 Optical image of AZ31B Mg Alloy As received from commercial supplier at 1000 times magnification

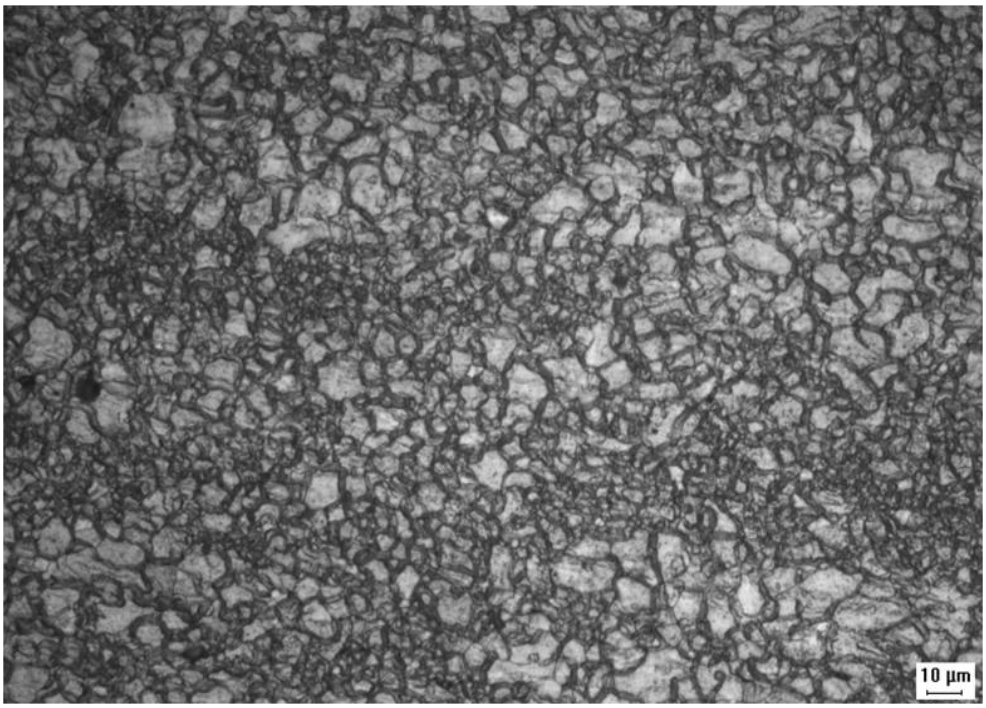

Figure 15 Optical image of AZ31B Mg Alloy annealed at 225˚C for 30 minutes at 500 times magnification

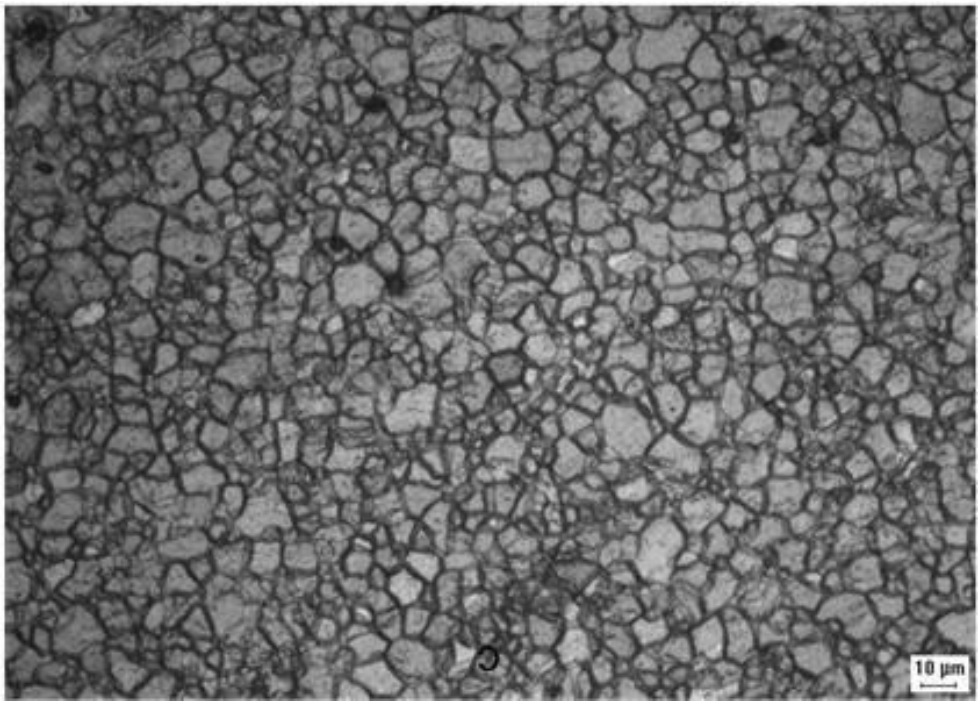

Figure 16 Optical image of AZ31B Mg Alloy annealed at 225˚C for 90 minutes at 500 times magnification

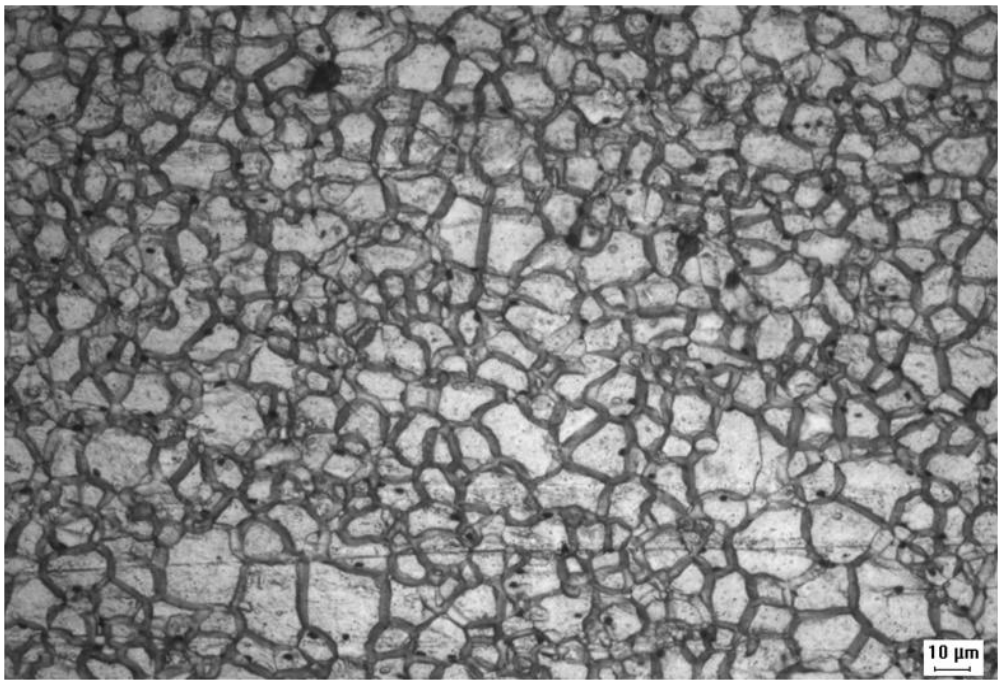

Figure 17 Optical image of AZ31B Mg Alloy annealed at 225˚C for 720 minutes at 500 times magnification

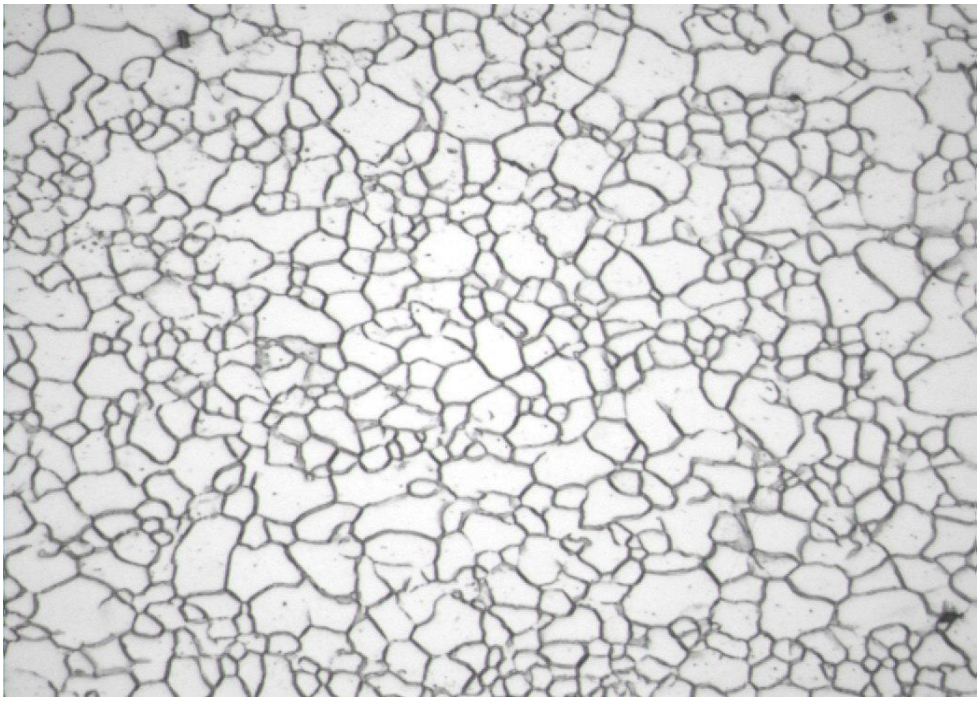

Figure 18 Optical image of the Mg AZ31 Sample annealed for 60 minutes at 225˚C. Image was taken with 625x magnification and is an example of those used to generate fit curves from Ecole des Mine d'Albi Carmuax in Albi France

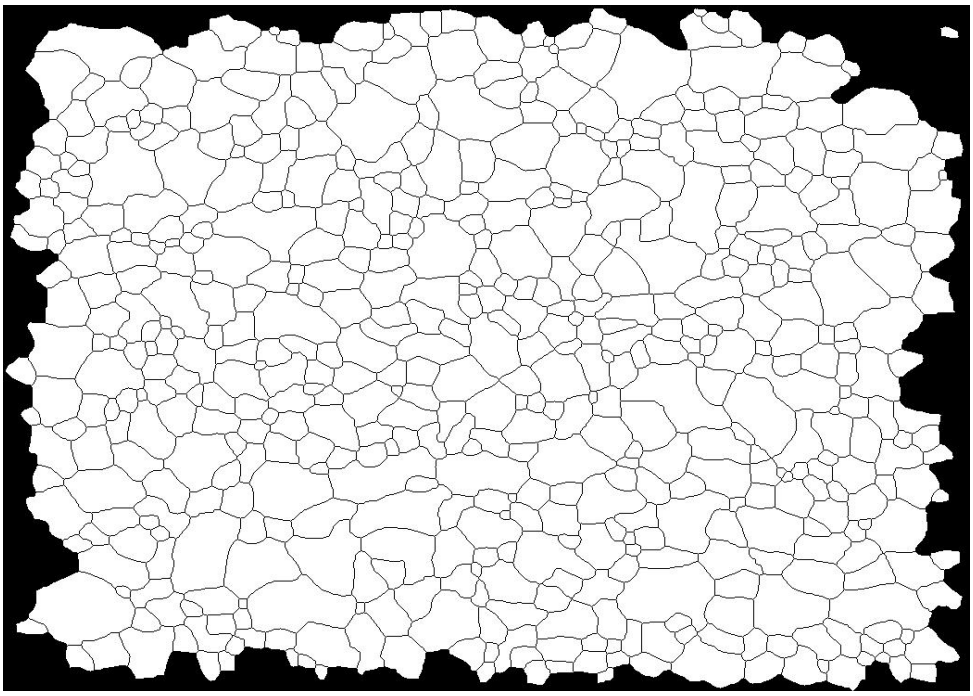

Figure 19 Digital representation of the image in Figure 18 generated from a Macro software for computer aided grain size measurement from Ecole des Mine d'Albi Carmuax in Albi France

Figure 18 is an example of an image taken at 625x magnification for the use of the static grain growth curves presented below. To generate the fits below, 10 pictures from each specimen marked in Table 3 as used for the annealing experiment were acquired and analyzed by a program called Aphelon 3.2. The software generated digital representations of the microstructure in the images by reconstructing the images using color gradients to determine boundaries as shown in Figure 19. After the images were regenerated, the software generated statistical data for each complete grain in the image by the pixel maps of the images and tabulating the information in a text document. The information was then imported into Microsoft Excel© and combined to generate the overall averages for each specimen. The results were then plotted for modeling and best fit purposes for late use in Chapters 4 and 5.

Figure 20 through Figure 27 are the fit plots for each temperature and sheet thickness. As can be seen from the figures, the fits are marginal due to the large variation in grain size mentioned above and shown in Figure 14 but do show rather consistent logarithmic trends. The grain growth exponents and constants vary greatly between temperature and sheet thickness for each trial. This is due to the complexity of annealing and microstructure and the inability to theoretically describe what occurs by equations 4.1 and 4.2. There are not even trends for the exponent and constant values that are functions of temperature as seen in Table 1. This leads to the determination that the static annealing curves are entirely material models based in the theory of static grain growth. The figures were combined into two 3-dimensional curves.

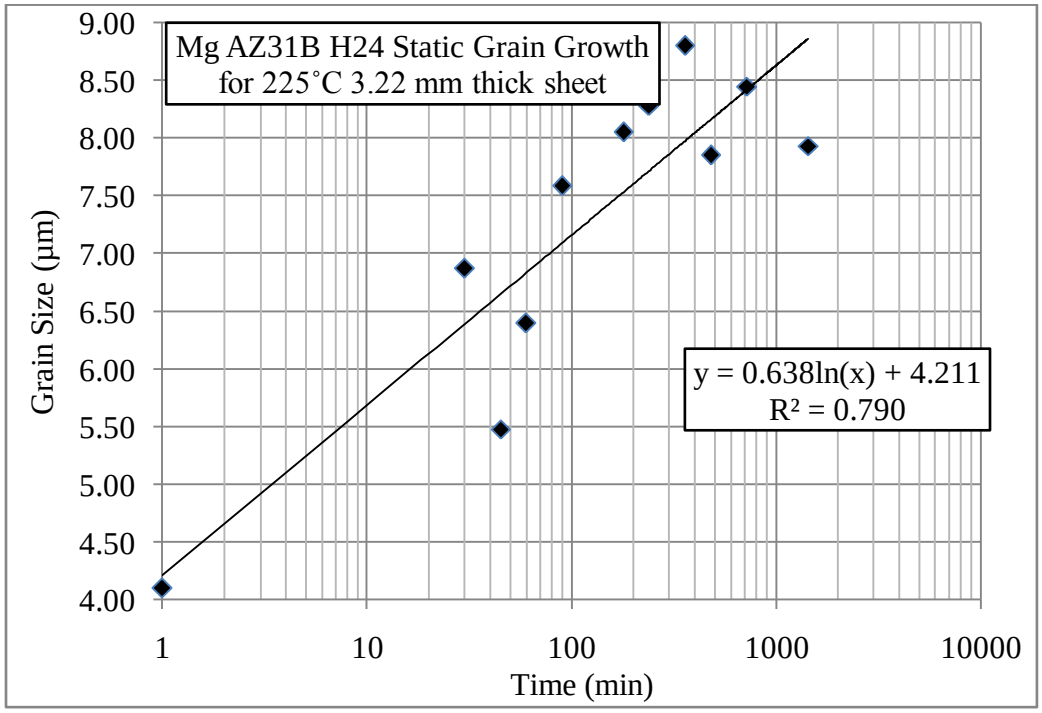

Figure 20 Logarithmic fit for Mg AZ31B annealing at 225˚C for the sheet thickness of 3.22 mm

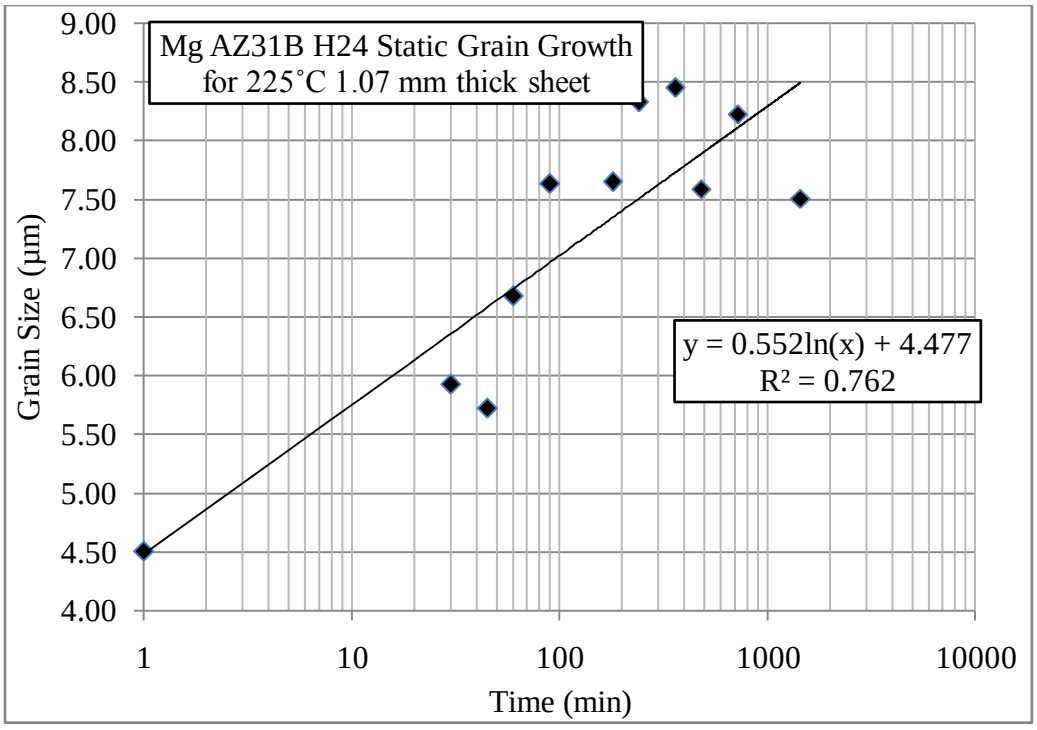

Figure 21 Logarithmic fit for Mg AZ31B annealing at 225˚C for the sheet thickness of 1.07 mm

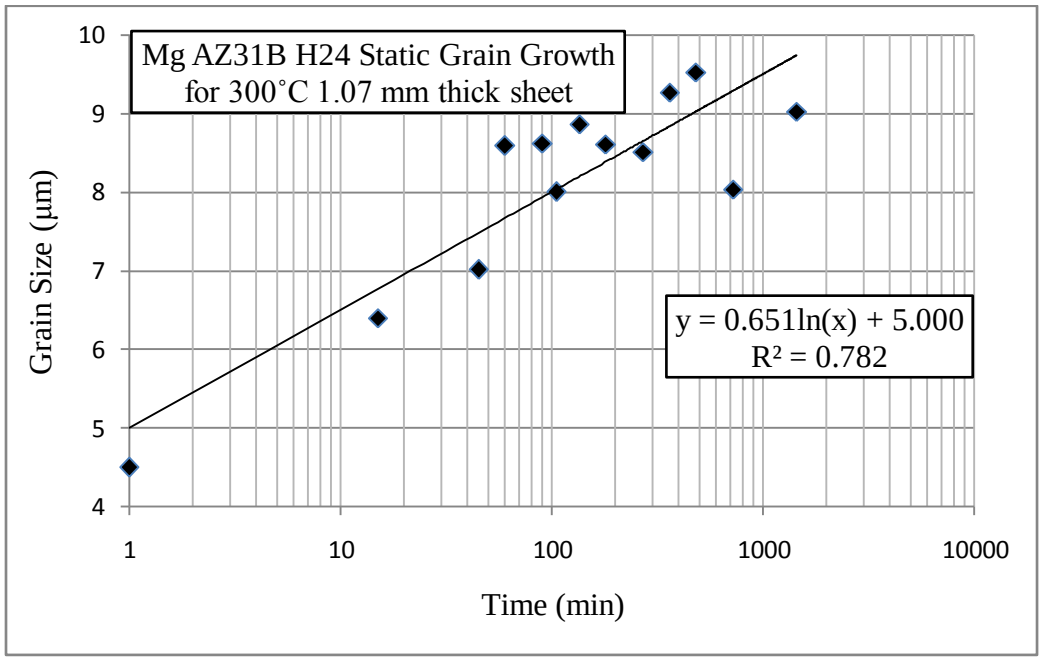

Figure 22 Logarithmic fit for Mg AZ31B annealing at 300˚C for the sheet thickness of 1.07 mm

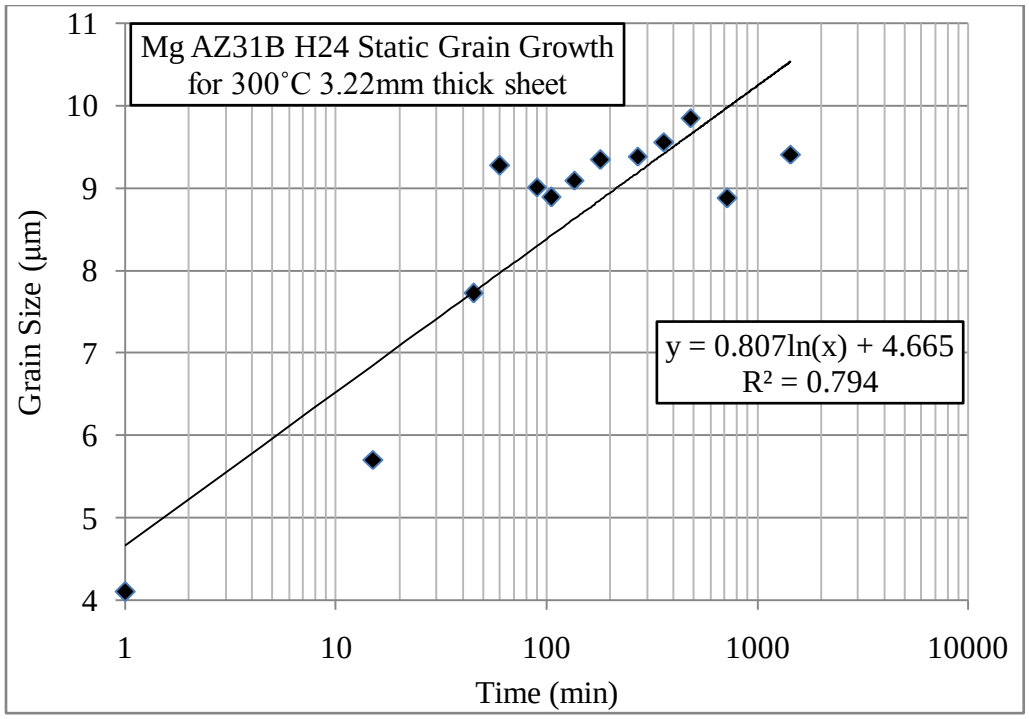

Figure 23 Logarithmic fit for Mg AZ31B annealing at 300˚C for the sheet thickness of 3.22 mm

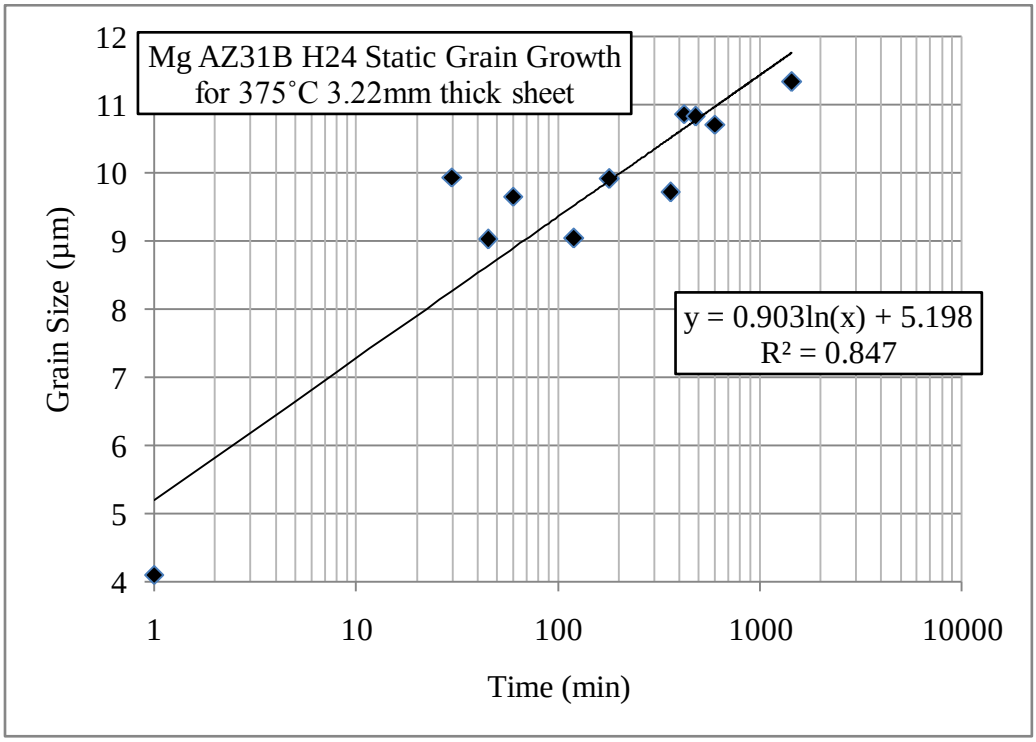

Figure 24 Logarithmic fit for Mg AZ31B annealing at 375˚C for the sheet thickness of 3.22 mm

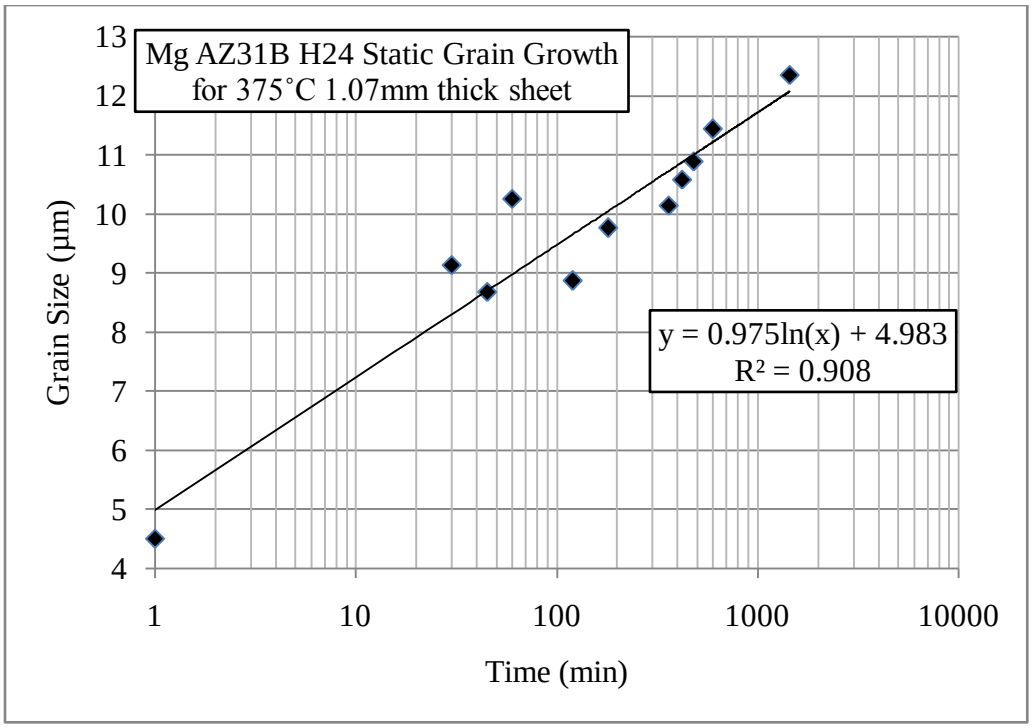

Figure 25 Logarithmic fit for Mg AZ31B annealing at 375˚C for the sheet thickness of 1.07 mm

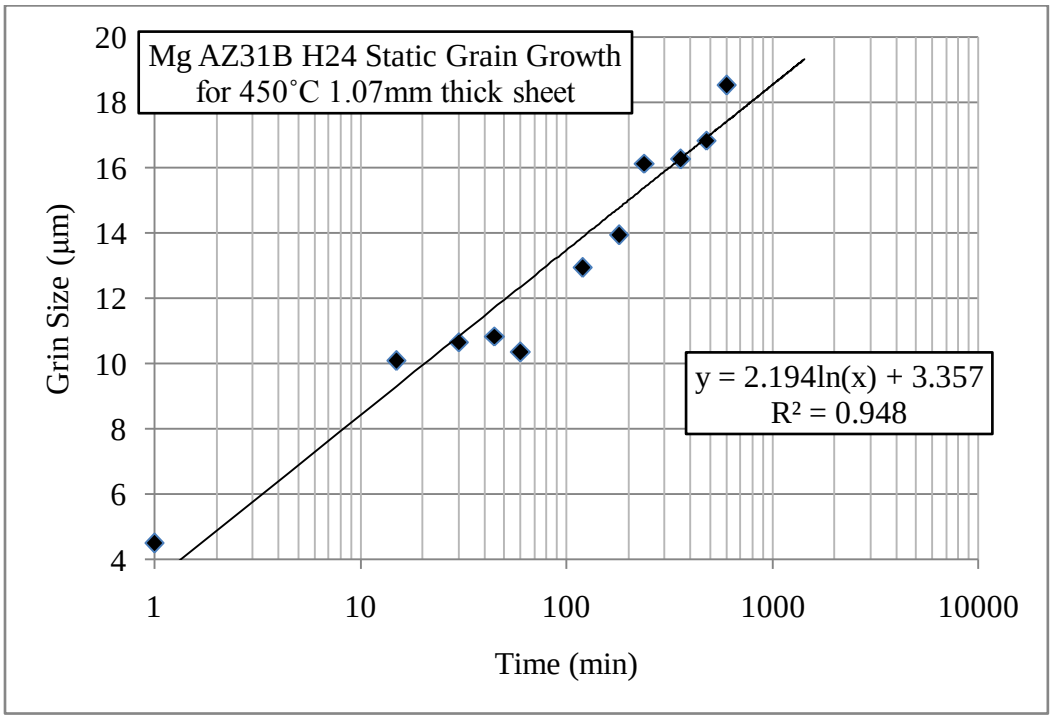

Figure 26 Logarithmic fit for Mg AZ31B annealing at 450˚C for the sheet thickness of 1.07 mm

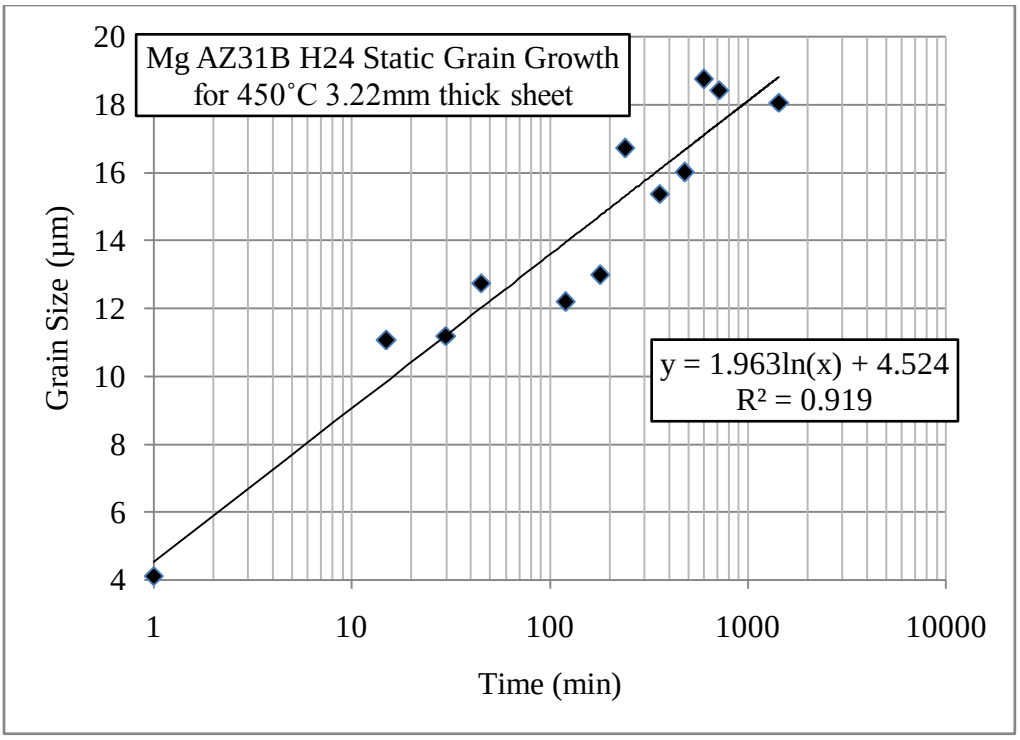

Figure 27 Logarithmic fit for Mg AZ31B annealing at 450˚C for the sheet thickness of 3.22 mm

Figure 28 and Figure 29 are the contour plots that were generated with the linear fit models above. With the 3-D contour plots, controlled experiment designs can be generated for selected heating experiments and application if the experiments are proven successful. But more importantly, the Contour plots can be used to control the grain size of SPF uniaxial tests presented in chapter 4, which is extremely necessary to produce a repetitive system for analysis in SPF annealing analysis and selective heating. Finally, if selective heating were ever to become used in industry, plots such as those below will be necessary due to the undesirable and unreasonable time required to examine microstructure of materials. Industry would never accept application with continual microstructure examination due to such costly measures with respect to time requirements.

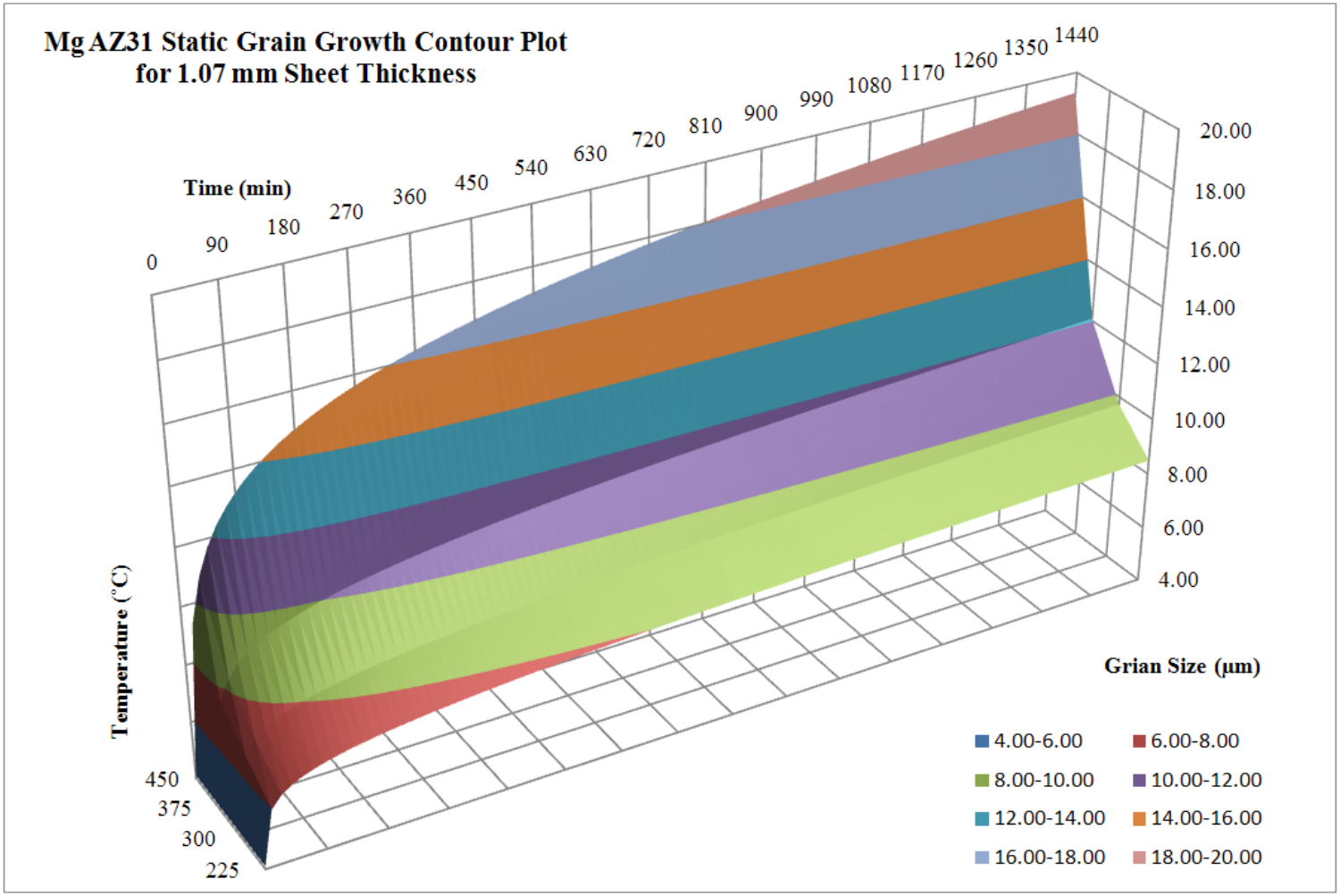

Figure 28 3-Dimensional static grain growth contour plot for the sheet thickness of 1.07mm of an Mg AZ31B-H24 alloy

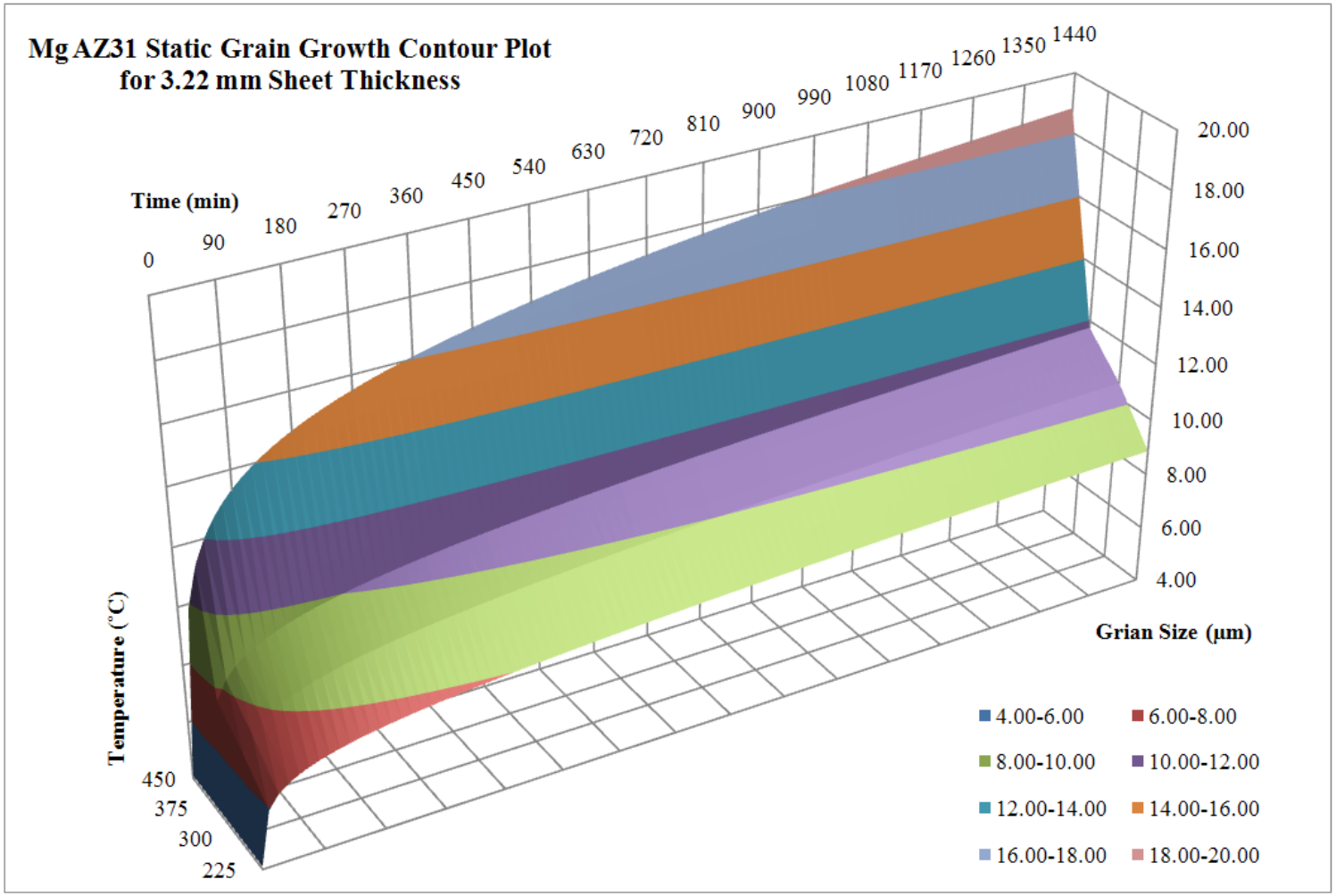

Figure 29 3-Dimensional static grain growth contour plot for the sheet thickness of 1.07mm of an Mg AZ31B-H24 alloy

CHAPTER 4 UNIAXIAL SPF

Overview

Selective microstructure gradients in SPF Mg AZ31 sheets are desired to determine the feasibility of their deformation properties in minimizing thinning while forming. In chapter 4, static grain growth curves were generated for the use in determining the desired annealing times in an attempt in controlling grain size. Chapter 5 provides an initial investigation of the effects of annealed grain size on the flow stress, ultimate stress and ductility of Mg AZ31 in uniaxial SPF. The experimental matrix for the investigation is based on the results of Abu-Farha and Khraisheh (2007) (21) who have provided a complete examination of the uniaxial properties of Mg AZ31 and determined the optimized SPF temperature for ~4.0 μm (non-certified) Mg sheet metal as processed by the mills.

A complete experimental analysis, design and explanation of the experimental set up used for the SPF uniaxial experiments is provided by Abu-Farha and Khraisheh (2007) (9). The work presented here is a summary to provide a brief background. For uniaxial testing at elevated temperatures, gripping is a major problem, to which several researchers have provided observations and techniques (9,34). The set up chosen here is due to the use of the same facilities as that of Dr. Fadi Abu-Farha and Dr. Marwan Khraisheh. Dr. Abu-Farha examined the slippage problem, and designed a tensile grip setup to which is shown in Figure 31. The grips are designed to pull the tensile specimens by their edge while clamped together through the center of the grip area to minimize the flow from the grip area into the gauge area.

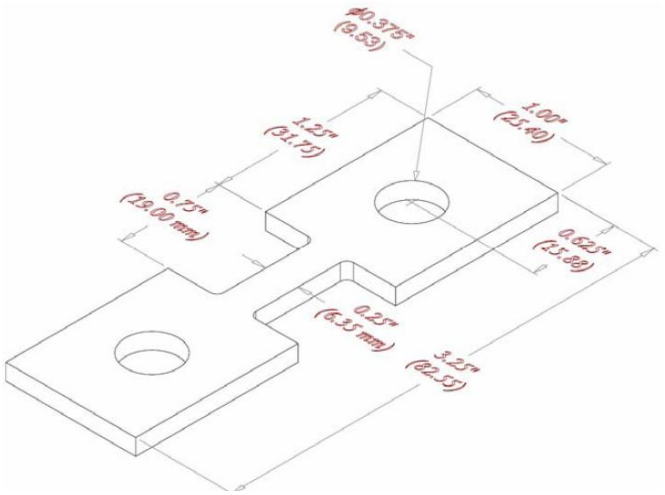

Figure 30 Tensile specimen geometry (9)

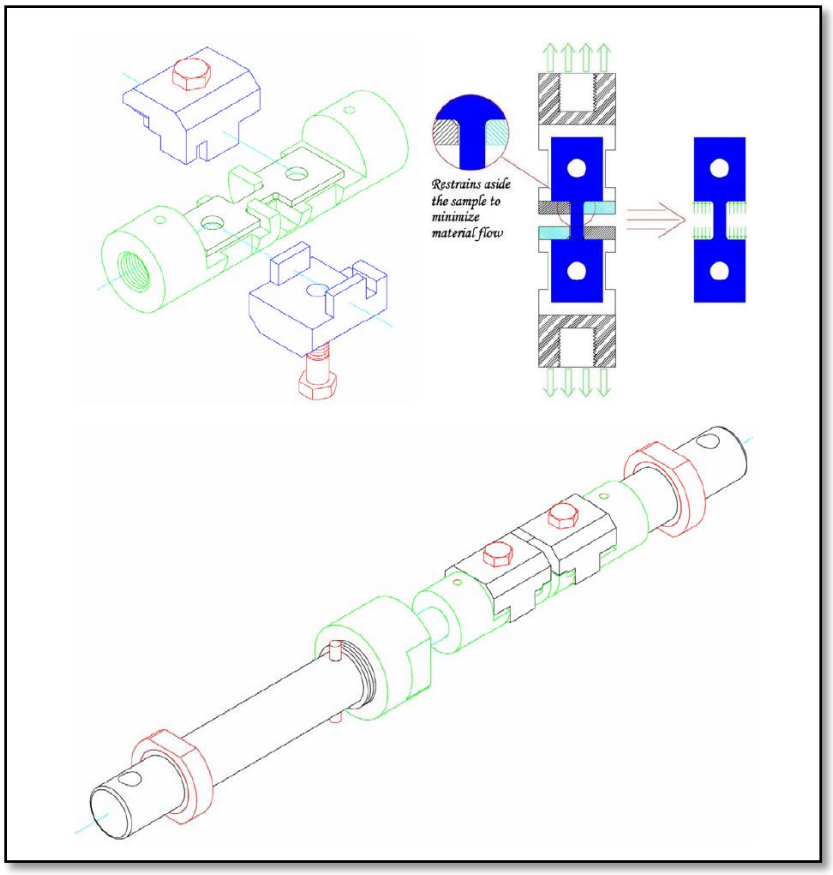

Figure 31 Tensile specimen gripping for SPF testing of Mg AZ31 (9)

Figure provides the geometry of the tensile specimens used in this work. A very important parameter that was determined by Abu-Farha (2007) was the results of a preheat test to determine the time required for the tensile system to achieve thermal equilibrium. It was concluded for the experimental setup to be used that there was a need for at least 65 minutes of preheat time for the system to reach thermal equilibrium. This results in static grain growth prior to experimental examinations that must be included in such work that revolves around grain size and its effects.

For direct comparison, uniaxial tests at constant strain rates $1.0x10^{-2}$ s^{-1}, $2.5x10^{-3}s^{-1}$, $5.0x10^{-4}$ s^{-1} and $1.0x10^{-4}$ s^{-1} were conducted to examine stress and ductility. In addition strain rate jump tests between strain rates of $2.5x10^{-3}$-$5.0x10^{-3}$ s^{-1} and $2.0x10^{-4}$-$5.0x10^{-4}$ s^{-1} were performed to generate strain rate sensitivity comparisons. Table 4 provides a test matrix that includes the annealing temperatures, times, and constant strain rate tensile tests.

Results

The results of the tensile tests are presented in the stress versus true strain plots in Figure through Figure . The darker blue curve in each of the figures is the results determined by Abu-Farha (2007) (2) and is used to provide the basis for what type of property shifts occur due to annealing. As can be seen, the ductility decreases with annealing which is to be expected due to the increase in grain size. This is also shown in Figure which presents % elongation versus strain rate for the 4 strain rates examined and the two annealing times versus that of the as received. At lower strain rates, the ductility of the annealed specimens decreased more due to the extended amount of dynamic grain growth that occurs. The dynamic grain growth is very important due to the direct link to the

deformation mechanism which is Grain Boundary Sliding (GBS). In GBS, the amount of grain boundary surface area influences the amount of deformation and as the grain boundary surface area decreases, so does the ductility in materials that are GBS dependant. For the annealed specimens, the ultimate stresses are sizably larger due to the static grain growth head start initialized by annealing. The ultimate stresses for both the annealed specimens and those for the as received are presented in Figure. Figure provides the flow stress results and the impacts of annealing which are similar to that of the ultimate stresses discussed above.

Table 4 Experimental matrix for uniaxial SPF analysis of the effects of annealing on SPF properties at 400˚C

			Annealing Time (min)							
			30				60			
Annealing Temperature (˚C)		Predicted Grain Size (μm) by Static Grain growth curves	7.35				7.81			
	300	Grain Size (μm) Measured	6.94	After Tensile Specimen Preheat to 400˚C testing temperature from 23˚C		8.89	6.89	After Tensile Specimen Preheat to 400˚C testing temperature from 23˚C		7.91
		Stress-Strain Strain rates	1.0×10^{-2}	2.5×10^{-3}	5.0×10^{-4}	1.0×10^{-4}	1.0×10^{-2}	2.5×10^{-3}	5.0×10^{-4}	1.0×10^{-4}
		Strain Rates for Jump Test	2.5×10^{-3} - 5.0×10^{-3}		2.0×10^{-4} - 5.0×10^{-4}		2.5×10^{-3} - 5.0×10^{-3}		2.0×10^{-4} - 5.0×10^{-4}	
		Predicted Grain Size (μm) by Static Grain growth curves	11				12.4			
		Grain Size (μm) Measured	9.32	After Tensile Specimen Preheat to 400˚C testing temperature from 23˚C		10.32	10.01	After Tensile Specimen Preheat to 400˚C testing temperature from 23˚C		10.32
	450	Stress-Strain Strain rates	1.0×10^{-2}	2.5×10^{-3}	5.0×10^{-4}	1.0×10^{-4}	1.0×10^{-2}	2.5×10^{-3}	5.0×10^{-4}	1.0×10^{-4}
		Strain Rates for Jump Test	2.5×10^{-3} - 5.0×10^{-3}		2.0×10^{-4} - 5.0×10^{-4}		2.5×10^{-3} - 5.0×10^{-3}		2.0×10^{-4} - 5.0×10^{-4}	

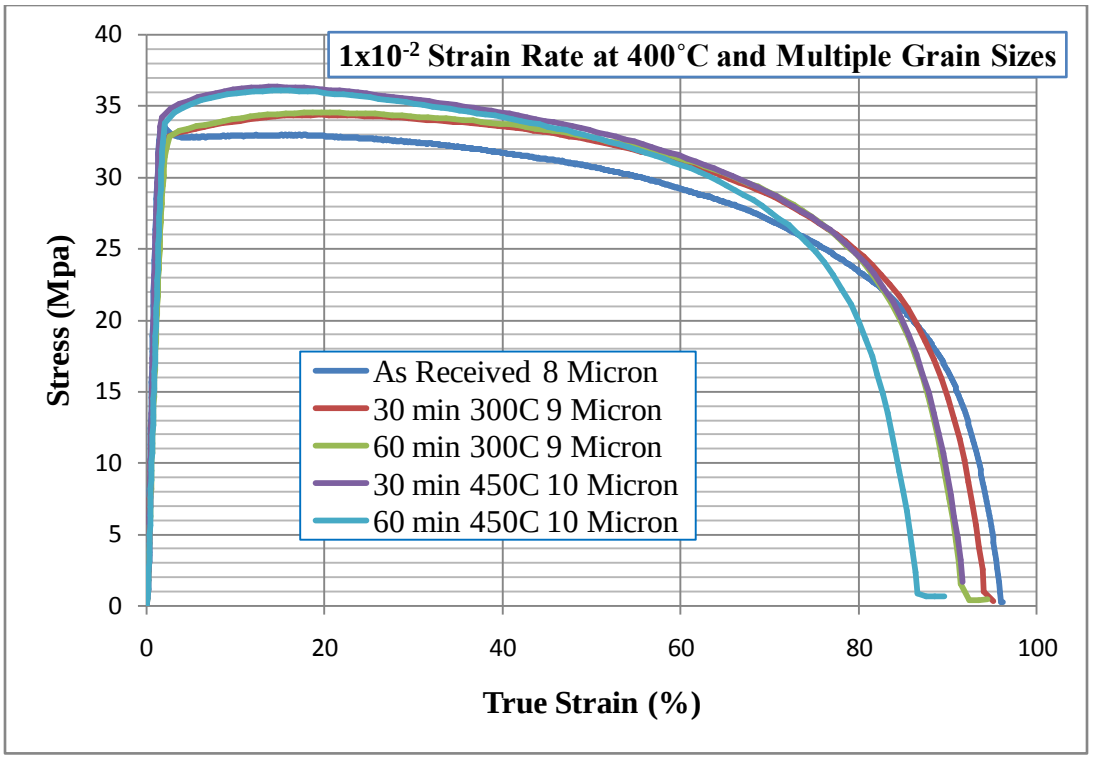

Figure 32 Stress Strain results for a strain rate of $1.0x10^{-2}$ s^{-1} at 400˚C

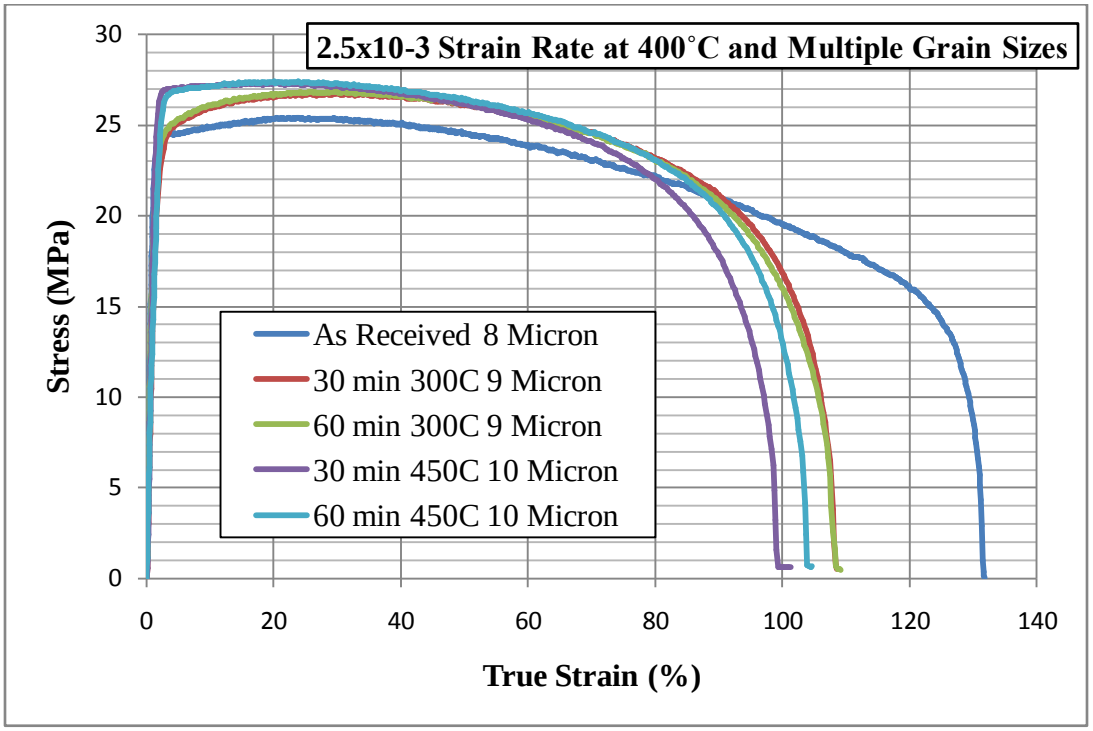

Figure 33 Stress Strain results for a strain rate of $2.5x10^{-3}$ s^{-1} at 400˚C

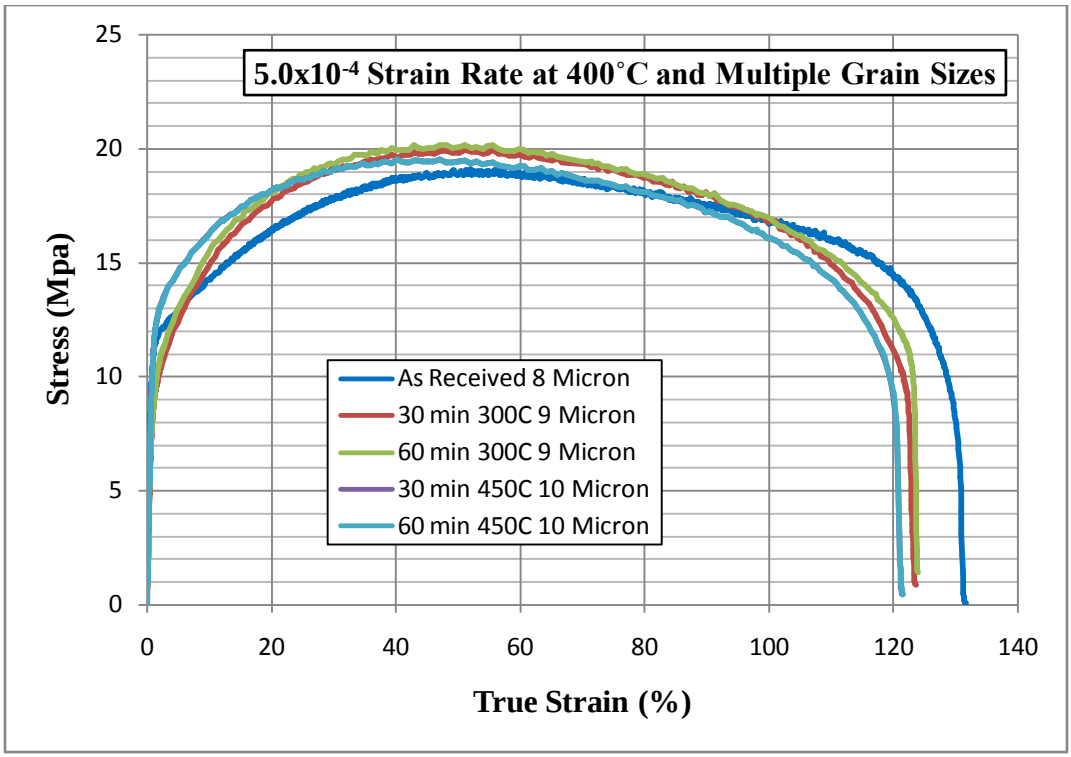

Figure 34 Stress Strain results for a strain rate of $5.0x10^{-4}$ s^{-1} at 400˚C

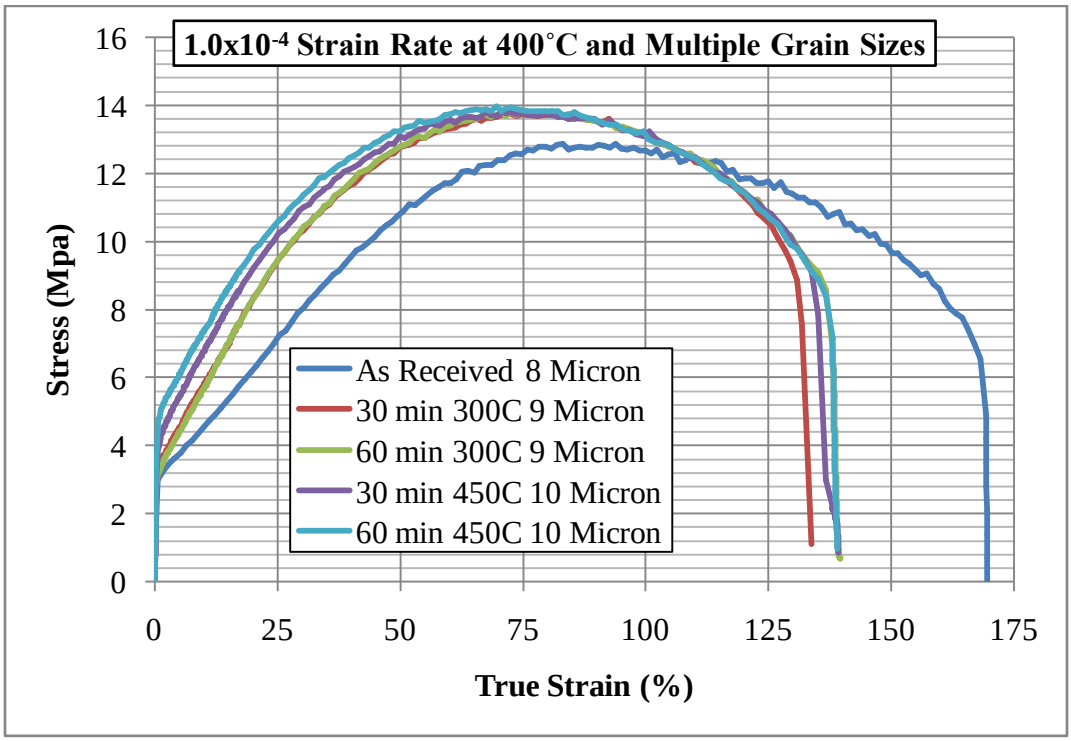

Figure 35 Stress Strain results for a strain rate of $1.0x10^{-4}$ s^{-1} at 400˚C

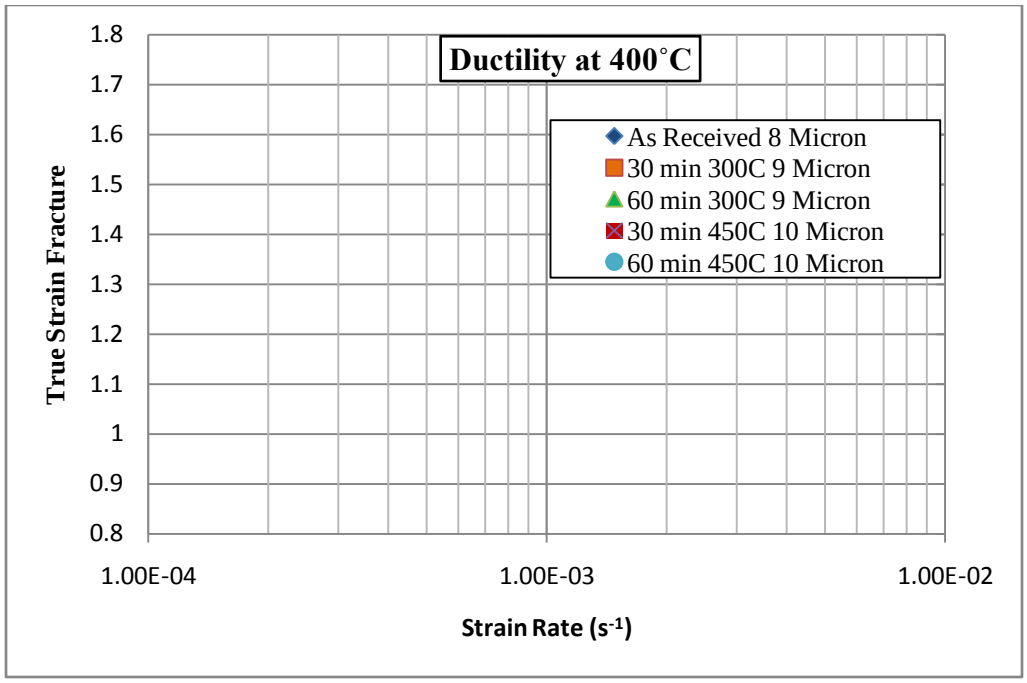

Figure 36 Superplastic Ductility for annealed Mg AZ31B alloy with respect to strain rate at 400˚C

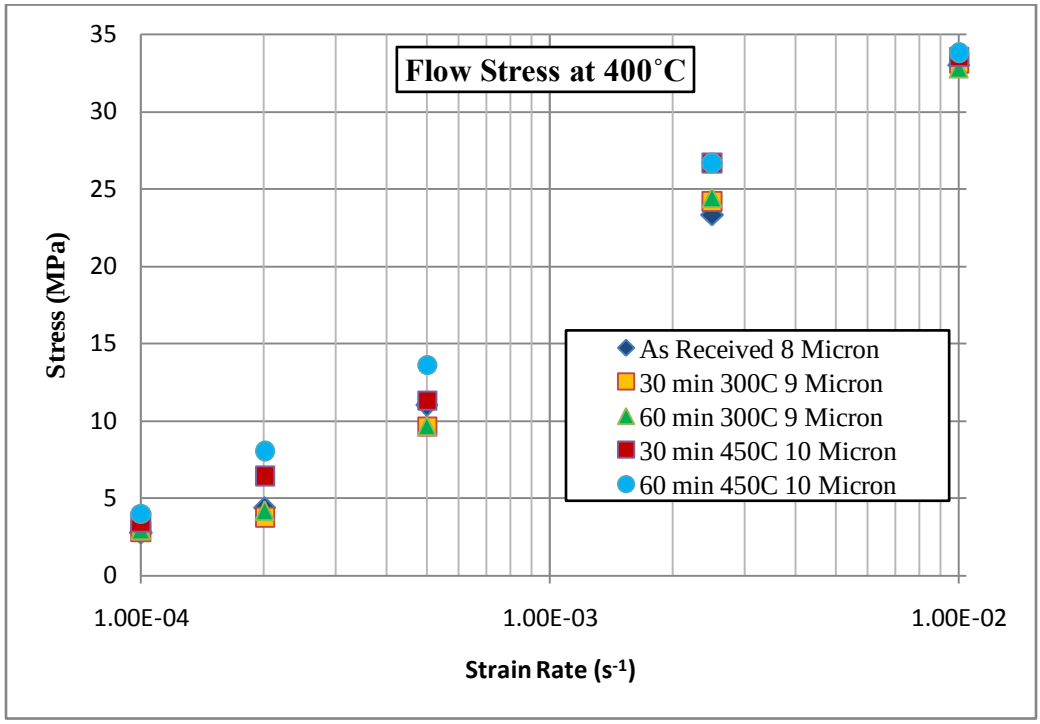

Figure 37 Superplastic Flow Stress of Annealed Mg AZ31B with respect to strain rate at 400˚C

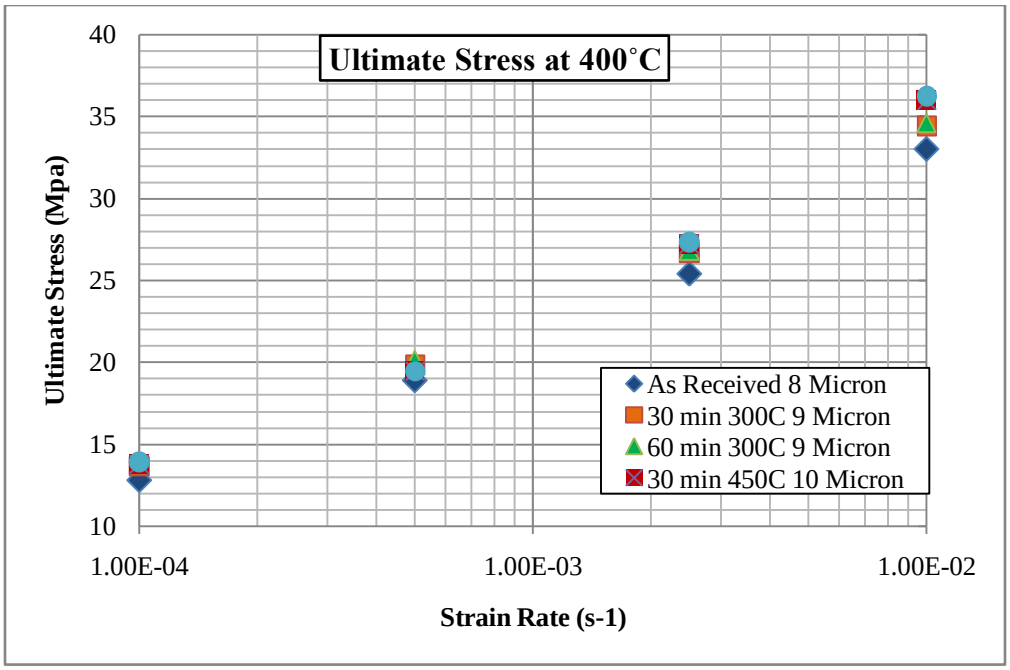

Figure 38 Superplastic Ultimate Stress of Annealed Mg AZ31B with respect to strain rate at 400˚C

The variation of the ultimate stresses at the larger strain rates are due to the lack of time to permit dynamic grain growth and thus allowing the microstructure to become similar for all the specimens. This leads to the determination that grain size gradients may need to be used to achieve larger flow stresses a. Of course, the 65 minute preheat does not exist for bulge forming specimens which for now makes it difficult to determine true as received material properties.

To perform an accurate comparison of the strain rate sensitivity of the annealed microstructure, strain rate jump tests were carried out for 2 strain rate combinations. The first strain rate jump was between $2.5e^{-3}$ s^{-1} and $5.0e^{-3}$ s^{-1} stain rates and a second jump between $2.0e^{-4}$ s^{-1} and $5.0e^{-4}$ s^{-1} provided a direct sensitivity comparison shown in Figure 41. The strain rate sensitivity is determined by the use of two stress and strain rate values during a single tensile test. A uniaxial test is carried out for a specific strain rate $\dot{\varepsilon_1}$ to a

predetermined true strain. At the predetermined true strain, the strain rate is changed to $\dot{\varepsilon_2}$. Since the strain rate sensitivity mirrors the flow stress sensitivity by definition, the strain rate sensitivity can be determine using equation 5.1 (9).

$$m = \frac{\log \sigma_{f2} - \log \sigma_{f2}}{\log \dot{\varepsilon}_2 - \log \dot{\varepsilon}_1} \qquad (5.1)$$

The uniaxial tensile strain rate jump tests are provided below as Figure and Figure . The strain rate sensitivity decreases a small amount due to the annealing. The grain size does not have as much effect as just the fact that the specimens were annealed for the larger strain rates. But at the smaller strain rates, the sensitivity begins to become more dependent on the grain size.

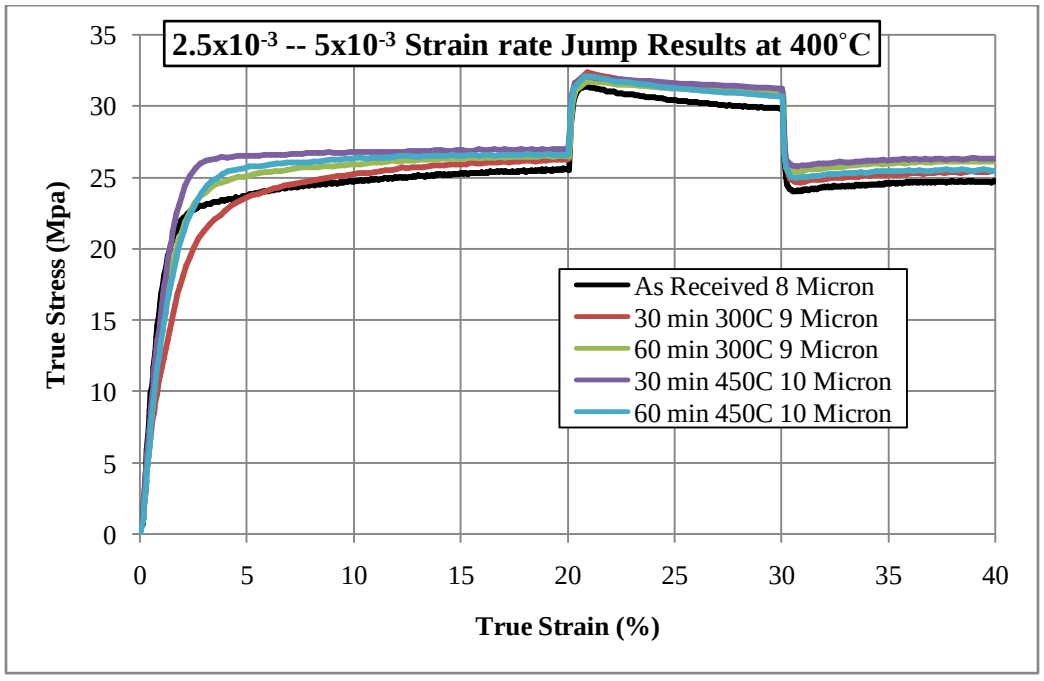

Figure 39 Strain rate jump tests from $2.5x10^{-3}$ to $5.0x10^{-3}$ for Mg AZ31B annealed specimens at 400˚C

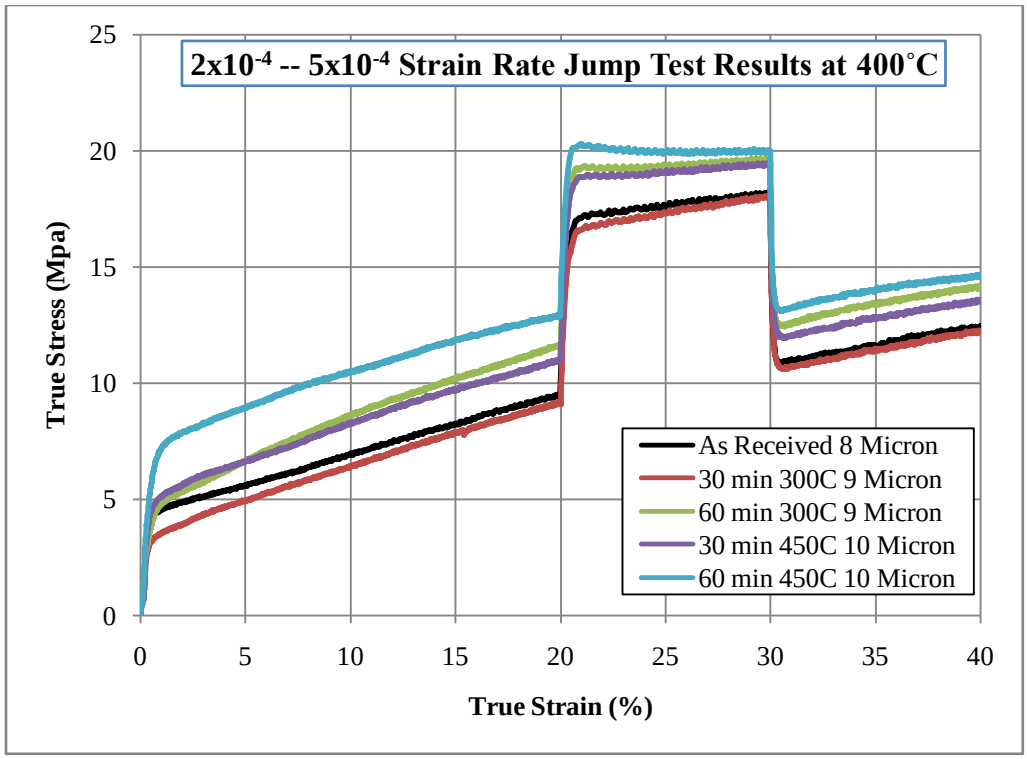

Figure 40 Strain rate jump tests from $2.0x10^{-4}$-$5.0x10^{-4}$ for Mg AZ31B annealed specimens at 400˚C

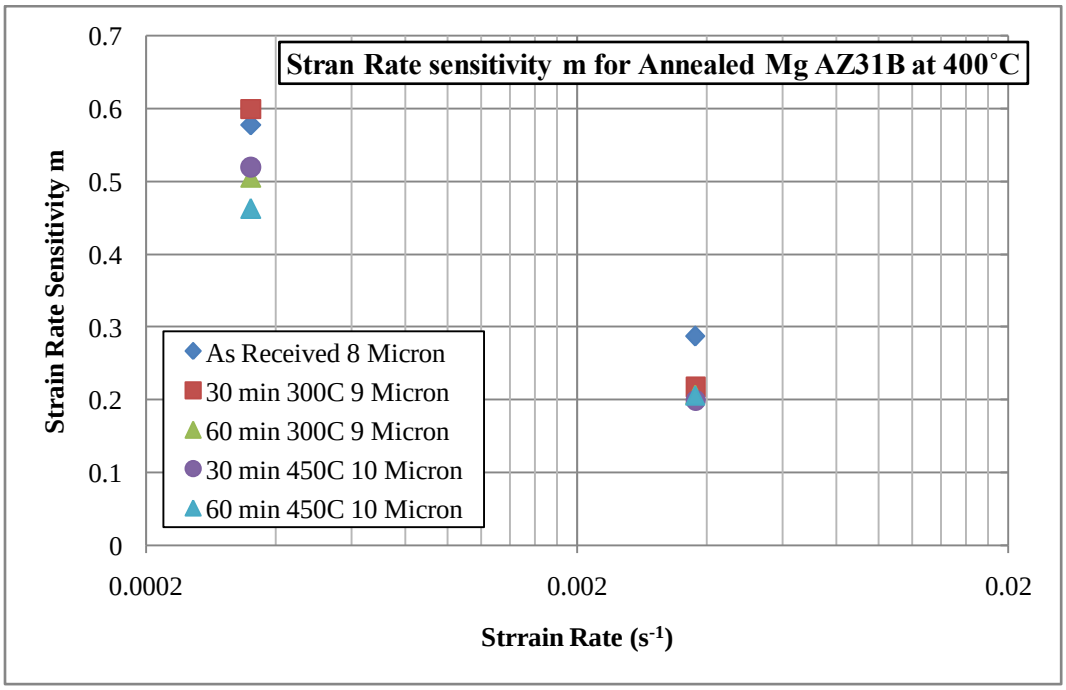

Figure 41 Strain rate sensitivity m for annealed Mg AZ31B at 400˚C

Discussion

Though the microstructure gradients in the tensile specimens are small, there are clear effects that can possibly be used to generate thickness control in SPF bulge formed sheets. To fully apply these results, the use of the static grain growth contour plots needs to be applied to a detailed series of tensile specimens to generate enough grain size dependent SPF properties to be modeled. Then, the uses of a material model in a FE simulation can be used to determine the magnitude of selecting static grain growth accurately enough to provide a reasonable temperature contour plot for selective heating experiments. Until this occurs, the selective heating experiments will be determined merely by guessing and thus providing faithful evidence to their benefits.

CHAPTER 5 SELECTIVE HEATING

Overview

Selective heating is one method to generate grain size gradients. Grain size gradients can be desired in SPF for their supposed ability to minimize thinning. Several researchers have attempted to selectively heat either a Zn 22Al or a Ti-6Al-4V alloy and bulge form. Though there were results that pointed to possible benefits, there have been no follow up work to generate conclusive results. A major influence to this is the use of such alloys being of low production rate parts in industry, such as aerospace. Since such material applications are of such low production rates, desires to minimize material used is not as important as other engineering problems and the rate of formation is of no problem due to the forming period of days instead of minutes. As for Magnesium alloys, their desire for automotive use specifically for weight reduction purposes provides a large desire to reduce thinning for material usage minimization as well as the determination of possible processing time decreases due to the properties of sheets with microstructure gradients.

Chapter 5 provided initial uniaxial observation into the effect of annealing and grain sizes on the SPF properties for Mg AZ31B alloy. Chapter 4 provided a detailed 3-dimensional static grain growth contour plot to allow the estimation of grain size growth during selective heating experiments in this chapter. The first task to complete for selective grain growth studies is the determination of applicable heating techniques. In this work, several were investigated, and due to equipment restrictions, several are mentioned with their pros and cons for such an application.

Hot Air Gun

The first selective heating technique was the use of a Steinel® hot air gun. Figure is a picture of the hot air gun with a nozzle modification used for selective heating experiments. A schematic of the experimental setup using the Steinel® hot air gun is shown in Figure . Figure through Figure provide pictures of the air gun being used to selectively heat 3 Mg AZ31B specimens.

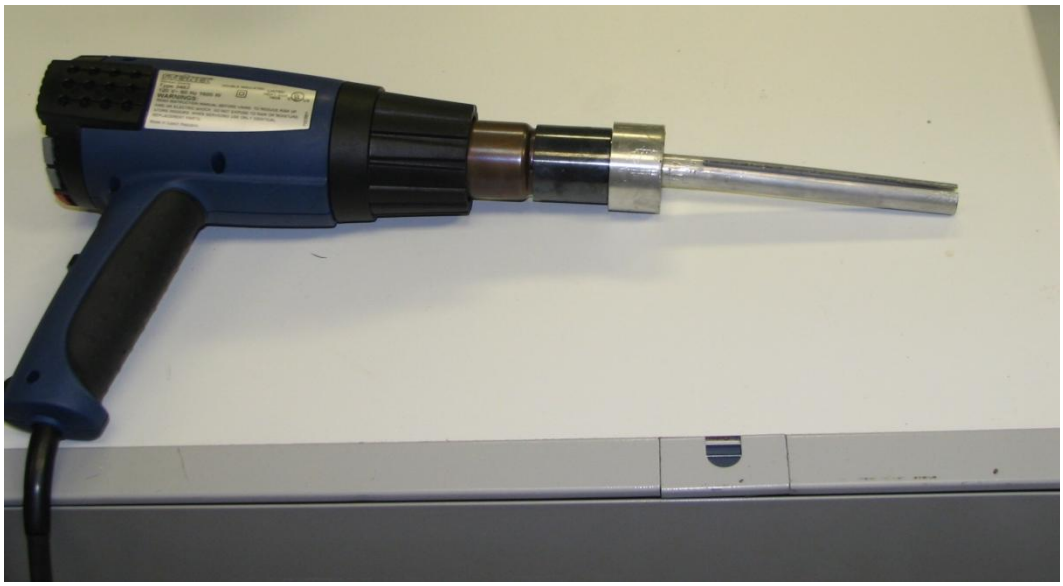

Figure 42 The Steinel® Hot air gun used for selective heating experiments capable of 600˚C

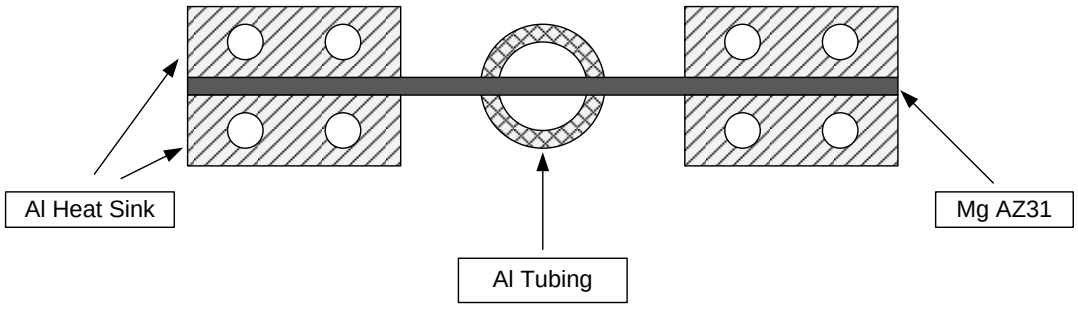

Figure 43 Schematic showing the breakdown of a selective heating experiment by the Steinel® hot air gun.

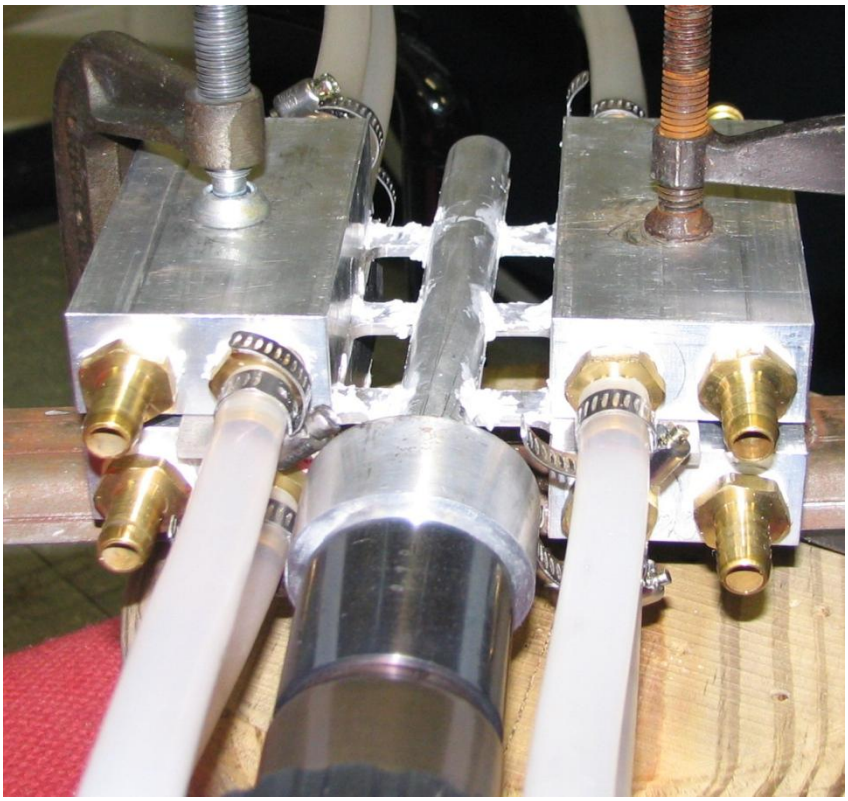

Figure 44 Mg AZ31B tensile specimens selectively heated using the Steinel® hot air gun

Figure 45 Steinel® hot air gun used to linearly heat Mg AZ31B bulge specimen

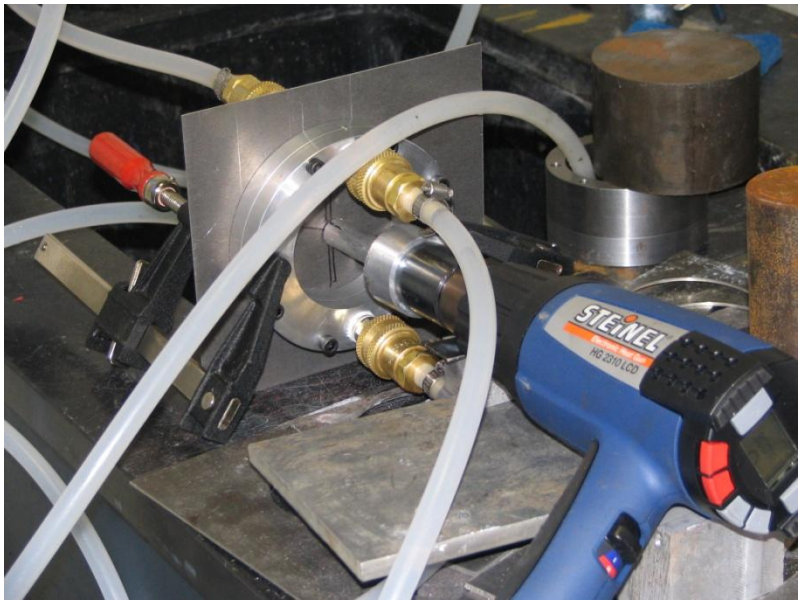

Figure 46 Steinel® hot air gun used to radially heat a Mg AZ31B bulge specimen

Five sets of tensile specimens were selectively heated. All five sets were heated with the Steinel® air gun. The heating times were as follows: set 1a was generated with 180 minutes of heating, set 1 was generated with 80 minutes of heating at 1200 °F gun setting, set 2 was generated with 93 minutes of heating at 900 °F gun setting, set 3 was generated with 625 minutes of heating at 1000 °F gun setting, and set 4 was generated a with 100 minutes of heating. Sets 1a, 1, 2, and 3 contained 3 tensile specimens that were of the same size. Set 4 was a set of 2 tensile specimens that were a bit larger and were chemically gridded with circles to show the material deformation. A tensile specimen from sets 1, 2, and 3 were cut at the center and near the edge of the heat exchanger and mounted, polished, etched to determine if the heating changed the microstructure.

For the bulge forming sheets, there were three sheets selectively heated. One of the sheets was linearly heated, and the remaining were heated with the circular heat exchanger. The linearly heated specimen was made using the Steinel® air gun. Two

circular heated samples were made using the Steinel® air gun. The microstructure for both the linearly and radially heated specimens were examined and are shown below.

The grain size results were estimated from acquired optical microscopy photos. A couple of the results are shown in Figure and Figure .

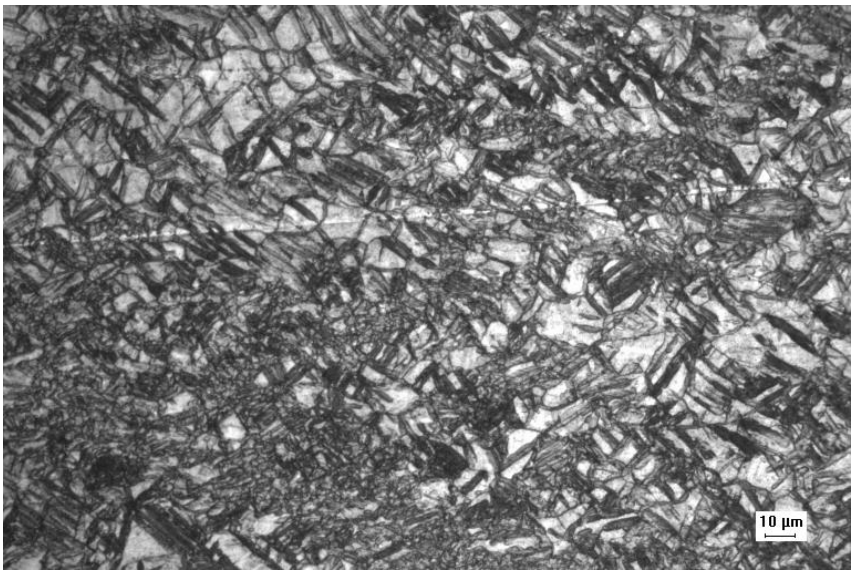

Figure 47 Grain size picture from the center of a radially heated bulge specimen generated with the Steinel® air gun

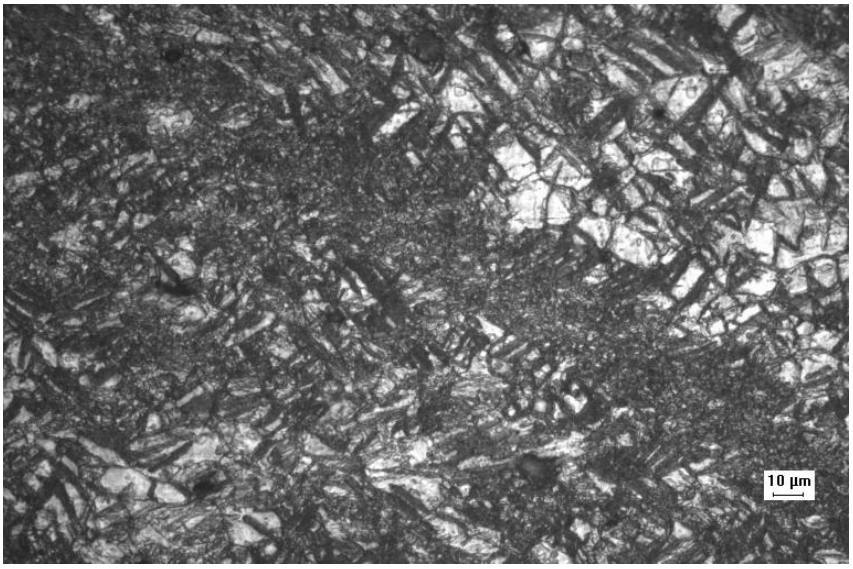

Figure 48 Grain size picture from the edge of a radially heated bulge specimen generated with the Steinel® air gun

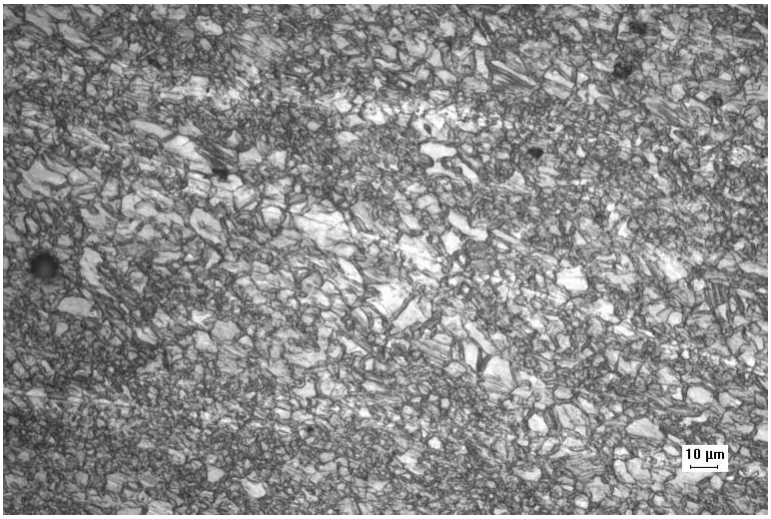

Figure 49 Grain size picture from the center of a tensile specimen from set 3 generated with the Steinel® air gun

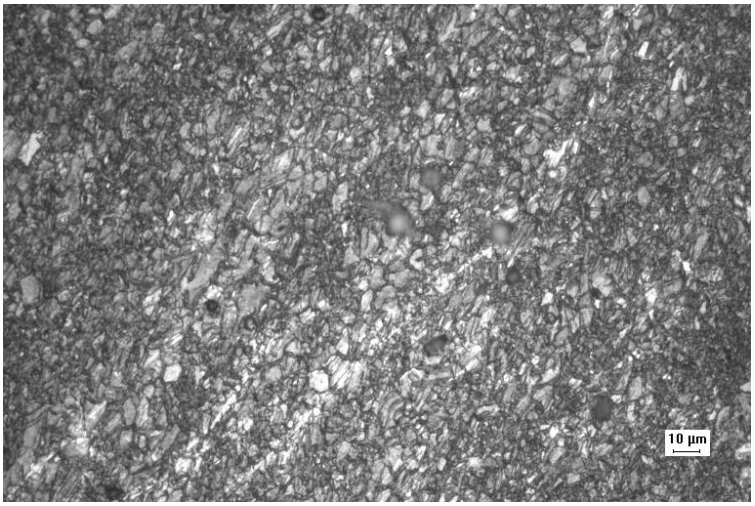

Figure 50 Grain size picture from the edge of a tensile specimen from set 3 generated with the Steinel® air gun

The results from the microstructure evaluation provided negligible results for the support of selective static grain growth. Also, the sample generated from the Steinel® air gun exhibited early failure due to deformation from heating. The sample had a slight bulge in the center where the heat was applied with the Steinel® air gun.

In the end, it was concluded that the temperature requirements for selective heating of the Magnesium alloy was not feasible for the Steinel® hot air gun even though it's supposed maximum temperature was 600˚C.

Electric Resistance Heaters

A second possible selective heating method is the use of electric resistance heaters. The manufacturers specs for a strip heater pictured in Figure was 550˚C and 450˚C for the bolt heater pictured in Figure . The heat from the electric resistance heaters was to be transferred to the surface of the Magnesium specimens to be selectively heated. A schematic of the process is presented in Figure .

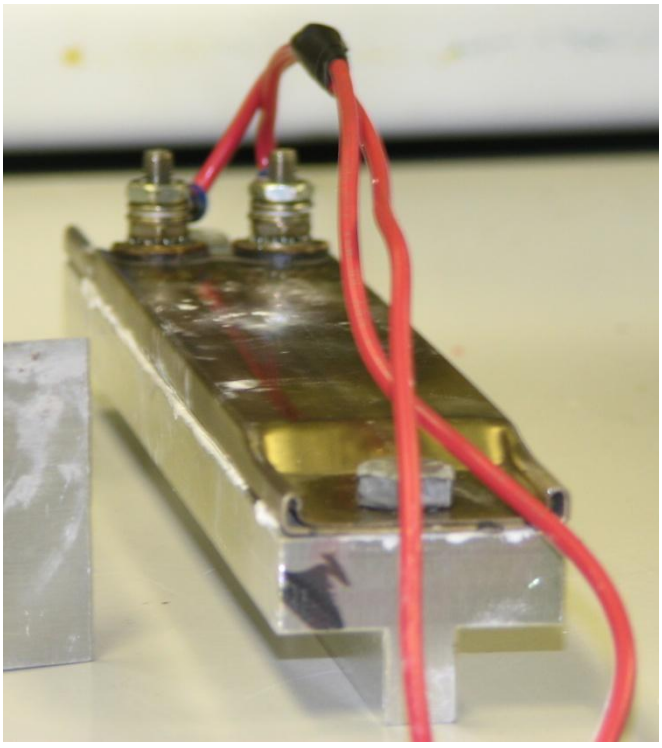

Figure 51 Electric resistance strip heater capable of 550˚C max temperature with a machined aluminum block to conduct heat to desired surface.

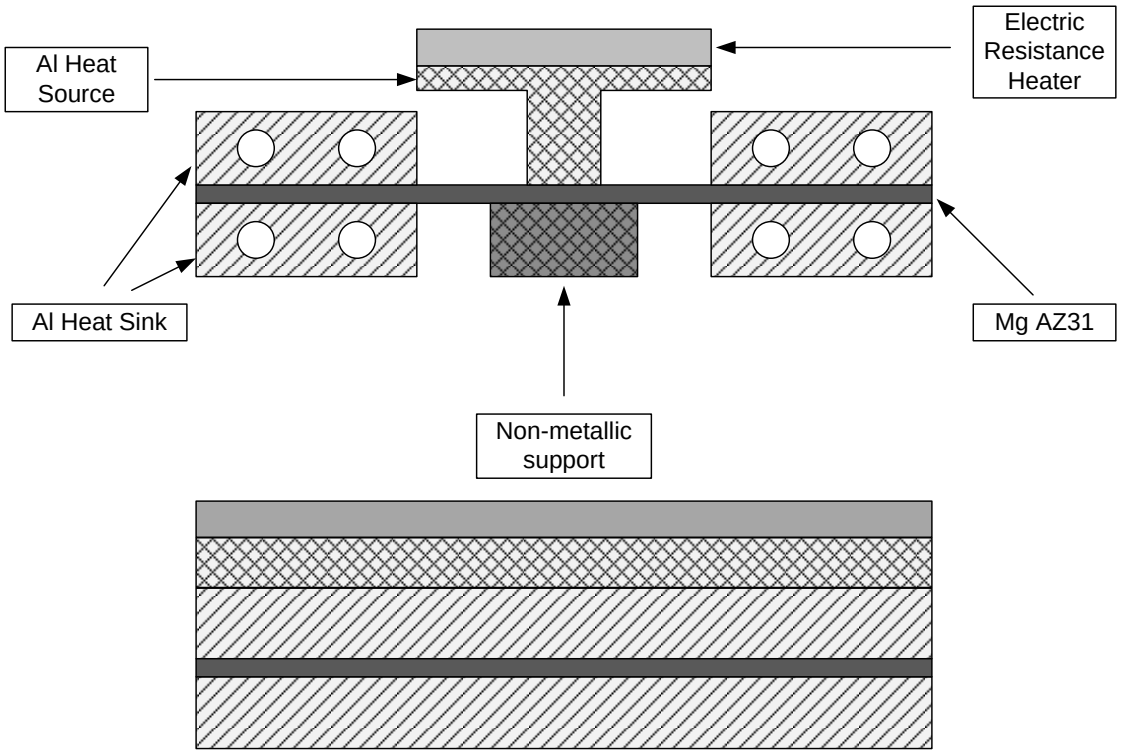

Figure 52 Schematic for the use of electric resistance heaters for selective heating

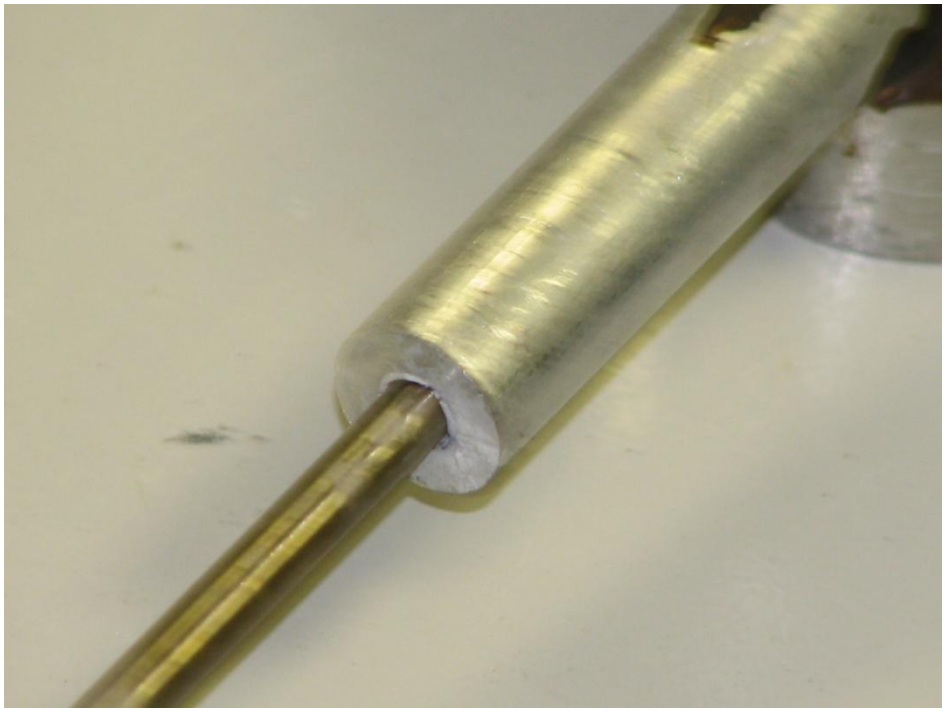

Figure 53 Photo of the bolt electric resistance heater capable of 450˚C

There were a single specimen radially heated by the bolt resistance heater and a single specimen linearly heated by the resistance heater. The radially heated specimen was bulge formed with little selective heating success expected due to the lack of microstructural evidence provided by the linearly heated specimen. The microstructure is not shown here because it is similar to the results shown in Figure and Figure .

For the bulge formed sample heated with the bolt heater, the forming time was 21 minutes where the non-heated bulge sample failed at 21 minutes. This specimen did not fail though. It also did not form to the same height. This specimen formed to a height of 31 mm versus 34 mm.

Though the results for the bulge specimen may seem hopeful, without the ability to generate large microstructure gradients, applicable results are not possible as shown by the tensile tests in chapter 5. In the end, it was concluded that the temperature requirements for selective heating of the Magnesium alloy were not feasible for the electric resistance heaters examined here even though the supposed maximum temperature was at least 450˚C which was plenty high enough. The heaters were just not capable of obtaining such temperatures without sufficient insulation.

Conduction from Furnace

A third method used to attempt selective static grain growth was conduction from a furnace, which was used for high temperature testing. Since the furnace was equipped with a circular opening at both the top and bottom to permit connections to an Instron machine for material testing, it was feasible to setup an experiment using Aluminum round bar protruding from the furnace to heat the sheet specimen. Figure shows a cross view schematic of the experimental setup. Figure , Figure, and Figure all provide

photographs of the actual experiments in use. It is important to note that this experimental setup was not to try and generate an obscure process for selective grain growth but to provide evidence that with the proper induction heating equipment that a piece of round bar of a material with the end that is in contact to the sample machined to a desired heating shape can be used to provide the necessary heat temperatures for selective heating.

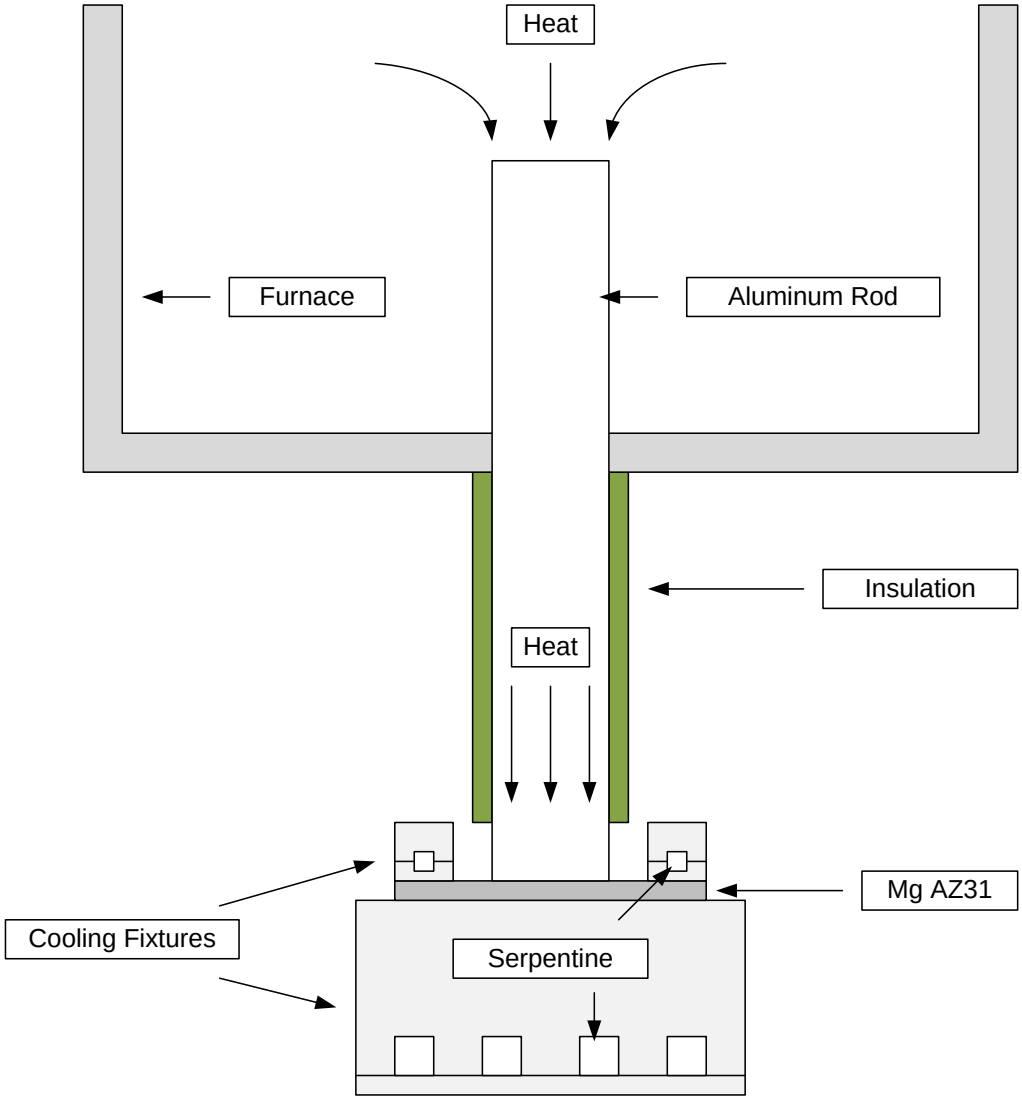

Figure 54 Schematic of selective heating using a furnace to create a heat sink from an 18 inch round bar of 6061 T6

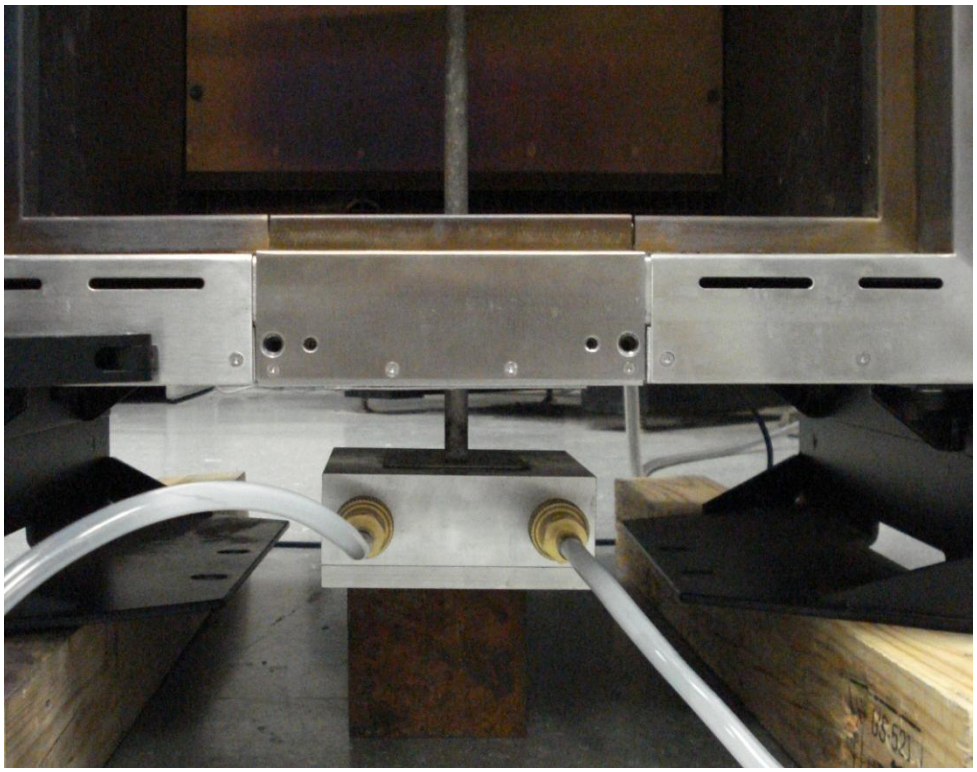

Figure 55 Picture of selective heating via conduction from a furnace and a ½ inch diameter 6061 T6 Aluminum rod as the heat source described in schematic above

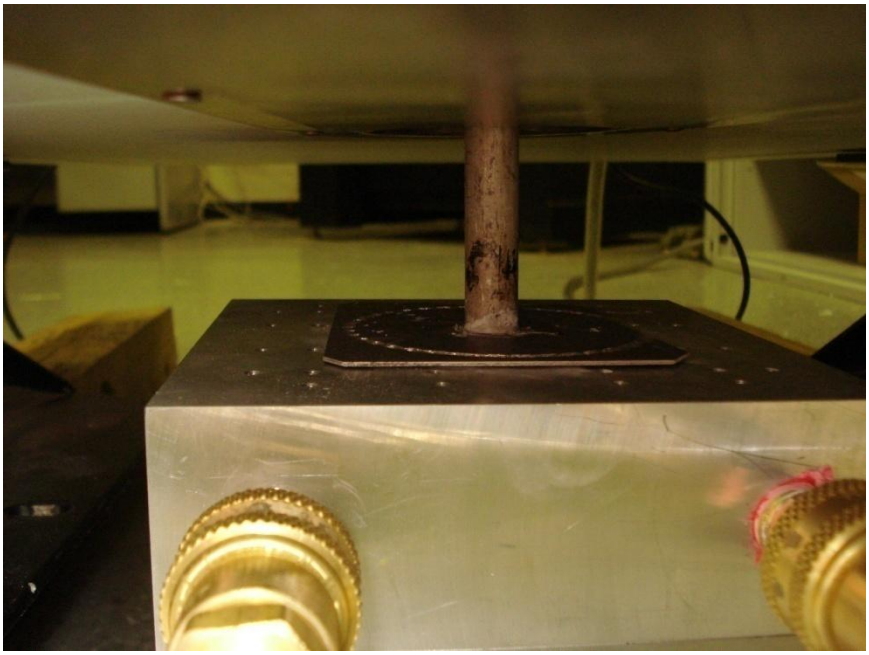

Figure 56 Picture showing the Magnesium sample being heated using conduction from a furnace

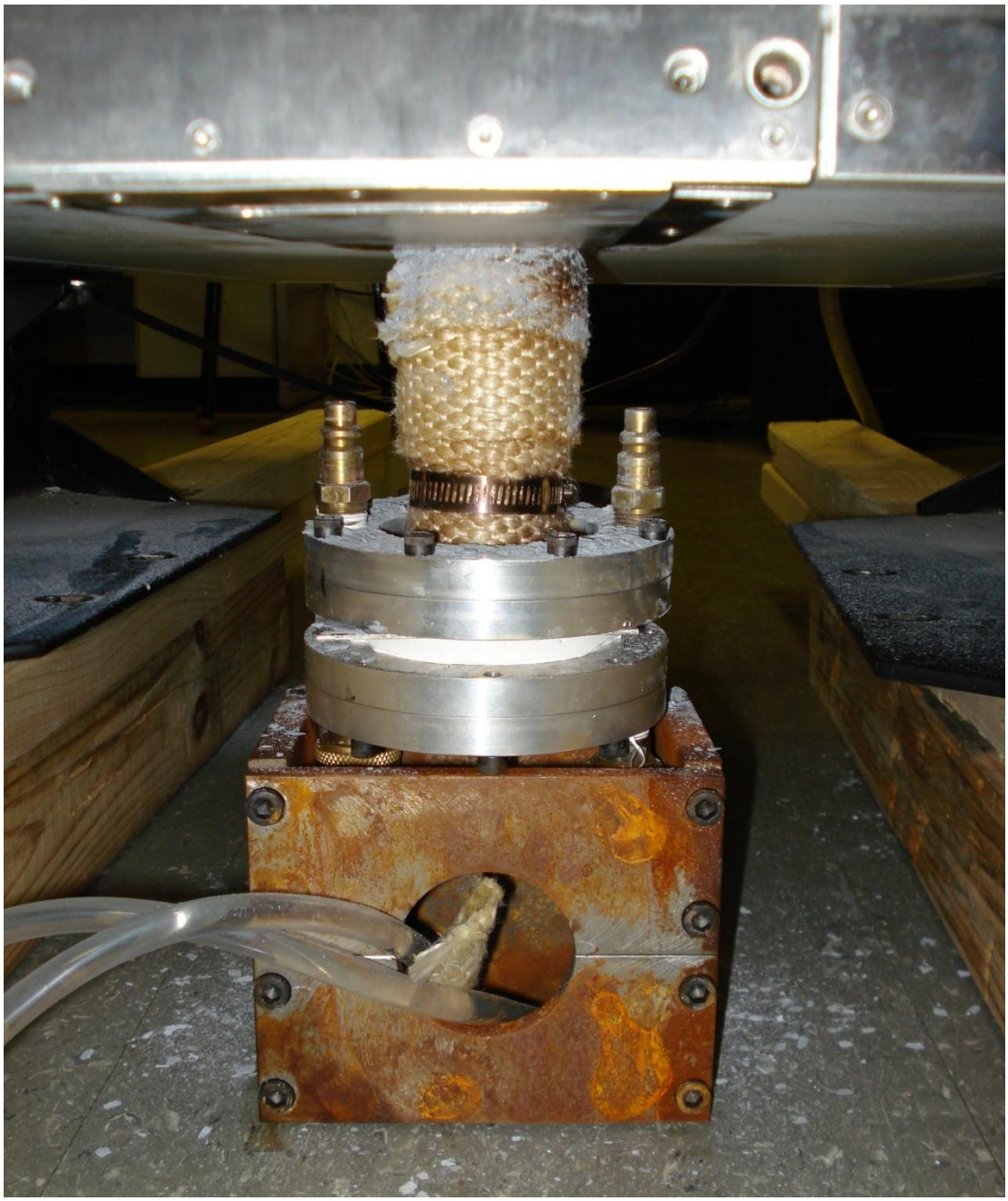

Figure 57 Picture of a different selective heating experiment using conduction from a furnace at 580˚C this time with a 6061 T6 Aluminum heat source that is 1.5 inches in diameter

To determine the capability of the furnace conduction experiment, microstructure analysis was performed to determine the heating affects. Figure and Figure provide little evidence that there was much selective heating. But with careful examination, one will

notice that both have a cleaner microstructure than that presented for the previous selective grain growth experiments. Though little, the ½ inch aluminum round bar provided a little bit of annealing for the complete specimen. So this lead to a second stage where a piece of 1.5 inch diameter round bar was used to perform another series of experiments.

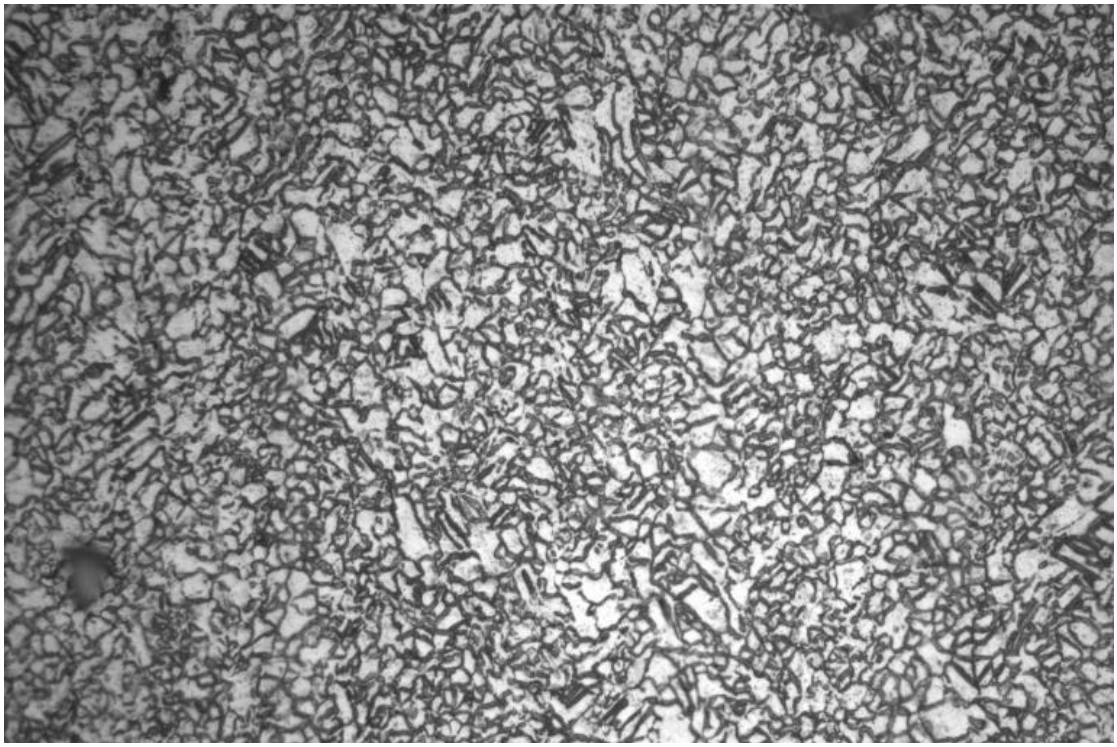

Figure 58 Optical microscopy photo at 500x obtained from the center of a specimen selectively heated by conduction from the furnace using the ½ inch Aluminum rod

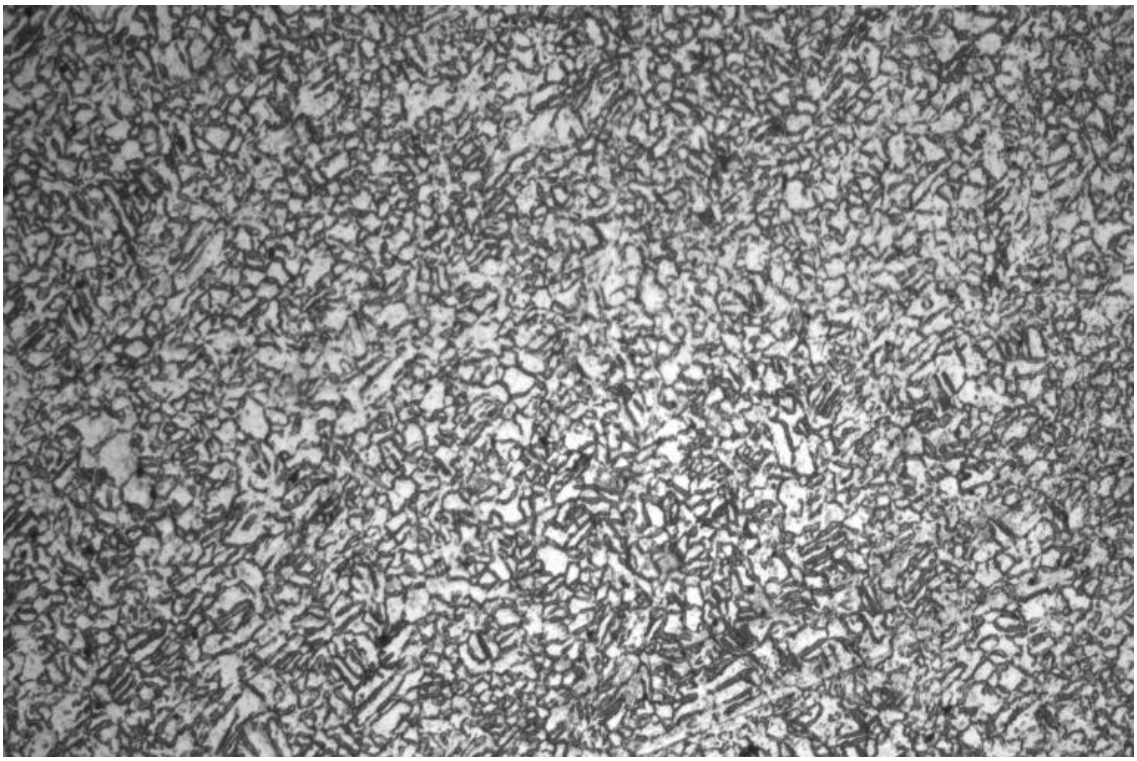

Figure 59 Optical microscopy photo at 500x obtained from the edge of a specimen selectively heated by conduction from the furnace using the ½ inch Aluminum rod

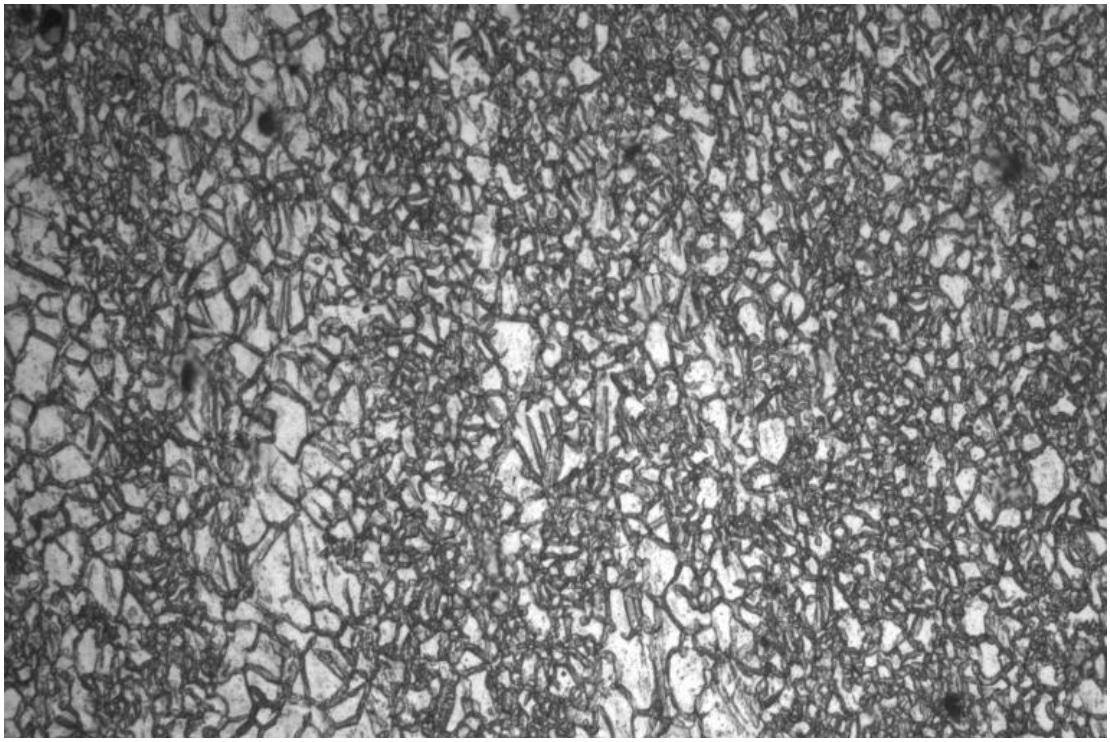

Figure 60 Optical microscopy photo at 500x obtained from the center of a specimen selectively heated by conduction from the furnace using the 1 ½ inch Aluminum rod

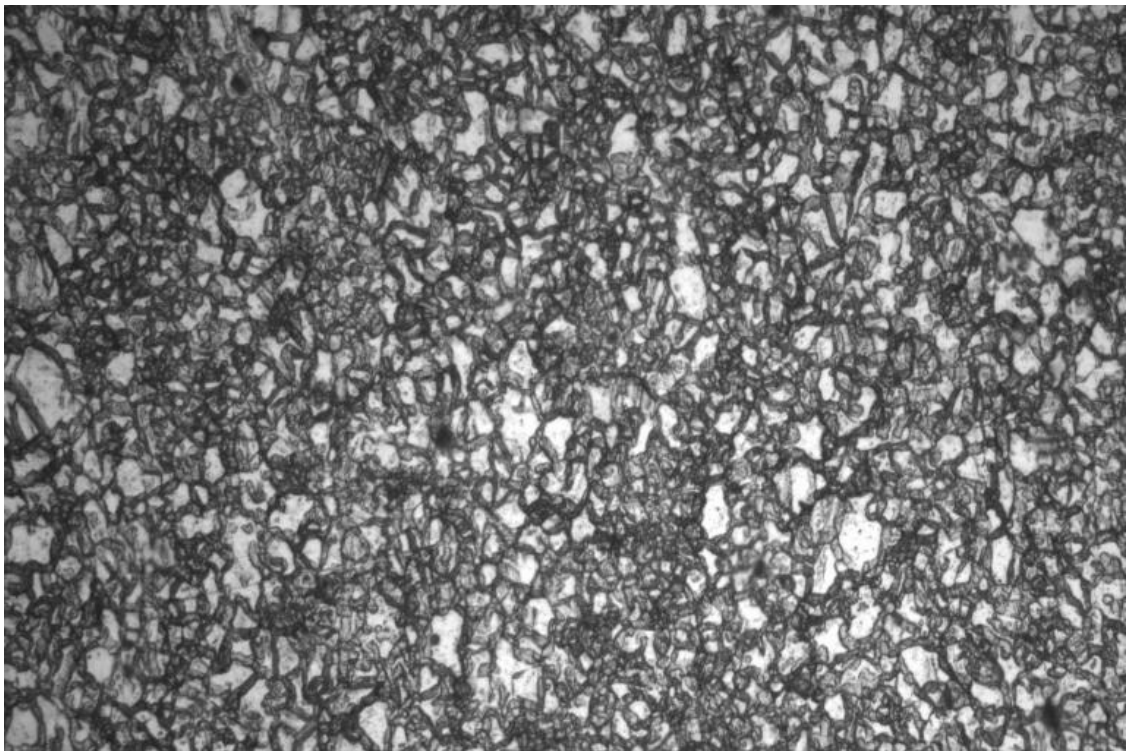

Figure 61 Optical microscopy photo at 500x obtained from the edge of a specimen selectively heated by conduction from the furnace using the 1 ½ inch Aluminum rod

Figure and Figure provide microstructure representation from a set of experiments for the 1.5 inch Aluminum round bar experiment. Again, there is very little difference in the size of the microstructure between the edge and the center, but annealing is even more apparent than before.

This leads to a conclusion that with the proper induction heating equipment, thus not a furnace, that selective grain growth is very achievable. There were two major problems with the furnace as the heating source. The first was the fact that the maximum temperature for the furnace was 600˚C. This temperature seems plenty high enough when 400˚C is the desired heating temperature, but there are two problems with it. One is that the temperature drop between the center of the furnace and the sample is quite large even when insulated. The other is that the temperature drop at the contact point due to the high

conductivity of Magnesium provides the remaining loss of energy that prevents the ability of selective heating. Based on the microstructure photographs and the static grain growth results in chapter 4, the maximum temperature achieved was about 200˚C given the experiments were carried out for 5 hours per specimen. The other large problem with the furnace was the fact that it was not designed to be used in such away which extremely limits the setups and makes the temperature analysis nearly impossible outside of microstructure analysis.

Though the results seem to be a bust, the results are actually promising. They lead to the conclusion that selective heating is achievable through conduction, but with the appropriate equipment. Thus future experiments with proper equipment are suggested, which may even be capable of creating selective heated tensile specimens to permit a more in depth material flow analysis with experimental results.

UV Light

The final selective heating method examined in this work was that of a UV light. The capability of the light was plenty with a maximum achievable temperature of 1500˚C. But one of the potential problems was the ability to focus the light. This section of research was carried out in a partnering facility called Ecole des Mine d'Albi Carmuax located in Albi France. The analysis for the temperature gradients was provided by the collection of inferred data collected during the experiment. The heating was carried out on 5 Mg AZ31B sheet samples that were approximately 3 in x 3 in and of a sheet thickness of 1.75 mm. The Samples were held vertically in front of the light source which had a polished shield to focus the light as best as possible. The IR camera was located behind the specimens heated and the data was saved using a DAQ loaded with IR

software ADDEILE. The specimens were coated with a black charcoal colored paint to permit accurate temperature readings. Figure provides the experimental schematic.

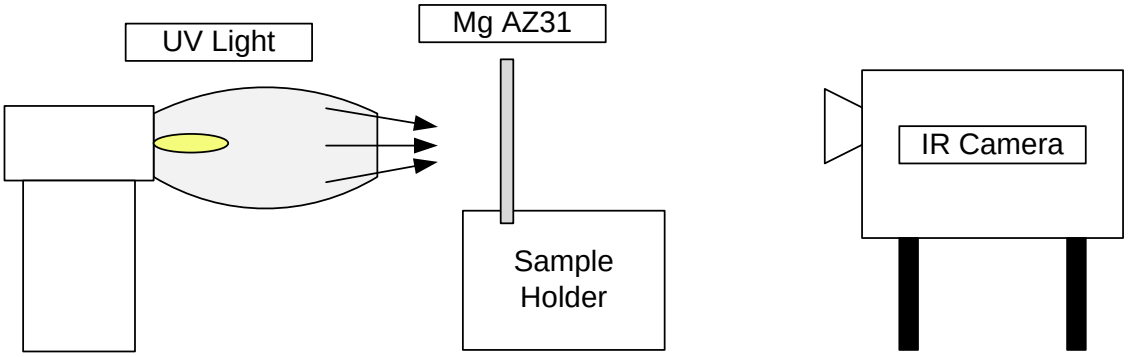

Figure 62 Schematic of the UV light heating setup

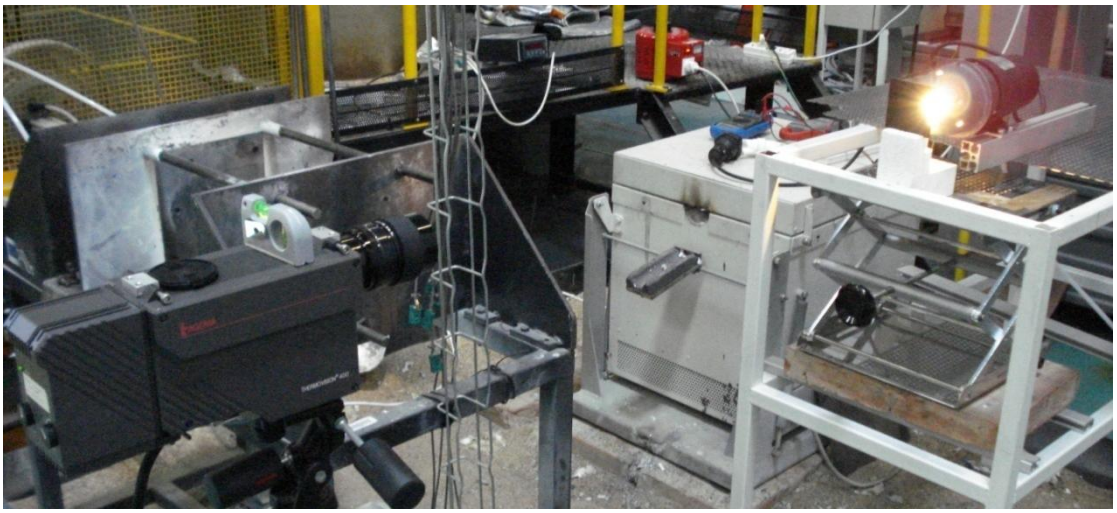

Figure 63 Photograph of the experimental setup and an experiment at Ecole des Mine d'Albi Carmuax in Albi France

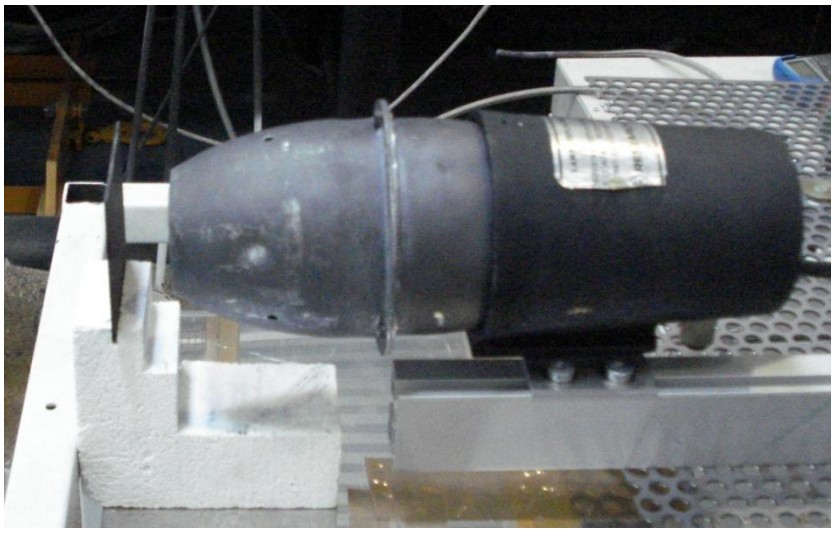

Figure 64 UV light with shield and a Magnesium specimen setup at Ecole des Mine d'Albi Carmuax in Albi France

Figure and Figure provide a visual representation of the experimental setup. As mentioned, the samples were held vertical for temperature measurements and were painted black for IR calibration purposes as shown in the figures above.

The heating profiles were captured as text files as well as several IR images to provide a basis for the temperature profiles that were achieved for the experiments. The heating experiments were broken up into three trials. The first trial was involved the use of the Mg AZ31B sample to be used for temperature versus voltage output to provide the basis of power to be supplied to achieve a specific temperature which are summarized in Table . It was determined that a 20 watt supply to the light source provided a 70˚C maximum temperature for the sample which was the starting point of the experiment. For a 40 watt setting, the maximum temperature was 150˚C, 60 watts created a maximum temperature of 235˚C, 80 watts created a maximum temperature of 320˚C, a 100 watt setting generated a max temperature of 395˚C, 110 watts created a maximum temperature of 430˚C, and finally 120 watts generated a maximum temperature of 460˚C.

Table 5 Temperature voltage relationships for UV heating experiments performed at Ecole des Mine d'Abli Carmaux in Albi France

Voltage Setting (watts)	Maximum Temperature (˚C)	Minimum Temperature (˚C)	Temperature Gradient(˚C)
40	150	125	25
60	235	205	30
80	320	280	40
100	395	345	50
110	430	340	90
120	460	360	100

Since the experiment was setup for natural convection to generate the temperature gradient desired due to lack of cooling fixtures, each wattage setting produced a different temperature gradient across the samples. The corresponding temperature gradients are as follows; 20 watts → 20˚C gradient, 40 watts → 25˚C gradient, 60 watts → 30˚C gradient, 80 watts → 40˚C gradient, 100 watts → 50˚C gradient, 110 watts → 90˚C gradient, 120 watts → 100˚C gradient. Figure through Figure provide a visual representation of the IR images captured during trial 1 experiments.

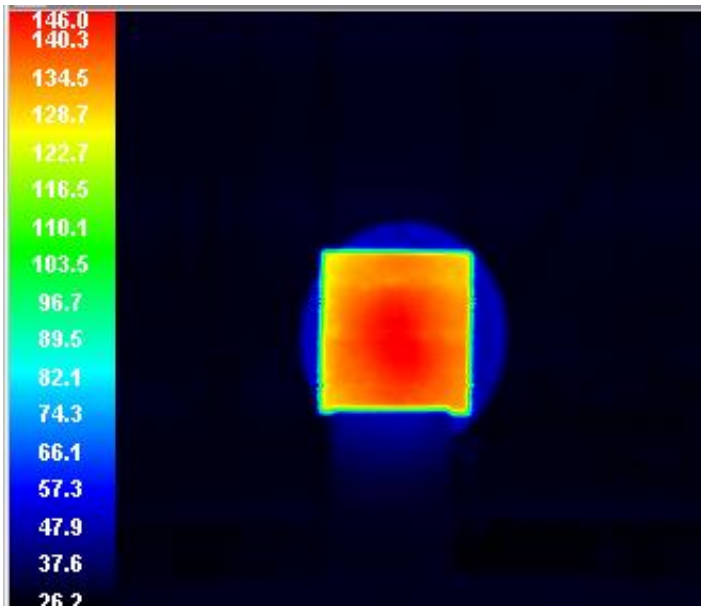

Figure 65 IR image of Mg AZ31B heated using a UV light to 145˚C with a wattage setting of 40 at Ecole des Mine d'Albi Carmuax in Albi France

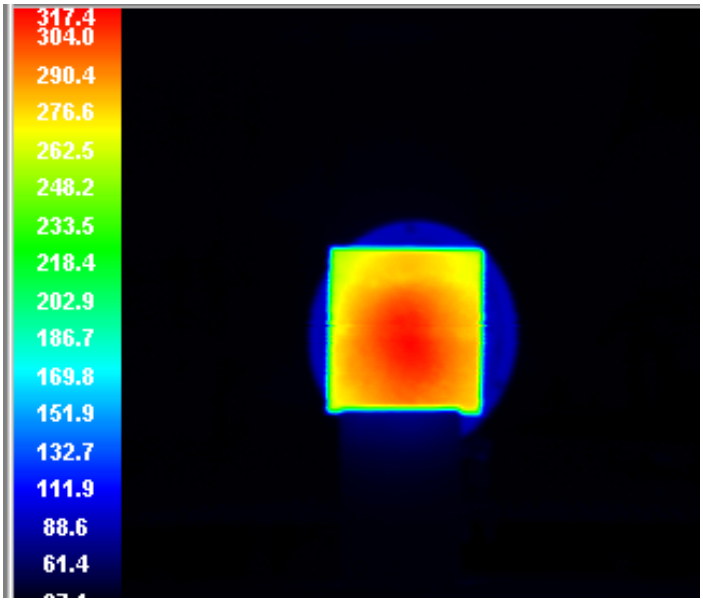

Figure 66 IR image of Mg AZ31B heated using a UV light to 320˚C with a wattage setting of 80 at Ecole des Mine d'Albi Carmuax in Albi France

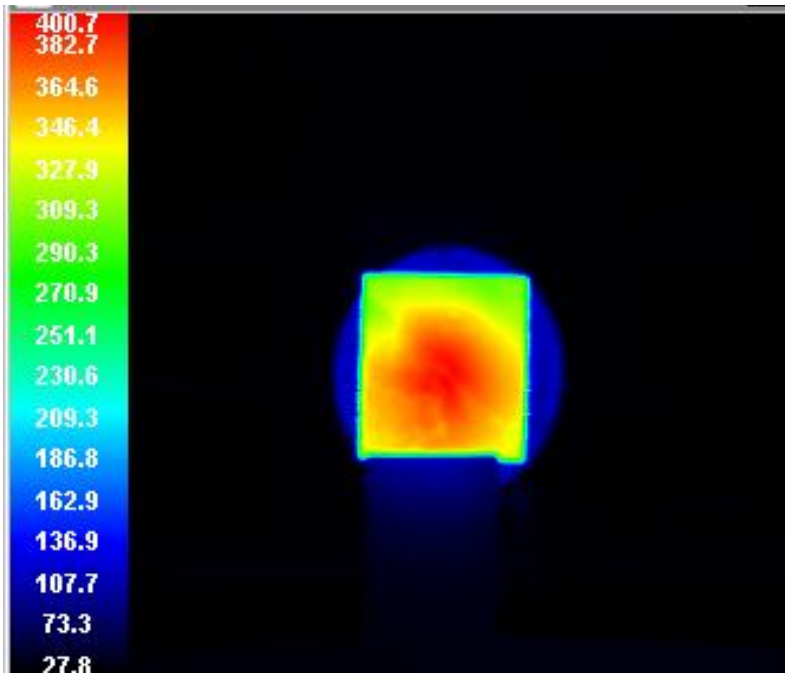

Figure 67 IR image of Mg AZ31B heated using a UV light to 400˚C with a wattage setting of 100 at Ecole des Mine d'Albi Carmuax in Albi France

The remaining specimens were heated under identical patterns. The samples were heated to a maximum temperature of 200˚C to warm the samples before jumping to the desired

temperature of 400˚C to minimize any transient static grain growth effects. Table provides the heating times for each specimen.

Table 6 heating trials for UV Light experiments performed at Ecole des Mine d'Abli Carmaux in Albi France

		Voltage Setting	Time (min)
Specimen	1	20	2
		40	3
		60	5
		80	5
		100	10
		110	5
		120	10
	2	100	25
	3	100	25
	4	100	25
	5	100	25

To verify the temperature gradient and to present the effect of the specimen holder, which was ceramic and thus prevented a perfectly symmetric heating pattern or maximum cooling, temperature profile curves through the center of the samples both horizontally and vertically were acquired and plotted. The profiles for specimens 2 and 3 are presented in Figure and Figure respectively. As provided by the temperature profile plots, the ceramic sample holder did create quit a large effect. Outside the holder though, the gradients are shown quit clearly. It can be noticed that there is a sharp temperature decline near the very edge of the specimens. Though this may seem promising, this area of the sheets is not incorporated in the forming area and represents the flange area of the bulge specimens. Part of the major temperature decline is due to non perpendicular light

emission from the edges. This provides a loss in IR imaging accuracy and therefore it is neglected during future examination.

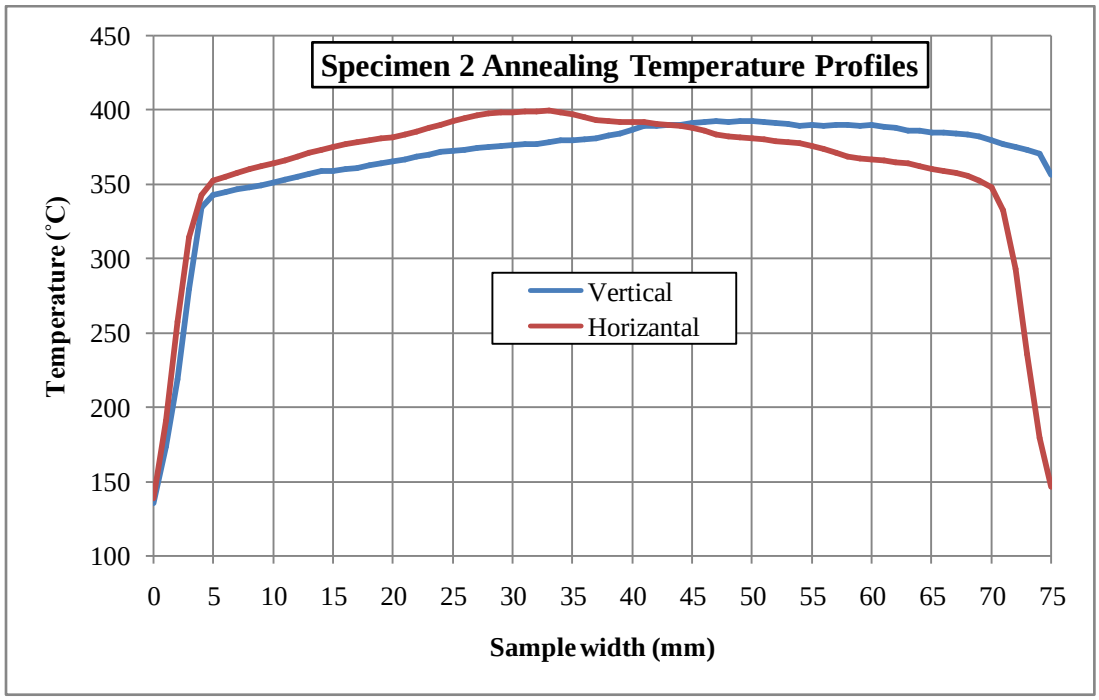

Figure 68 Temperature profiles for specimen 2

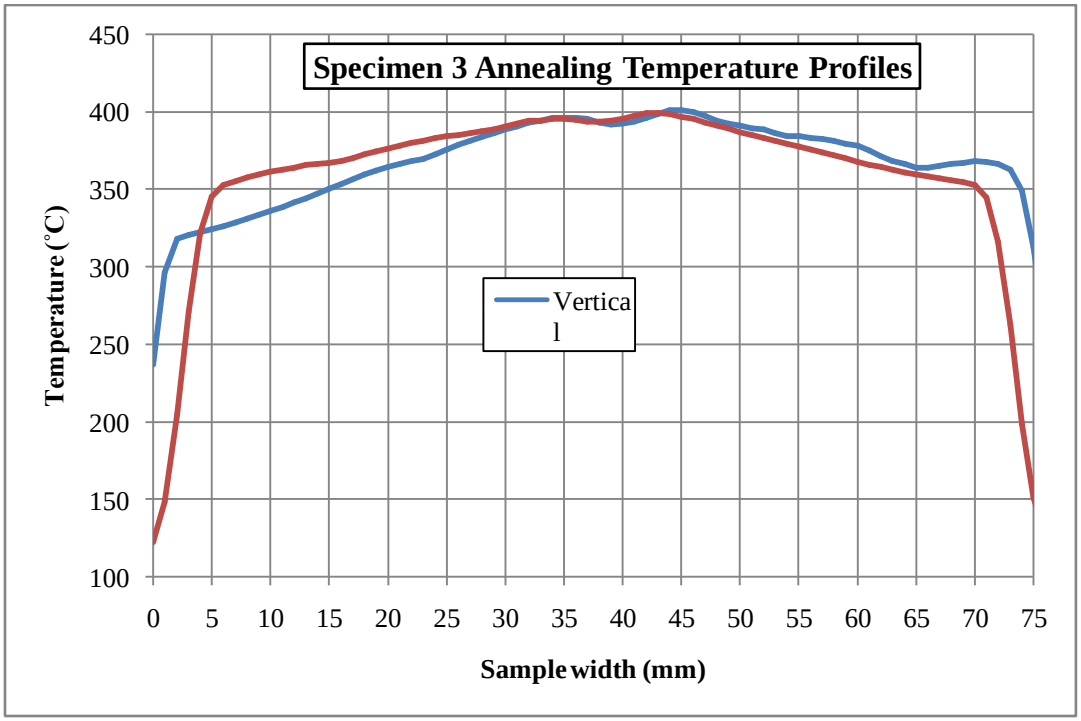

Figure 69 Temperature profiles for specimen 3

Microstructure examination was used to verify the temperature gradients with comparison to the static grain growth curves presented in Chapter 3. Due to mishap in mounting of the specimen, specimen 4 was lost as well as Specimen 5 which was examined in France with a SEM provided inconclusive evidence of grain growth due to difficulty in polishing and etching. Specimen 3 was cut, mounted and examined at UK and provided reasonable results. Microscopy images at 500x magnification are presented in Figure and Figure . By mean linear intercept method, the grain size for the edge was estimated to be 7.5 μm and the center was estimated to by 8.5 μm. From the static grain growth curves in Figure 28 and Figure 29, the grain size at the edge of the specimen was expected to be 7.5 μm and for the center, between 8.5 and 9 μm. This provides excellent proof that the static annealing curves are applicable as well as the UV light Selective heating method.

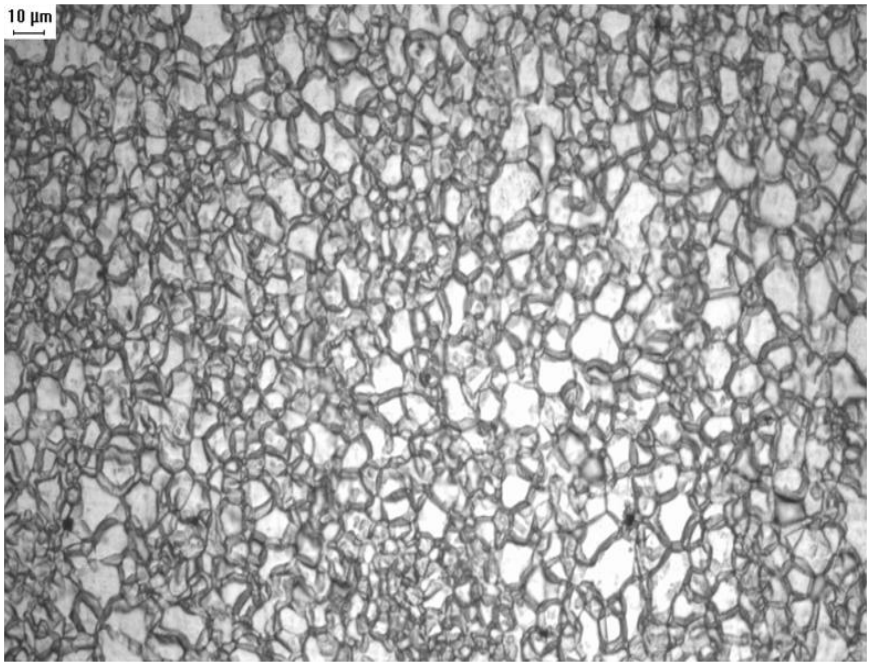

Figure 70 Optical Microscopy image at 500x magnification from the edge of UV selectively heated Mg AZ31B specimen 2. By method of MLI grain size estimated as 7.5 μm

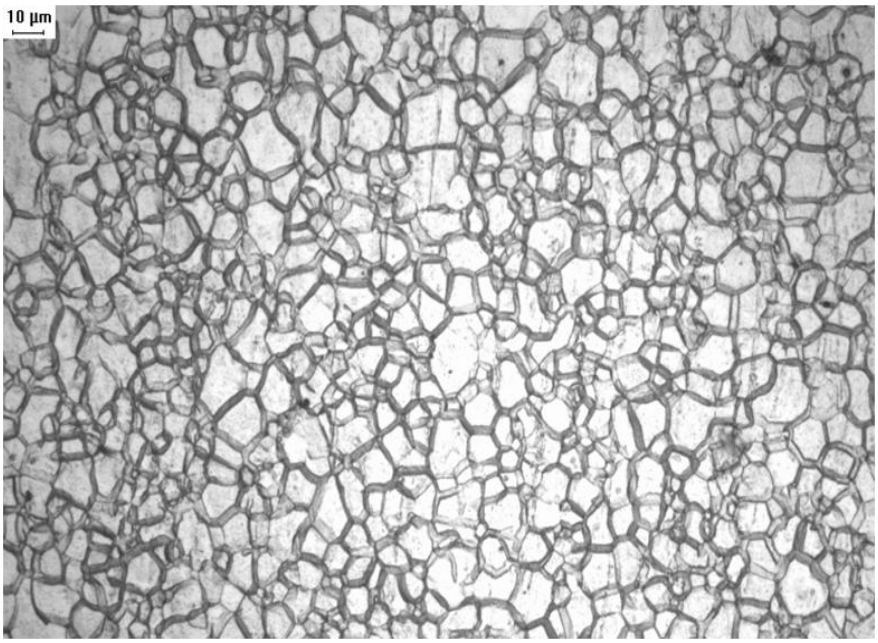

Figure 71 Optical Microscopy image at 500x magnification from the center of UV selectively heated Mg AZ31B specimen 2. By method of MLI grain size estimated as 8.5 µm

Bulge forming

SPF bulge forming was carried out for UV light specimens 1 and 2 from the UV light selective heating experiments. The experimental setup for bulge forming is described in detail by Abu-Farha (2007) (2) as was the tensile setup since he was the one to develop the experimental setup. Figure provides a detailed setup schematic for the SPF experiments carried out.

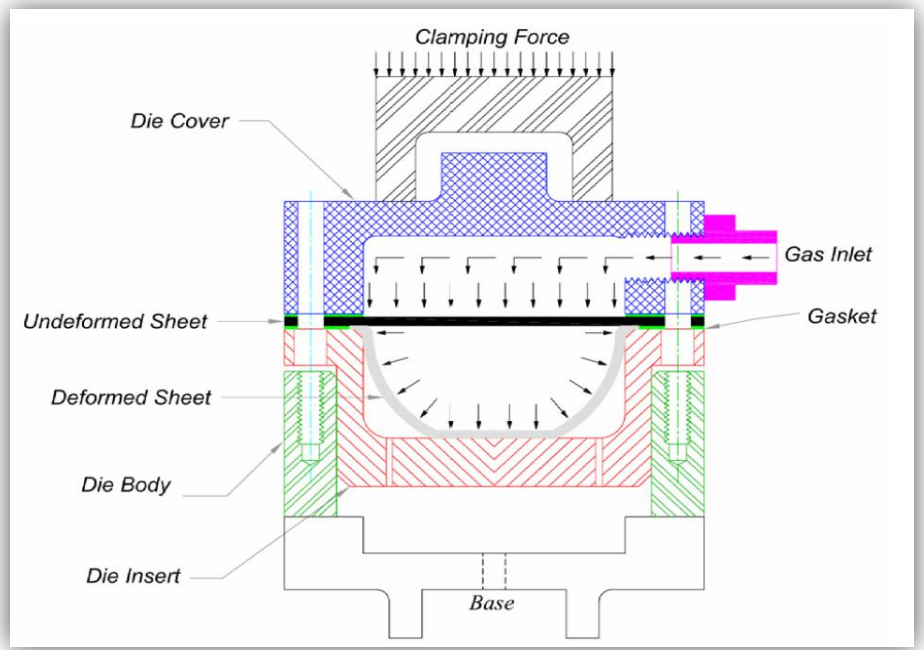

Figure 72 Schematic of the SPF bulge forming setup used for this work (9)

For experimental analysis, thickness distribution was the main concern of the work. A pressure profile was determined from the analytical solution by Dutta (36) and modified briefly to provide complete bulging to failure of as received specimens used to determine the effects of the selective heating. Typical forming time for as received specimens is ~930 seconds at a constant dome strain rate of 1.0×10^{-3} s^{-1} at 400˚C. Figure is the plots of the bulge forming results. The measurements were determined by using an angular coordinate system set as the center of the specimen prior to forming. A visual representation of the angular coordinate system for the thickness measurements is presented in Figure as well as a table with the formed results in

Table .

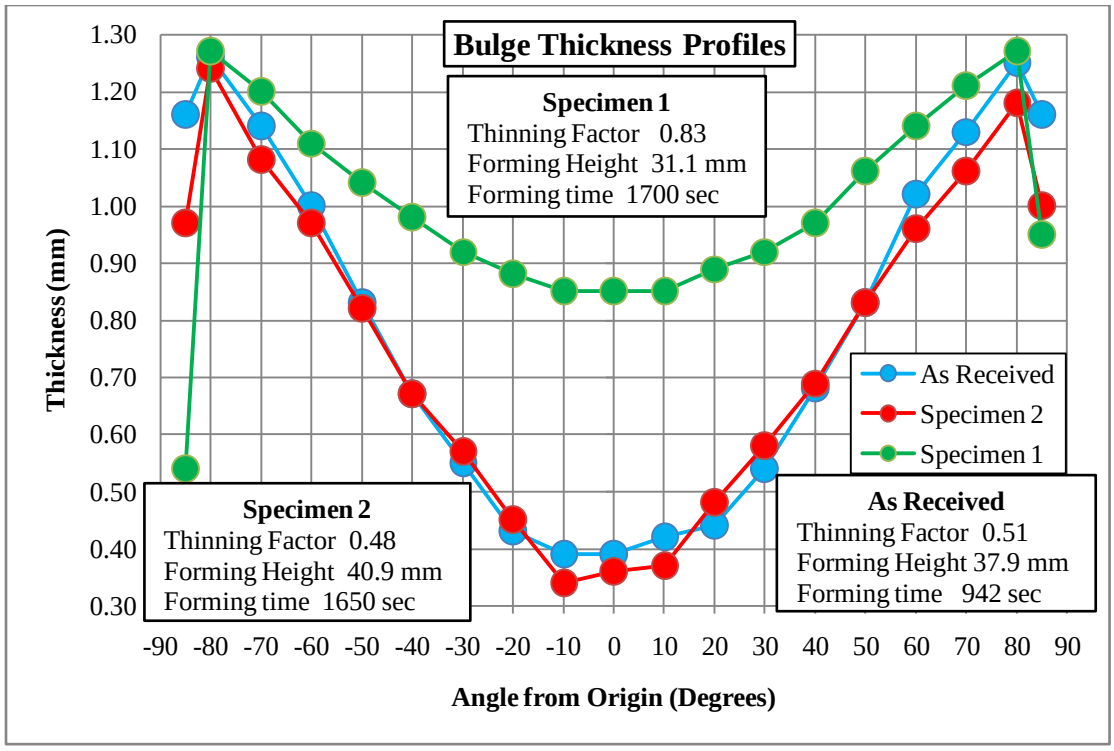

Figure 73 Bulge forming thickness profiles for the UV light bulge specimens compared with an as received specimen

Table 7 Bulge forming results performed at a dome strain rate of 1.0×10^{-3} s^{-1} at 400˚C

	As Received	Specimen 1	Specimen 2
Forming Temperature (˚C)	400	400	400
Thinning Factor	0.51	0.84	0.48
Forming Height (mm)	37.9	31.1	40.9
Forming Time (s)	962	1700	1650
Minimum Thickness (mm)	0.36	0.34	0.85
Failure	Yes	No	Yes

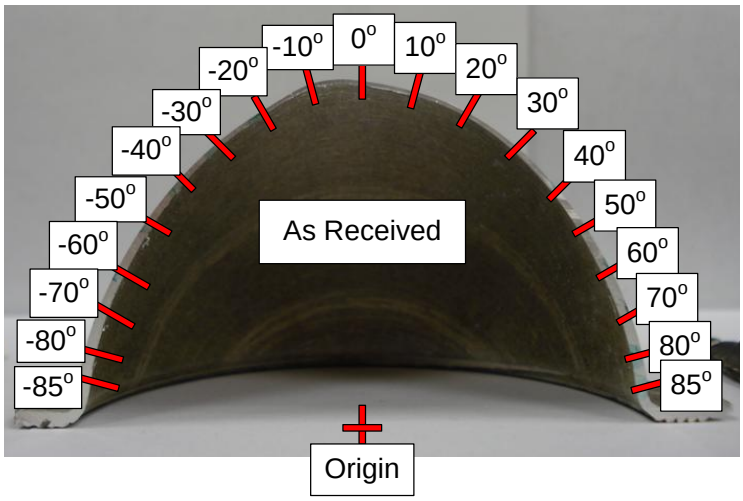

Figure 74 Angular coordinate system for thickness measurements of bulge samples shown on the as received specimen

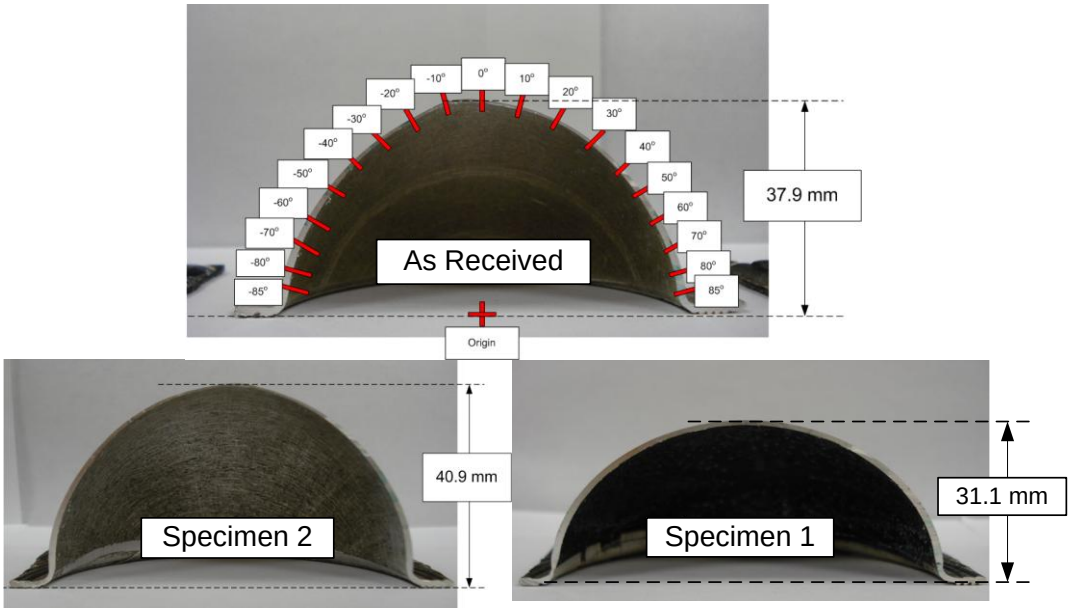

Figure 75 All three bulge formed specimens with forming height

With Figure as a physical representation, Figure provides the complete collection of results from the bulge forming experiments. The forming heights provide evidence of the annealing effects on SPF of Mg AZ31B. Specimen 1 was selectively heated for nearly 40 minutes which is 15 minutes longer than the remaining specimens. Also, specimen 1 was heated to temperatures of 425˚C and 460˚C which would create a major difference in the

microstructure by nearly 2 microns granted the evidence from the microstructure examination carries from specimen 3 to the remaining specimens. This difference in the microstructure explains why the specimen failed to approach failure with a pressure profile for the as received microstructure. The 1700 + second forming without failure provides secondary evidence to the results from SPF tensile tests in chapter 4. As for specimen 2, it did fail, but again the forming time was ~1650 seconds which is substantially longer than expected if there were no microstructure effects from selectively heating.

As for the tinning effects, it was hypothesized prior to forming that there would be negligible effects since the grain size gradients were so small. It was desired to achieve a gradient of at least 3 microns before thinning effects could be examined which was not possible due to the lack of proper cooling fixtures for the UV light experiments in Albi France. Though, if one looks at the forming heights, specimen 3 did provide a taller bulge which means that the material needed to stretch more, but this is most likely due to the slower strain rate during forming which also provides a major influence on forming thickness (9).

But, for specimen 1, if one looks closely at the two edges of the plot, a major drop in thickness is noticed at - 85˚ versus 85˚. If one recalls the temperature profiles, Figure and Figure , the vertical profiles present a major temperature drop off near the top versus the bottom due to the ceramic holder. This means that the grain growth would be much different between top and bottom. And if this occurs, then the material flow stress is a bit lower at the top verses the bottom even for small grain size differences as presented in chapter 5 from the tensile tests. Therefore, specimen 1 provides a very little but important

result towards thinning influences and thus presenting reason to continue the research. Especially since the temperature gradients achieved versus those desired are much different in that an ideal temperature gradient profile would provide a maximum temperature of 200˚C slightly inside the forming die edge and at least a temperature of 350˚C near the center in order to allow for substantial grain growth in the middle in the order of 5 microns versus minimal grain size growth near the edge.

This leads to a conclusion that the research has provided a small amount of insight to selective heating using a UV light source.

CHAPTER 6 CONCLUSIONS

Results

Through a collective series of samples for different temperatures, annealing times and sheet metal thicknesses, 3-dimensional contour plots for static grain were generated. The contour plots are to be used for future annealing research and selective grain growth studies as well as for the work presented here. Chapter 5 selective heating results verified the results for the contour plots are applicable. This seems marginal, but when one accurately accounts for the time and cost requirements to perform microstructure analysis, the results are substantial for future Mg AZ31B research dealing with any temperature effects in SPF since microstructure requirements provide that a grain size of less than 10 μm is important and the microstructure of the commercially received Magnesium alloy used for this work are of ~4 μm.

Chapter 4's uniaxial SPF results provide a basis for future research to provide a major annealing/grain size examination. With this work, one can begin to fit constitutive material models to these results and determine the necessary future work required to generate accurate simulations of multi grain sized sheets. Ultimately, this will be required to completely determine if grain size gradients will offer a major contribution to high production rate SPF for industry.

Finally, the selective heating research presented here is marginal in the determination of thinning effects generated by grain size gradients. This work does however provide proof that two methods of heating are applicable to such research and suggestions on future experimental setups is provided below. The bulge results do provide biaxial proof to that of the uniaxial results presented in Chapter 5. The major

effect of annealing on forming time and height provides a reason to continue such research further in selective heating of Mg AZ31B.

Recommendations For Future Work

My recommendations for future work are of two fold. If it desired to simply provide physical proof that grain size gradients can permit positive thinning influence in SPF bulge forming, than it is recommended to recreate the UV light selective heating experiments but with the heat sinks shown in Figure . These heat sinks were used with the air gun and use water as a coolant connectable to a sink.

Figure 76 Circular heat sinks

This will provide the necessary cooling requirements to generate a 100˚C + temperature gradient. Now, if an induction heater meant for heating purposes of more than 1000˚C is

available, selective heating should be achievable by similar means as the furnace which was used to conduct the need energy to the samples surface. Just, the heat source will be capable of providing such energy where as the furnace was not capable of such requirements.

Now if future work is desired to put forth an applicable selective grain growth study to prove its abilities, then a more in depth research effort is needed. First, it would be suggested that a complete uniaxial SPF analysis be performed now that the contour plots in Chapter 4 are complete to generate proper grain size experiments larger than those presented here and in more detail. At the same time, it is also suggested that a constitutive material model be adapted to represent the uniaxial results such as the one Abu-Farha (2007) (2) presented for the as received experiments. Then, accurate modeling efforts can be used to determine necessary grain size gradients to obtain substantial results in the thinning effects as well as necessary temperature gradients and heating times can be determined logically with the static grain growth curves presented in chapter 4 of this work. And finally the heating experiments can be carried out to provide a basis for accuracy of the constitutive model and whether such work is feasible and thus desirable to continue to pursue. That is, if such methods are successful, than industrial application means would still need to be researched and proof would need to be provided that the work can be used in industry.

REFERENCES

1. Superform *Superform Aluminum.* www.superform-aluminium.com.
2. *Ti-6Al-4V Dental Implant Structure.* R.V. Curtis, A.S. Juszcyk, B. Swale, and J.D. Walter**.** London , 1996, Institute of Metals, pp. 1784-1791.
3. R.V.Curtis. *Face On.* 2005, Materials World, pp. 20-22.
4. K.A. Padmanabhan, R.A. Vasin, and F.U. Enikeev**.** "Superplastic Flow: Phenomenology and Mechanics". Berlin : Springer Verlag, 2001.
5. H. Watanabe, H. Tsutsui, T. Mukai, M. Kohzu, S. Tanabe, and K. Higashi. *Deformation Mechanism in a Coarse-Grained Mg-Al-Zn Alloy at Elevated Temperatures.* 2001, International Journal of Plasticity, Vol. 17, pp. 387-397.
6. Y. Lui, K. Shue, and X. Wu. *Superplasticity and Microstructural Ecolution of a Large-Grained Mg Alloy.* 2000. Proceeding of the ASME, Manufacuring in Engineering Division. Vol. 11, pp. 275-280.
7. Y. Liu and X. Wu**,** *Superplasticity of Coarse-Grained Magnesium Alloy.* 4, 2002, Scripta Materialia, Vol. 46, pp. 269-274.
8. H. Watanabe, T. Mukai, K. Ishikawa, M. Mabuchi, and K. Higashi. *Realization of High-Strain-Rate Superplasticity at Low Temperatures in a Mg-Zn-Zr Alloy*, 2001, Materials Science and Engineering, Vol. A307, pp. 119-128.
9. F. Abu-Farha *INTEGRATED APPROACH TO THE SUPERPLASTIC FORMING OF MAGNESIUM ALLOYS*. Univeristy of Kentucky, 2007, Disssertation.
10. C.H. Hamilton, H.M Zbib, C.H. Johnson, and S.K. Richter. *Dynamic Grain Coarsening and Its Effect on Flow Localization in Superplastic Deformation.* Hiba-shi, Japan, 1991. Japan International SAMPE Symposium and Exhibition. pp. 272-279.
11. C.H. Johnson, C.H. Hamilton, H.M. Zbib, and S.K. Ricter. *Designing Optimized Deformation Paths for Superplastic Ti-6Al-4V.* The Minerals, Metals and Materials Society, 1993, Advances in Superplasticity and Superplastic Forming, pp. 3-15.
12. C.H.Hamilton and A.K. Ghosh *Influence of Material Parameters and Microstructure on Superplastic Forming.* May 1982, Metallurgical Transactions A, Vol. 13A, pp. 733-743.
13. K. Mallikarjun, S. Suwas, S. Bhargava. *Effect of Prior Beta Processing on Superplasticicty of (Alpha+Beta) Thermo-Mechanically Treated Ti-632Si alloy.* 2003, Journal of Materials Processing Technology, Vol. 134, pp. 35-44.
14. C.H.Hamilton and A.K. Ghosh *Mechanical Behavior and Hardening Characteristics of a Superplastic Ti-6Al-4V Alloy.* June 1979, Metallurgical Transactions A, Vol. 10A, pp. 699-706.
15. C.H. Hamilton and N.E. Paton *Microstrutural Influences on Superplasticity in Ti-6Al-4V.* February 1978, Metallurgical Transactions A, Vol. 10A, pp. 241-250.
16. R. Imayev, N. Gabdullin and G. Salishchev. *Effect of Grain Size on Superplastiity of an Intermetallic Ti3Al Compound.* 1997, Intermetallics, Vol. 5, pp. 229-236.
17. Z.Y. Ma, R.S. Mishra, and M.W. Mahoney. *Superplastic Deformation Behavior of Friction Stir Processed 7075 AL Alloy*. 2002, Acta Materialia, Vol. 50, pp. 4419-4430.
18. R.S Mishra and Y. Wang *Finite Element Simulation of Selective Superplastic Forming of Fricion Stir Processed 7075 Al Alloy.* 2007, Materials Science and Engineering, Vol. 463, pp. 245-248.

19. H. Watanabe, H. Tsutsui, T. Mukai, K. Ishikawa, Y. Okanda, and K. Higashi. *Superplastic Behavior in Commercial Wrought Magnesium Alloys.* 2000, Materials Science Forum, Vols. 250-351, pp. 171-176.
20. *M.* Khraisheh and F. Abu-Farha *On the Superplastic Forming of AZ31 Magnesium Alloy*. Dresden Germany, 2006. 7th International conference on Magnesium Alloys and Their Applications .
21. M. Khraishehand F. Abu-Farha *Analysis of Superplastic Deformation of AZ31 Magnesium Alloy.* In Press, Journal of Advanced Engineering Material.
22. L.A. Neumeier and M.M. Tilman *Superplasticity in Commercial and Experimental Compositions of Magnesium Alloy Sheet.* United States Department of the Interior, Burea of Mines. US Government, 1982. Report of Investigations.
23. R.H. Bricknell. *The Effect of Grain Size on the Maximum Strian Rate Sensitivity Observed in Superplastic Alloys.* 1979, Scripta Metallurgica, Vol. 13, pp. 605-610.
24. *R.* Raj and A.K. Ghosh *Grain Size Distribution Effects in Superplasticity*. 1981, Acta Metallurgica, Vol. 29, pp. 607-616.
25. *M.C*. Chaturvedi and B.P. Kashyap *The Effect of Prior Annealing on High Temperature Flow Propeties and Microstructural Evolution in SPF grade IN718 Superalloy.* 2007, Materials Science and Engineering A, Vols. 445-446, pp. 364-373.
26. *M.S.* Soliman *Effect of Strain Rate and Grain Size on the Ductility of Superplastic Pb-62% Sn Eutectic At Room Temperature.* 6, 1995, Scripta Metallurgica et Materialia, Vol. 33, pp. 919-924.
27. *A.K.* Ghosh and D.H. Bea *Grain Size and Temperature Dependence of Superplastic Deformation in an Al-Mg Alloy Under Isostructural Condition.* 2000, Acta Materialia, Vol. 48, pp. 1207-1224.
28. D. Garriga-Majo, R.J. Paterson, R.V. Curtis, R. said, R.D. Wood, and J. Bonet. *Optimisation of the Superplastic Forming of a Dental Implant for Bone Augmentation using Finite Element Simulations.* 2004, Dental Materials, Vol. 20, pp. 409-418.
29. J. Bonet, R.D. Wood, R. Said, R.V. Curtis and D. Garriga-Majo. *Numerical Simulation of the Superplastic Forming of Dental and Medical Prosthses.* 2002, Biomechan Model Mechanobiol, Vol. 1, pp. 177-196.
30. *L.D.* Hefti. *Advances in Fabricating Superplastically Forming and Diffusion Bonded Components for Aerospace Structures.* 2004, Journal of Materials Engineering and Performance, Vol. 13, pp. 678-682.
31. G. Davies, J. Edington, C. Cutler, and K. Padmanabhan. "Superplasticty: A Review". 1970, Journal of Materials Science, Vol. 5, pp. 1091-1102.
32. W. backofen and D. Avery *A Structural Basis for Superplasticity*. 1965, Transactions of ASM, Vol. 58, pp. 551-556.
33. E. Hart. *A Theory for Flow of Polycrystals.*1967, Acta Metallurgica, Vol. 15, pp. 1545-1549.
34. H. Raman, G. Luckey, G. Kridli, and P. Friedman. *Development of Accurate Constitutive Models for Simulation of Superplastic Forming.* 2007, Journal of Materials Engineering and Performance, Vol. 16, pp. 284-292.
35. A.Mukherjee *The Rate Controlling Mechanism in Superplasticity.* 1971, Materials Science and Engineering, Vol. 8, pp. 83-89.
36. A. Mukherjee and A. Dutta *Superplastic Forming: an Analytical approach.* 1992, Materials Science and Engineering A, Vol. 157, pp. 9-13.

37. R. Sharma and A. Dutta *Prediction of Initial Blank Thickness and Thickness Profile after Superplastic Forming.* 1994, Materials Science Forum , Vols. 170-172, pp. 757-762.
38. B. Rao and J. Jeyasingh *On the Thinning Variation of a Superplastically Formed Titanium Alloy Spherical Domes.* 2005, Journal of Materials Processing Technology, Vol. 160, pp. 370-373.
39. X.D. Ding, H.M. Zbib, C.H. Hamilon and A.E. Bayoumi. *On the Optimization of Superplastic Blow-Forming Processes.* 1995, Journal of Metarials Engineering and Performance, Vol. 4, pp. 474-485.
40. H. Jintao and J. Qualin *Superplastic Constitutive Realtion and its Application.* 1997, Materials Science Forum, Vols. 243-245, pp. 170-184.
41. T. Langdon and R. Gifkins *Grain Boundary Displacement Due to Diffusional Creep.* 1970, Scripta Metallurgica, Vol. 4, pp. 563-567.
42. F. Abu-Farha and M.K. Khraisheh. *Microstructure-Based Modeling of Anisotropic Superplastic Deformation.* 2003, Transactions of North American Manufacturing Research Institute, Vol. 31, pp. 41-47.
43. F. Abu-Farha and M.K. Khraisheh. *Microstructure-Based Modeling and Simulation of Superplastic Forming Process.* Albi, France. 2004 Proceedings to European Conference on Superplastic Forming. pp. 75-80.
44. M.K. Khraisheh, F. Abu-Farha, M.A. Nazzel and K.J. Weinmann. *Combined Mechanics-Materials Based Optimization of Superplastic Forming of Magnesium AZ31 Alloy.* 2006, Annuals of the CIRP, Vol. 55, pp. 233-236.
45. B.H. Cheong, J. Lin and A.A. Ball. *Modelling the Efects of Grain-Size Graidents on Necking in Suerplastic Forming*. 2003, Journal of Materials Processing Technologies, Vol. 134, pp. 10-18.
46. T-K. Kim and F.P.E. Dunne. *Modelling Heterogeneous Microstructures, Inhomogeneous Deformation and Failure in Superplasticity.* 1998, Journal of Materials Processing Technology, Vols. 80-81, pp. 96-100.
47. K. Droder and E. Doege. *Sheet Metal Forming of Magnesium Wrought Alloys - Formability and Process Technology.* 2001, Journal of Materials Processing Technology, Vol. 115, pp. 14-19.
48. K.F. Zhang, G.F. Wang, D.Z. Wu, and Z.R. Wang. *Research on the Controlling of the Tickness Distribution in Superplastic Forming.* 2004, Journal of Materials Processing Technology, Vol. 151, pp. 54-57.
49. H. Watanabe, T. Mukai, M. Mabuchi, and K. Higashi. *High-Strain-Rate Superplasticity at Low Temperature in a ZK61 Magnesium Alloy Produced by Powder Metallurgy.* 2, 1999, Scripta Materialia, Vol. 41, pp. 209-213.
50. D.G. Sanders. *The Current State-of-the-Art and the Future in Airframe Manufacturing Using Superplastic Forming Technologies.* 2001, Materials Science Forum, Vols. 357-359, pp. 17--22.
51. P.A. Friedman, S. Luckey, W. Copple, C. Miller, and C. Young. *Overview of Superplastic Forming Research at Ford Motor Company.* 2004, Journal of Materials Engineering and Performance, Vol. 13, pp. 670-677.
52. G.S. Cole. *How Magnesium Can Achieve High Volume Usage in Ground Transportation.* Rome, Italy : s.n., 1999. The 56th Annual Meeting of the International Magnesium Associate. pp. 21-30.

53. F. Abu-Farha and M.K. Khraisheh. *An Experimental Investigation of Post-Superplastic Forming Properties of AZ31 Magnesium Alloy.* 2007, Annuals of the CIRP, Vol. 56.
54. E. Aghion, B. Bronfin and D. Eliezer. *The Role of the Magnesium Industry in Protecting the Environment.* 2001, Journal of Materials Processing Technology, Vol. 117, pp. 381-385.
55. B. Bronfin and E. Aghion. *Magnesium Alloys Development towards the 21st Century.* 2000, Materials Science Forum, Vols. 350-351, pp. 19-28.
56. G.S. Cole. *Issues that Influence Magnesium's Use in the Automotive Industry.* 2003, Materials Science Forum, Vols. 419-422, pp. 43-50.
57. F. Friedrick and S. Schuman. *The use of Magnesuim in Cars - Today and in the Future.* 1998, Mg Alloys and thier Applications, pp. 28-30.
58. A.M. Sherman and G.S. Cole. *Lightweight Materials for Automotive Applications.* 1995, Materials Characterization, Vol. 35, pp. 3-9.
59. B.L. Mordike and T. Ebert. *Magnesium Properties - Application - Potential.* 37-45 2001, Material Science and Engineering, Vol. A302.
60. S. Schumann and H. Friedrick. *Research for a "New Age of Magnesium" in the Automotive Industry.* 2001, Journal of Materials Processing Technology, Vol. 117, pp. 276-281.
61. A. Mertz. *Improved Design Possibilities by Applying Magnesium Extrusions.* Munich, Germany, 2002. International Congress Centre.
62. M. Beyer and A. Jambor. *New Cars - New Materials.*, 1997, Materials and Design, Vol. 18, pp. 203-209.
63. S. Schumann and H. Friedrich. *The Second Age of Magnesium Research Strategies to Bring the Automotive Industry's Vision to Reality.* Sdom, Israeli, 2000. The 2nd Israeli International Conference on Mg Science and Technology. pp. 9-18.
64. U. Dragugelates, A. Schram and C-C. Kedenburg. *Superplasticity of Magnesium-Based Alloys.* 2000, Magnesium Technology, pp. 341-344.
65. J. Bohlen, A. Horstmann, F. Kraise, A. Styczynski, D. Letzig, and K.U. Krainer. *Influence if the Thermomechnical Treatment on the Microstructure of Magnesium Alloy AZ31.* 2003, Magnesium Technology, pp. 253-258.
66. A-W. El-Morsy, K. Manabe, and H. Nishimura. *Superplastic Forming of AZ31 Magnesium Alloy Sheet into a Rectangular Pan.* 10, 2002, Materials Transactions, Vol. 43, pp. 2443-2448.
67. A. Takara, Y. Nishikawa, H. Watanabe, H. Somekawa, T. Mukai, and K. Higashi. *Secondary Processing of AZ31 Magnesium Alloy Concomitant with Grain Growth or Dynamic Recrystallization.* 7, 2004, Materials Transactions, Vol. 45, pp. 2377-2382.
68. Wu and Q. Jin. *Superplastic Formign Behaviors and Microstructure Characters of Magnesium Alloy Sheet AZ31B. H.* Columbus Ohio: American Institute of Physics, 2004. 8th International Conference on Numerical Methods in Industrial Forming Processes. Vol. 712.
69. J.C Huang and C.J. Lee. *Cavitation Characteristics in AZ31 Mg alloys during LTSP or HSRSP.* 2004, Acta Materialia, Vol. 52, pp. 3111-3122.
70. H. Watanabe, A. Takara, H. Somekawa, T. Mukai, and K. Higashi. *Effect of Texture on Tensile Properties at Elevated Temperatures in an AZ 31 Magnesium Alloy* 2005, Scripta Materialia, Vol. 52, pp. 449-454.

71. D.L. Yin, K.F. Zhang, and G.F. Wang. *Microstructure Evolution and Fracture Behavior in Superplastic Deformation of Hot-Rolled AZ31 Mg Alloy Sheet.* 2005, Materials Science Forum, Vols. 475-479, pp. 2923-2926.
72. L. Wang, M. Song, and R. Lui. *Superplasticity and Superplastic Instability of AZ31B Magnesium Alloy Sheet.* 2006, Transactions of Nonferrous Metals Society of Chine, Vol. 16, pp. 327-332.
73. S. Yi, S. Zaefferer, and H. Brokmeier. *Mechanical Behavior and Microstructural Evolution of Magnesium Alloy AZ31 in Tension at Different Temperatures*. 2006, Materials Science and Engineering A, Vol. 424, pp. 275-281.
74. M.A. Nazzal, M.K. Khraisheh, and F. Abu-Farha. *The Effect of Strain Rate Senesitivity Evolution on the Deformation Stability During Superplastic Forming.* 2007, Journal of Material Processing Technology, Vol. In Press.
75. Z.Y. Ma, R.S. Mishra, and M.w. Mahoney. 2002, Acta Materialia, Vol. 50, p. 4419.
76. P.S. Bate and J.Q. Jiang. 1996, Metallurgical and Materials Transaction A, Vol. 27A, pp. 3250-3258.
77. S. Rhaipu. *The Effect of Microstructural Graidents on Superplastic Forming of Ti-6Al-4V.* 1998, Journal of Materials Processing Technology, Vols. 80-81, pp. 90-95.
78. J. Wadsworth and T.G. Nieh. *Effect of Grain Size on Superplastic Behavior of Y-TZP.* 1990, Scripta Metallurical and Materialia, Vol. 24, pp. 73-766.
79. J.J. Bucki and K.J. Kurzydlowski. *Flow Stress Dependence on the Distribution of Grain Size in Polycrystals.* 1993, Acta Metallurical et Materialia, Vol. 41, pp. 3141-3146.
80. F.P.E. Dunne. *Inhomogeneity of Microstructure in Superplasticity and its Effect on Ductility.* 4-5, 1998, International Journal of Superplasticity, Vol. 14, pp. 413-433.
81. F. Hung, C. Shih, L. Chen, and T. Lui. *Microstructures and High Temperature Mechanical Properties of Friction Stirred AZ31-Mg Alloy.* 2007, Journal of Alloys and Compounds, Vol. 428, pp. 106-114.
82. B.M. Darras, M.K. Khraisheh, F.K. Abu-Farha, and M.A. Omar. *Friction Stir Processing of Commercial AX31 Magnesium Alloy.* 2007, Journal of Materials Processing Technology, Vol. 191, pp. 77-81.
83. Y.S. Sato, A. Sasaki, A. Sugimoto, A. Honda, and H. Kokawa. *Enhancement of Formability in Magnesium Alloy AZ31B via Friction Stir Processing.* 2007, Materials Science Forum, Vols. 539-543, pp. 3775-3780.
84. C.H. Hamilton. *Simulation of Static and Deformation-Enhanced Grain Growth Effects on Superplastic Ductility.*1988, Metallurgical Transactions A, Vol. 20A, pp. 2783-2792.
85. K. Woo and T. Lou. *Influences of Grain Size on Fracture of Superplasticity.*February 2002, Materials Letters, Vol. 52, pp. 374-377.
86. A. Dutta. *Thickness-profiling of Initial Blank for Superplastic Forming of Uniformly Thick Domes.*2004, Materials Science and Engineering A, Vol. 371, pp. 79-81.
87. R. Abbaschain and R.E. Reed-Hill. "Physical Metallurgy Principles". 3rd. Boston : PWS Publishing Company, 1994.
88. R.S. Mishra and A. Sepulveda. *An Analysis of Grain-Growth Data in Duplex Materials on Static Annealing and During Superplastic Deformation.* 1987, Journal of Materials Science, Vol. 22, pp. 2153-2157.
89. Metals Handbook. "Properties and Selection: Nonferrous Alloys and Special-Purpose Materials". [10th ed.] ASM International, 1990. Vol. 2.

90. H. Furuya, N. Kogiso, S. Matunaga, and K. Sendra. *Applications of Magnesium Alloys for Aerospace Structure Systems.*2000, Material Science Forum, Vols. 350-351, pp. 341-348.
91. P.P. De. Marco and P. Cavalier. *Effect of Friction Stir Processing on Mechanical and Microstructural Properties of AM60B Magnesium Alloy.* 2006, Journal of Material Science, Vol. 41, pp. 3459-3464.
92. N. Ridley and J. Pilling. "Superplasticity in Crystalline Solids". 1989, The Institute of Metals, London.
93. K. Osada. *Commercial Applications of Superplastic Forming.* 1997, Journal of Materials Processing Technology, Vol. 68, pp. 241-245.
94. Z. Li, and H. Guo. *Application of Superplastic Forming and Diffusion Bonding in the Aerospace Industry*. 2005, Materials Science Forum, Vols. 475-479, pp. 3037-3042.
95. L.D. Hefti. *Commercial Aiplance Applications of Superplastically Formed Aluminum Sheet.* ASM International, 2007, Journal of Materials Engineering and Performance, Vol. 16, pp. 136-141.
96. J. del Valle, F. Penalba, and O.A. Ruano. *Optimiation of the Microstructure for Improving Superplastic Forming in Magnesium Alloys.* 2007, Materials Science and Engineering A, Vol. In Press.
97. E. Ruibal, J.J. Urcola, and M. Fuentes. *Static Recrystallization Kinetics, Recristallized Grain Size, and Grain Growth Kinetics After Hot Deformation of a Low Alloy*. 1985, Z. Metallkde, Vol. 76, pp. 568-576.

VITA

Michael Christopher Cusick was born on July 17th 1983 in Greenville Pennsylvania. He was awarded a BS of Mechanical Engineering from the University of Kentucky. In pursuit of a Master's of Science, he was awarded a GAANN Fellowship as well as a IREE NSF grant for the year of 2007 for collaborative work with Ecole des Mine d'Albi Carmuax Campus in Albi France.